

## **Session 4:**

# **Early warning systems for drought and desertification**

# **Integrated modeling and remote sensing approach: toward a sustainable management of water resources in a semi-arid region**

A. Chehbouni<sup>a</sup>, R. Escadafal<sup>a</sup>, G. Boulet<sup>a</sup>, B. Duchemin<sup>a</sup>, V. Simonneaux<sup>a</sup>, G. Dedieu<sup>a</sup>,  
B. Mougenot<sup>a</sup>, A. Oliso<sup>b</sup> and H. Hanich<sup>c</sup>

<sup>a</sup> Centre d'Etudes Spatiales de la BIOSphère (CESBIO CNES-CNRS-UPS-IRD)  
18, avenue Edouard Belin, 31401 Toulouse Cedex 9 – France,  
email: ghani@cesbio.cnes.fr

<sup>b</sup> INRA, Avignon, France

<sup>c</sup> Université Cadi Ayyad, Faculté des sciences Semlalia, Marrakech, Maroc

## **ABSTRACT**

The Sudmed project is an international, multidisciplinary project whose objective is to understand the integrated hydro-ecological functioning of a semi-arid basin in central Morocco through combination of process modeling and multispectral/multiresolution remote sensing data. This project has been conceived by CESBIO/IRD in a close connection with Moroccan scientists, managers, decision makers and other stake holders. In addition to this scientific objective, the sudmed project also aims to provide operational tools to managers and guidance to decision makers which help to make informed decision where the need for the growth/development and the sustainability of water are balanced. In this presentation, we will first outline the specific objectives of the program. Second, we will provide the initial results, ongoing and future investigations.

**Keywords:** Semi-arid, land-surface interactions, sustainability, remote sensing, integrated modeling, long term variability.

## **1 INTRODUCTION**

Population growth has resulted in intense demands on the quantity and quality of water resources worldwide. The sustainability of water resources in the 21st Century will depend on our ability to correctly manage water resources systems under a more variable future climate. Semi-arid regions are in particular jeopardy, which are experiencing rates of population development that exceed those of other climatic regions and are highly sensitive to increasing anthropogenic pressures, variations in climate, and the disruptions associated with long-term climate change.

In southern Mediterranean regions, water consumption has increased by 60% in the last decades and continues to rise while available water resources are becoming increasingly scarce [3]. This situation has raised public awareness of long-term water resources issues. However, due to a combined shortage of expertise and funding, little has been attempted toward the development of a basin-wide hydrological understanding of its functioning, natural and/or human induced stresses and the consequent hydrological responses to those stresses. The development of improved management strategies and viable interventions to meet these challenges should entail unprecedented coordination and integration across a broad range of disciplines and actors/players.

However, understanding of critical hydrological processes at the basin scale and more importantly addressing them through an integrated research program is not trivial. A close integration of the individual components of hydrological cycle, i.e., vegetation functioning, surface water ground - water interaction, surface-atmosphere interactions is required. Such integration is made difficult by the discrepancy of time-space scales at which each of these processes is pertinent and thus needs to be addressed. Further complications are induced by the specificity of the space representation required for each component (Grid versus Area Representative for example). Additionally the issue of the degree of complexity required to accurately describe the processes is scale dependent and varies according to individual processes.

Understanding the complex processes involved cannot be fulfilled without making a full use of historical data and newly developed technology such as remote sensing, GIS, and other ground instruments such as scintillometer, isotopic analysis, numerical modeling and data assimilation. Here also one has to address the issue of the link

between ground and remotely sensed data as well as the scale discrepancies between remotely sensed data emanating from different platforms.

The objective of this paper is to present the sudmed project ([www.irrimed.org/sudmed](http://www.irrimed.org/sudmed)). We first present the objectives of the project, as well as the general structure and the thrust areas. Second we present the study site, followed by an overview of the initial results, ongoing and future investigations. Finally, the issue of transposing the results obtained in Morocco to other semi-arid regions of the world will be discussed.

## **2 OBJECTIVES AND STRUCTURE OF THE SUDMED PROJECT**

The sudmed project has been conceived by CESBIO/IRD in a close connection with Moroccan scientists, managers, decision makers and other stake holders whose general objectives are to understand the integrated hydrological functioning of a semi-arid basin in Morocco and to provide guidance and tools to managers, decision makers and stake holders for sustainable management of water resources in the basin. The specific objectives of the program are:

- a- What are the changes that occurred in the basin during the past 30 years or so, and what drove these changes and what are the impact on water and vegetation resources in a semi-arid basin?
- b- Describe in integrated manner, the dominant processes that control the overall hydrological functioning of the basin by making full use of recent technological and scientific developments (Modelling, Remote Sensing, Assimilation)
- c- Develop scenarios in terms of the sustainability of water and vegetation resources in response to different hypothesis associated with natural and/or human induced environmental changes.
- d- Provide operational tools to managers while assuring compatibility between level of technology and the user's ability.

To achieve the above objectives, the program has been structured into the following thrust areas:

- Basin characterisation and Geographic Information System development
- Basin scale Evapo-Transpiration estimates and the quantification of the origin of water used (dam, rain , pumping)
- Quantifying precipitation and its partitioning between runoff and infiltration in the mountain area as well as quantifying snow, snowmelt and its contribution to recharge and to spring runoff and ground water surface water interaction (recharge and pumping)
- Development of a generic vegetation functioning model
- Integrative modelling and quantitative remote sensing and data assimilation
- Education, capacity building and knowledge transfer.

## **3 SITE DESCRIPTION AND EXPERIMENTAL SETUP**

### **3.1 Site Description**

This study took place in the Tensift basin which represents the focus study region for the SUDMED program. The basin originates in the atlas mountain and flows west to the Atlantic Ocean. The basin embodies a number of characteristics which make it an exceptional outdoor laboratory for addressing a large number of scientific challenges in arid and semi-arid hydrology, meteorology, ecology, and social and policy science. In the basin in characterized by a significant topographic and vegetation variation, and a highly variable climate. The annual rainfall ranges from around 150 mm in the dry part to 1000 mm in the mountain, with the majority of annual precipitation occurring during the winter season. The precipitation pattern depicts strong annual to inter-annual variability (figure 1).

Carte de la pluviométrie moyenne du Tensift 1972-2001

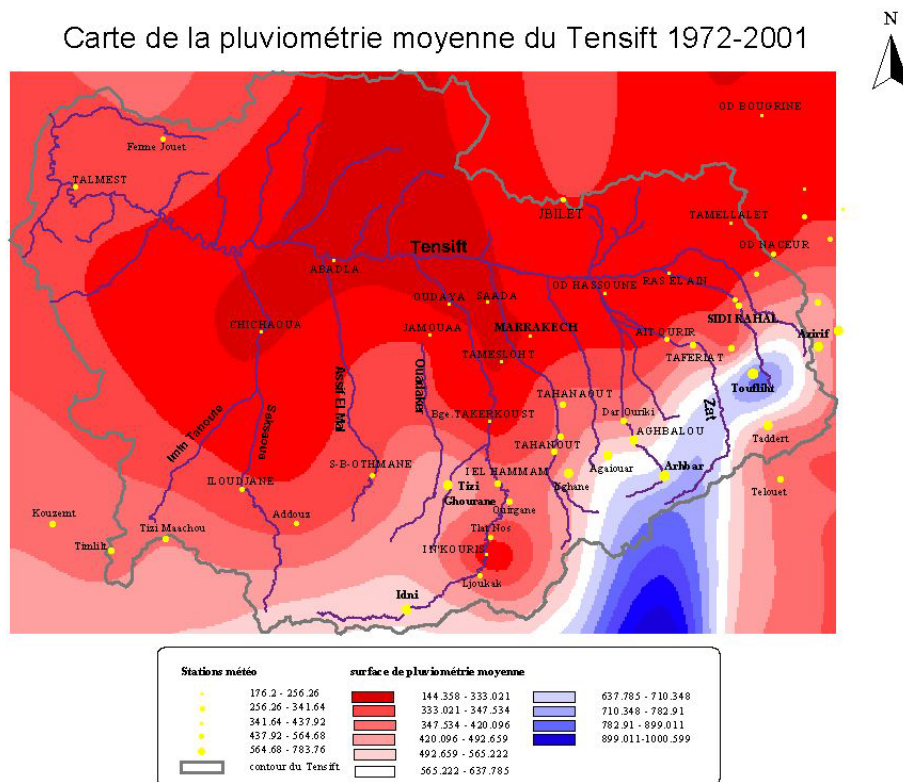


Figure1. 30 years average rainfall over the basin.

In this basin about 85% of available water is used in the plain by agriculture. Major irrigated vegetation types include olive (40% of national production), oranges and wheat. As shown in figure 2, irrigated surfaces increase tremendously during the past two decade which leads to an overexploitation to ground water [1].

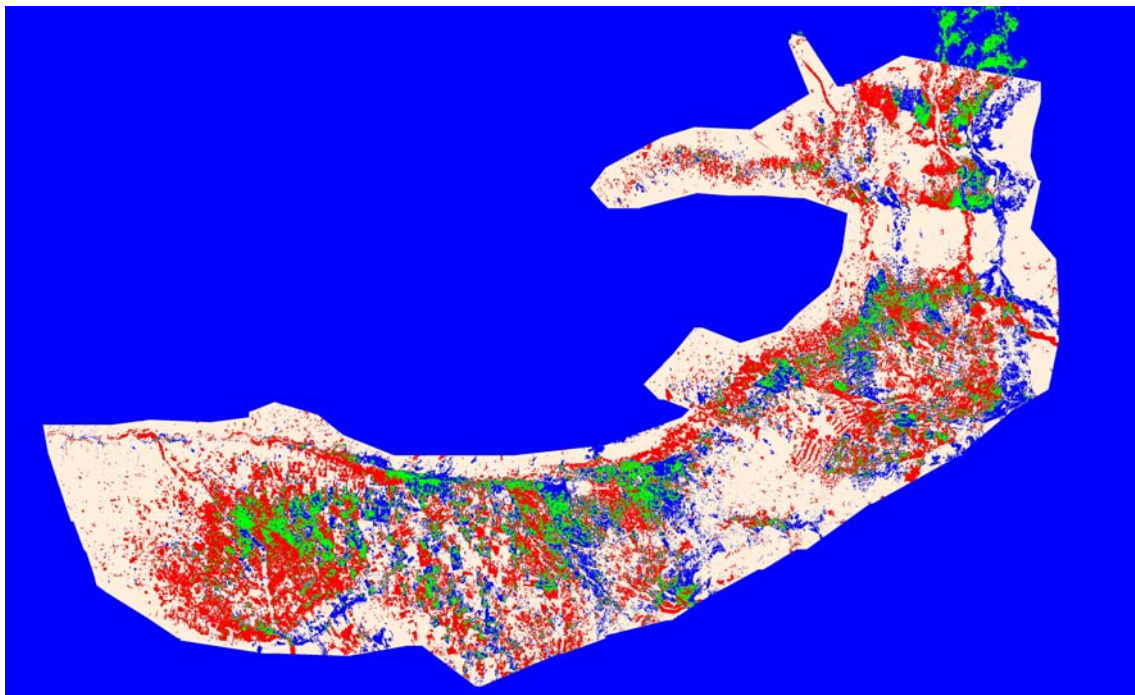


Figure2. Variation of irrigated cultures from 1986 to 2000 (blue = decrease, green = stable, red = increase).

In dry part of the basin, ground water level drops about 1m every year (figure 3).

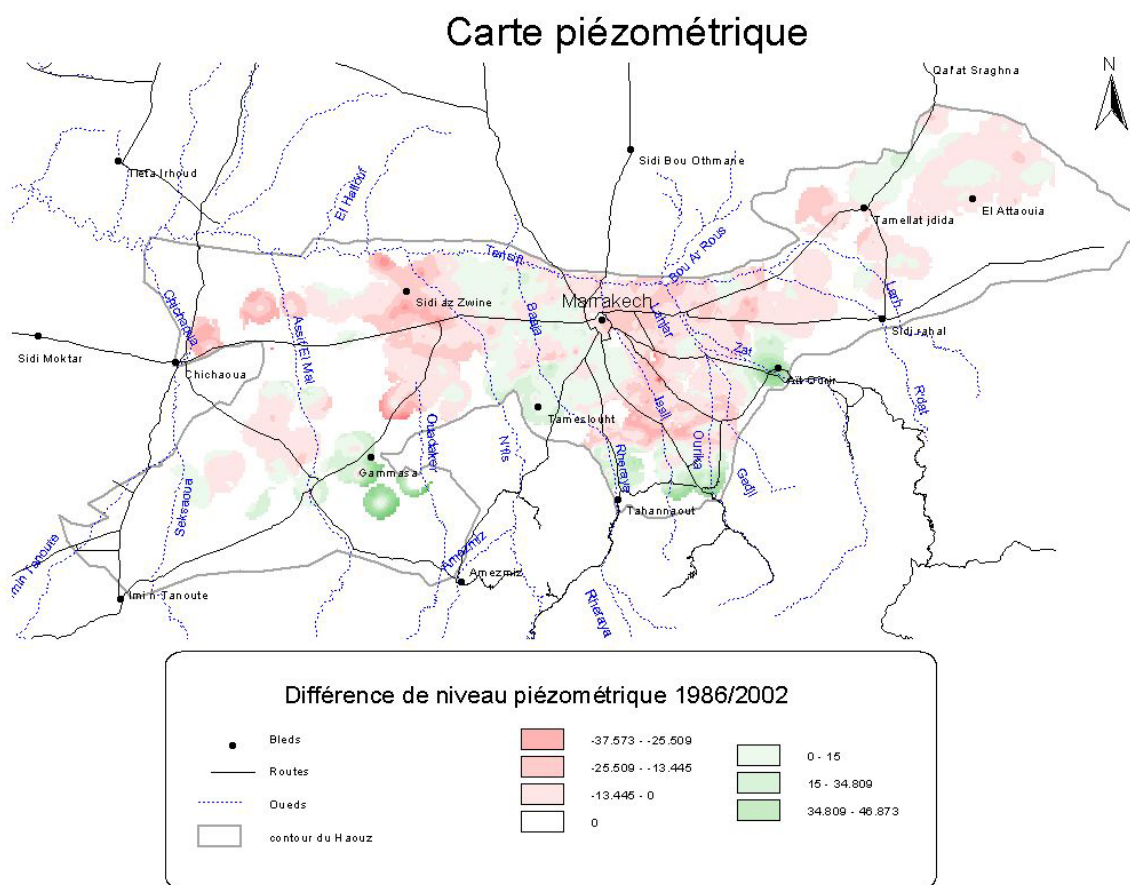


Figure 3. Variation of water table level between 1986 and 2002 [1].

### 3.2 Experimental setup

For this study, a comprehensive experimental was designed to achieve the objectives of the study. A basin wide meteorological network made up of 9 automatic stations that measure incoming radiation, wind speed and direction, air temperature and humidity, rainfall. In the mountain site a dense network of rain gauges was deployed to capture the spatial variability of the rainfall. In the plain section, complete flux stations (eddy correlation) were deployed over the 3 dominant vegetation types (olives, oranges and wheat). A large aperture scintillometer (LAS) that measures sensible heat flux over large surfaces (up to 5 km) was also deployed over the olives site in 2002-2003, wheat site in 2003 and oranges site in 2004 [9]. Additionally, surface temperature, soil moisture and soil temperature were collected over each sites. During the 2003 season the olives site was equipped with device to measure sapflow and thus plant transpiration. At the same time isotopic sampling were used to separate soil and vegetation contribution to total evapotranspiration [12].

Regarding remote sensing data, ground based surface reflectance and temperature were collected throughout the growing seasons using a hand held radiometers (cropscan). Historical satellite data were acquired over a period of 30 years (MSS and LANDSAT). Additionally time series of SPOT and TM, VEGETATION images were ordered starting 2002. Finally a sun photometer (CIMEL) was installed in 2003 to collect atmospheric data required for atmospheric correction.

## 4 PRELIMINARY RESULTS

In the following section, significant preliminary results associated with each thrust area mentioned above are provided.

### Basin characterisation and Geographic Information System development

A complete basin wide Geographic Information System was developed that includes several information layer: topography, soil map, geological map, land use and land cover, groundwater map, etc.

### **Basin scale Evapo-Transpiration estimates**

Several models ranging from the most simple (FAO-56) to the most complex one (i.e. SVATs) were implemented to estimate the spatio-temporal variability of evapotranspiration. The results show that the physically based SVAT provides the best estimates of surface fluxes over all sites but the model required several input parameters which are not routinely available. The FAO-56 model was adapted to use satellite based vegetation index and the results show that despite the simplicity of the model and some theoretical limitation of its parameterisations, estimates of ET were reasonable. However, the model was not able to separate soil and vegetation contributions to ET [6, 8].

### **Quantifying precipitation and its partitioning between runoff and infiltration in the mountain**

This talk has been talked in the context of Chaponniere's PhD. thesis [4]. The SWAT model has been implemented in mountainous sub-watershed. The result shows that the fact that a hydrological model provides accurate estimates of the runoff does not necessary means that the other hydrological components are well described. For example, the snow parameterisation in SWAT as well as surface-subsurface one were not realistic while the total runoff was well reproduced. Future work is dedicated toward the improvement of the other components of hydrological cycle in SWAT.

### **Development of a generic vegetation functioning model**

Here also several vegetation growth models have implemented. STICS model has been validated over an irrigation district. The results show that when the model is forced by remotely sensed data, the estimates of biomass, yield and water balance are well reproduced. Similarly to other complex models, STICS needs several input parameters which are not routinely available at the appropriate space-time scales [11, 10]. To tackle this problem a simpler and generic model has been developed (SAFYE: [7]). This model requires only a few parameters and most of them can be obtained from remotely sensed data. Despite the simplicity of this model, the simulation results compared well the those of STICS

### **Integrative modelling and quantitative remote sensing and data assimilation**

Remote sensing data has been used for different purposes. First historical data, has been processed to estimates changes in land used and land cover for a period of 25+ years. Actual data were used to produce land cover maps and to monitor snow cover in the atlas [4]. Second SPOT data has been used in conjunction with FAO-56 and with STICS and SAFYE to map evapotranspiration. Finally Thermal infrared data (TM) has been used in conjunction with a SVAT and assimilation scheme to invert the quantity of irrigation water.

### **Education, capacity building and knowledge transfer.**

9 PhD students (6 from Morocco and 3 from Europe) as well as 12 Masters students have been working un the context of the sudmed project. Additionally several training sessions in remote sensing, geographic information systems, micrometeorology were organized in Marrakech this the course of the project. These training sessions were open for students, young scientists and engineers working for different government agencies partners in the project. Finally a Decision Support System for better management of irrigation water is under development.

## **5 CONCLUDING REMARKS**

Substantial results have been obtained during this first phase of the sudmed project. A remote sensing data base has been constructed. Advances in each thrust area have been accomplished. However it should be mentioned that we are far from achieving all the objectives of the project. The second phase of sudmed will build up on the achieving of the first phase and it will be directed towards:

- Integrative modeling
- Aggregation and desegregation issues
- The use of low to very low resolution satellite data (VEGETATION, MSG, SMOS).
- Completing the development of the Decision Support System

## **REFERENCES**

[1] ABOURIDA, A., ERROUANE, S., CHEHBOUNI, A., AND CHEGGOUR, A., 2004: Caractérisation hydrogéologique de la plaine du Haouz dans le cadre du programme scientifique Sud-Med. in: Conf. Int., Ouarzazate (Maroc), 1er-2 Avril/2004.

- [2] ABOURIDA, A., ERROUANE, S., CHEHBOUNI, A., AND CHEGGOUR, A., 2004: Impact of the dryness on the underground water potentialities of the Haouz plain (Central Morocco). in: 1st Gen. Assem., Nice (France), 25-30 April/2004.
- [3] BOULET, G., CHEHBOUNI, A., BRAUD, I., DUCHEMIN, B. AND LAKHAL, A., 2004: Evaluation of a two-stage evaporation approximation for contrasting vegetation cover. *Wat. Resour. Res.*, 40, W12507, doi:10.1029/2004WR003212.
- [4] CHAPONNIERE, A.B.G., MAISONGRANDE, P. AND CHEHBOUNI A., 2003. Simulation of the hydrological regime of a small semi-arid mountainous watershed in Morocco. in: EGS-AGU Joint meet., Nice, France.
- [5] CHEHBOUNI, A., ESCADAFAL, R., DEDIEU, G., ERROUANE, S., BOULET, G., DUCHEMIN, B., MOUGENOT, B., SIMONNEAUX, V., SEGHERI, J. AND TIMOUK F., 2003: A multidisciplinary program for assessing the sustainability of water resources in semi-arid basin in Morocco: SUDMED. EGS - AGU - EUG Joint Assembly, Nice, France, 6-11 April 2003.
- [6] DUCHEMIN B., ER-RAKI, S., GENTINE, P., MAISONGRANDE, P., CORET, L., BOULET, G., RODRÍGUEZ, J.C., SIMONNEAUX, V., CHEHBOUNI, A., DEDIEU, G. AND GUÉMOURIA N., 2003: Estimating Cereal Evapotranspiration using a Simple Model driven by Satellite Data. in: 23th Int. Geosci. and Remote Sens. Symp. (IGARSS), Toulouse (France), 21-2 July /2003.
- [7] DUCHEMIN, B., HADRIA, R., ER-RAKI, S., BOULET, G., MAISONGRANDE, P., CHEHBOUNI, A., ESCADAFAL, R., EZZAHAR, J., HOEDJES, J.C.B., KHARROU, M.H., KHABBA, S., MOUGENOT, B., OLIOSO, A., RODRÍGUEZ, J-C. AND SIMONNEAUX, V., 2005: Monitoring wheat phenology and irrigation in Central Morocco: on the use of relationships between evapotranspiration, crops coefficients, leaf area index and remotely-sensed vegetation indices. *Agric. Wat. Manage.* (In press).
- [8] ER-RAKI, S, CHEHBOUNI, A., GUÉMOURIA, N., DUCHEMIN, B., EZZAHAR, J. AND HADRIA, R., 2005: Combined FAO-56 model-remote sensing approaches to estimate water wheat consumptions in semi arid region. *Agric. Wat. Manage.* (In press ).
- [9] EZZAHAR, J., CHEHBOUNI, A.G., HOEDJES, J.C.B., CHEHBOUNI, A., ER-RAKI, S. AND HADRIA R., 2005: Combined a large Aperture Scintillometer and the aggregation model to integrate Area-averaged sensible and latent heat fluxes over two adjacent of olive. in: 6ème Conf. Int. Europ. Wat. Resour. Assoc., Palais de l'Europe, Menton (France), 7-10 Septembre/2005.
- [10] HADRIA, R., DUCHEMIN, B., LAHROUNI, A., KHABBA, S., ER-RAKI, S., DEDIEU, G. AND CHEHBOUNI A., 2005: Monitoring of irrigated wheat in a semi-arid climate using crop modeling and remote sensing data : Impact of satellite revisit time frequency. *Int. Journ. Remote Sens. (IJRS)*. (In press)
- [11] RODRÍGUEZ, J.C., DUCHEMIN, B., HADRIA, R., WATTS, C., GARATUZA, J., CHEHBOUNI, A., KHABBA, S., BOULET, G., PALACIOS, E. AND LAHROUNI A., 2004: Wheat yield estimation using remote sensing and the STICS model in the semiarid valley of Yaqui (Mexico). *Agron.*, 24 (2004 ), pp. 295-304.
- [12] WILLIAMS, D.G., CABLE, W., HULTINE, K., HOEDJES, J.C.B., YEPEZ, E.A., SIMONNEAUX V., ER-RAKI, S., BOULET, G., DE BRUIN, H.A.R., CHEHBOUNI, A., HARTOGENSIS, O.K. AND TIMOUK., F., 2004: Evapotranspiration components determined by stable isotope, sap flow and eddy covariance techniques. *Agricultural and Forest Meteorology* 125, pp. 241-258.

# A fuzzy anomaly indicator for environmental status assessment based on EO data: preliminary results for Africa

P.A. Brivio<sup>a</sup>, M. Boschetti<sup>a</sup>, P. Carrara<sup>a</sup>, D. Stroppiana<sup>a</sup> and G. Bordogna<sup>b</sup>

<sup>a</sup> IREA CNR, Institute for Electromagnetic Sensing of the Environment,  
Via Bassini 15, 20133 Milano, Italy. email: brivio.pa@irea.cnr.it

<sup>b</sup> IDPA CNR, Via Pasubio 5, 24044 Dalmine (BG), Italy

## ABSTRACT

New opportunities for the assessment of global environmental status and changes are offered from the exploitation of satellite remote sensing data coupled with appropriate geoinformation processing. The assessment of environmental status is generally based on complex models that require large dataset and whose performance depends on expert knowledge and specific tuning. In this paper we propose a synthetic indicator which is evaluated by aggregating the scores of diverse observable factors that reinforce the convergence of anomaly evidence. The factors evaluation and aggregation are framed within Fuzzy Set theory and approximate reasoning methods so as to take into account the uncertainty and incompleteness affecting the collection of factors, the estimation of their importance and the complexity of their interrelationship. The methodology is described and its operational capabilities are shown in the case of Africa using parameters derived from the analysis of rainfall and NOAA-AVHRR GAC NDVI time series data.

**Keywords:** environmental indicator, approximate reasoning, land cover change, continental scale.

## 1 INTRODUCTION

The assessment of environmental status is a very broad term that can hardly be precisely defined without delimiting the context and identifying the perspective from which the issue is approached. For example, environmental assessment can be the impact assessment, i.e. the evaluation of the response of the environment to a driving force, the assessment of the environment conditions in relation to a specific context, e.g by comparison between natural and managed/degraded systems, the assessment of the environment vulnerability to different stressors or the evaluation of environment degradation based on the analysis of land-use land-cover change [1, 2, 3]. In such a wide context, several initiatives have been promoted and methodologies have been developed with the objective of depicting the status of the environment. The choice of the most suited approach is a trade off between the type of information that are to be provided, the users and project's requirements, and the constraints given by data and implementation tool availability.

In the framework of GeoLand, an Integrated Project of the European Union 6<sup>th</sup> Framework Program, the Observatory for Land cover and Forest change (OLF) has to provide information addressing international concerns related to the global environmental protection and global change issues to support EU policies and international conventions such as the UN Forum on Forest (UNFF) and the Convention to Combat Desertification (CCD). The OLF's objective is the development of indicators, based on Earth Observation (EO) data, for environmental status assessment at continental scale on two priority areas, Boreal Eurasia and Africa.

In this context, environment is therefore assumed to refer to the vegetation compartment of the ecosystems, and status is assumed to refer to the conditions of vegetation cover and changes. Note that, although commonly used with a negative meaning, a change is not necessarily an adverse effect on the vegetation cover [3].

Different methodologies for vegetation status assessment have been developed and are currently in use. They include physical approaches describing specific ecosystem characteristics, such as Net Primary Production (NPP) through Light Use Efficiency (LUE) models [4], conceptual models using neural network to analyse specific processes, such as deforestation [5], and multivariate regressive models addressing human and natural interactions [6]. These approaches have predictive capabilities although their application requires the prior knowledge about the phenomena, the independent and predicted variables must be known and measured, and application is mainly at local and regional levels where the ecosystems are better understood and models can be tuned to the specific conditions.



The understanding and quantification of the nature of land-use/cover change at global and continental scale and its impacts on the environment can be formalised by complex models that, due to the interdisciplinary character of the dynamics involved, require a large set of data which are difficult to collect continuously on the long term especially over large areas. For these reasons it is increasingly hard to develop and implement continental and global models.

Environmental indicators can overcome these limitations by providing a synthetic picture of the phenomena under analysis. An environmental indicator can be defined as a mean devised to reduce a large quantity of data to its simplest form, retaining essential meaning of the questions that are being asked for the data, and supplying simplified information about complex system, or not easy measurable criteria [7].

Moreover, Earth Observation (EO) systems partially solve the issue related to the availability of datasets over large areas and long periods of time. Long-term EO data can be exploited for monitoring the vegetation compound thus retrieving useful information on the status of the environment. Yet the data made available by satellite imagery analyses have to be interpreted and integrated in order to synthetically describe the conditions of the environment. An example of this type of analysis is the vegetation conditions indicator which integrates in a multivariate regression two contributing factors derived from NOAA-AVHRR NDVI and BT (Brightness Temperature) [8]. The indicator's temporal and spatial trends have been shown to correlate well with ENSO (El Nino/Southern Oscillation) events that strongly affects vegetation conditions.

This paper proposes a new approach based on approximate reasoning techniques [9, 10] that make it possible to integrate a set of contributing factors into a synthetic indicator of anomaly. The contribution of each factor is evaluated through the use of fuzzy score functions and the aggregation is performed by a multi-criteria approach. The objective is the periodic monitoring at continental scale for the identification of alarming conditions: that is, to enhance those areas where the occurrence of events, given the ambient conditions, may determine situations where changes are presently undergoing or are likely to occur in the near future. The anomaly indicator allows the integration of different sources of data (e.g. vegetation conditions and phenology, climate and socio-economic) in order to provide a synthetic picture of the environmental status.

We present the general approach for the development of the anomaly indicator and the preliminary results obtained over Africa using parameters derived from the temporal analysis of NOAA-AVHRR GAC data and rainfall data.

## 2 METHODOLOGY

The basic idea for identifying anomalies at continental scale is to use a multi-criteria integration approach where individual factors contribute to the indicator of anomaly through the concept of reinforcement of evidence brought by each factor in terms of departure from a reference.

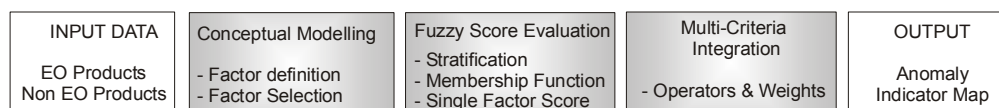
The multi-criteria integration approach can be summarized in the following expression:

$$AI = F(p_1, \dots, p_n, I_1, \dots, I_n) \quad (1)$$

where

- $AI$  is the anomaly indicator, intended as a proxy of the process under analysis and it is the higher-level product derived from multi-criteria integration. The integration of the contributing factors, i.e. the available parameters that interact with the process, is realised with the concept of reinforcement of evidence.
- $F$  is the operator that realises the multi-criteria integration of the contribution of each factor, by means of Ordered Weighted Averaging aggregation (OWA) operators which make it possible to take into account flexible compensations of the judgements [10].
- $p_j$  is a contributing factor, i.e. a variable/parameter, which is relevant for the computation of the synthetic indicator. Its computation is realized in the framework of the fuzzy sets theory [9, 11]: it is a real number in the [0,1] range associated to each elementary unit (usually the pixel) of the area under investigation. This value is not intended as a quantitative measure of a process under analysis, instead it is an evaluation of its contribution in term of anomaly to the multi-criteria integration.
- $I_j$  is the importance associated to each contributing factor.

Figure 1 summarizes the main steps of the proposed methodology which is described in detail in the following sections. The introduction of fuzzy paradigm is suggested by its potential in managing complexity especially for the system with a mathematical model that is difficult to derive. The general experience is that the more complex the problem involved, the greater the superiority of fuzzy methods [12].



**Figure 1.** Block-diagram of the main steps in the proposed methodology for the environmental status assessment.

## 2.1 Conceptual Modelling

The conceptual model behind the proposed methodology is that, whereas a single contributing factor is not sufficient to assess the status of a phenomenon, a synthetic indicator could be generated from several factors combined together to reinforce-weaken this assessment.

Factors contributing to the environmental assessment may include different type of information concerning both physical parameters and socio-economic information of the region. Physical parameters of the ecosystem related to the vegetation phenology, water resources, fire activity, etc. can be derived from satellite observations [13, 14]. Presently several coarse spatial resolution sensors, such as the MODIS, SPOT-Vegetation, NOAA-AVHRR, are available that allow to monitor the status of the environment at continental scale. Among these low resolution EO data, NOAA-AVHRR GAC data with 10 km spatial resolution have been used in this work being the more easily accessible data and covering more than twenty year period. Each factor contributes to the anomaly indicator in terms of the departure of current observation parameter's value from a reference value, usually its long term average. Thus EO products can be used either directly or after a specific processing, that includes:

- temporal syntheses from each pixel's temporal profile (e.g. max and min value over a given period);
- spatial syntheses over an area, fixed grid or polygon, surrounding each pixel (e.g. difference with respect to the land cover class average value);
- a combination of the previous two (e.g. max of the difference with respect to the land cover class mean value).

Although the design of the indicators is open to include expert knowledge (heuristics), if available, this step implies the introduction of a more complex and region-specific model. The integration of this component may definitely improve the accuracy of the results but it may be hardly modelled at continental scale. For this reason the methodology to assess anomaly at continental scale include only observable component or evidences. For example, it is an evidence that the higher the fAPAR (fraction of Absorbed Photosynthetically Active Radiation) the greater the vegetation amount. Hence, the decrease of the seasonal maximum fAPAR with respect to the Long Term (LT) average indicates ecosystem degradation. Although this statement hides a model, no one would argue about its robustness. The anomaly indicator has been conceived on a way that makes use only of these evidence type components: in these terms, the multi-criteria approach can be thought as the co-occurrence of evidences.

## 2.2 Evaluation of fuzzy factor score

The contribution of each factor to the indicator score is described by a fuzzy score function. The choice of a method based on the fuzzy sets theory is driven by its ability to deal with vague and incomplete information as well as the possibility of applying a gradual degree for score extraction instead of crisp value. Indeed in environmental assessment it is more likely to deal with a smooth change between two different conditions rather than an abrupt change [15]. Moreover, fuzzy functions allow the standardization of each factor contribution to the [0-1] range. This step, besides being necessary for the integration of factors derived from various sources, has the advantage to make more understandable to the user the relative contribution of different factors in the overall indicator score.

- *Stratification into homogeneous areas.* The fuzzy membership functions for each contributing factor are defined over homogeneous areas where the factors are assumed to have on average the same behaviour. Over a homogeneous area the factor's variability is assumed to be solely due to changes in the status of the environment and not to be related to the spatial variability of the ecosystem characteristics. The choice of the most suited stratification scheme is an important step since it influences the shape of the factor score function. A possible stratification criterion can be derived from either the WWF eco-regions thematic map [16] or from the intersection of more information layers such as the eco-regions and the land cover map, such as GLC2000 [17].

- *Membership function and factor score.* The score functions are used to map the value of each contributing factor into a fuzzy membership degree, i.e. the factor score. The factor score functions can be derived by following three different approaches: completely data-driven, partially data-driven, user-driven [18]. In the case of the

completely data-driven approach, the factor score functions are defined purely on the basis of the statistical analysis of a set of values assumed by a specific contributing factor. For example if the contributing factor is the difference between the present value and its long term average, its statistical distribution (frequency histogram) shows how the factor behaves on average and which range of values can be assumed as normal. The interpolation of the histogram provides the normality function: values generating scores close to 1 are considered as fully normal, while values with scores close to 0 indicate anomaly. Otherwise a function complementing the interpolation of the histogram means the departure from normality of the observed phenomenon: 0 is not anomalous and 1 is max anomaly. This second type of function is better suited to anomaly analysis. In the other two approaches domain experts have a role in defining membership functions.

### 2.3 Multi-criteria integration

The integration of the contributing factors is performed by an operator that aggregates the fuzzy factor scores into a synthetic indicator score. Aggregation operations on fuzzy sets are operations that combine several fuzzy sets in a desirable manner to produce a single fuzzy set [12].

The proposed integration methodology try to avoid the use of complex models to describe the relationships between the contributing factors and the indicator. Moreover, the integration has been conceived so as to allow the selection of the way in which factor scores are aggregated to obtain a final indicator, as well as the definition of the 'importance' of each contribution. These are concerns related to multi-criteria decision-making (MCDM), a field in which procedures have been established to combine opinions about alternatives associated to different points of view. In particular, fuzzy logic allows decision making with estimated values under incomplete or uncertain information, which is particularly suitable to satisfy the requirements of methodology robustness.

Within this formal framework the Ordered Weighed Averaging (OWA) operators were introduced thus offering a flexible and comprehensive way to define a complete family of integration operators reflecting different attitudes in combining a set of contributing factors [10]. An OWA operator of dimension  $n$  is a function  $F: \mathbb{R}^n \rightarrow \mathbb{R}$ , that has associated a set of weights  $(w_1, \dots, w_n)$ , so that  $w_i \in [0, 1]$  and  $\sum_{i=1}^n w_i = 1$ , and is defined to aggregate a list of values  $(p_1, \dots, p_n)$  according to the following expression,

$$F = \sum_{j=1}^n w_j b_j \quad (2)$$

where  $b_j$  is the  $j$ -th largest (or more important) element of the set  $(p_1, \dots, p_n)$ . By changing the definition of the weighting vector the aggregation operator changes as well, i.e. the purpose of weights is to allow distinguishing the different OWA operators. Particular cases of OWA are the OR and AND connectives, as well as the traditional arithmetic mean, so that exact approaches are limiting cases of fuzzy approaches.

The definition of the weighting vector can be accomplished by either exploiting a learning mechanism or trying to assign some semantics or meaning to the weights, such as in the area of quantifier guided applications [10]. In fact, the OWA operators have been used to implement the concept of fuzzy majority in the aggregation phase of fuzzy criteria by means of a fuzzy linguistic quantifier [19] which indicates the proportion of criteria 'necessary for a good solution' [20]. Furthermore, the calculation of the weighting vector can also take into account the importance  $I_i$  attributed to each considered factor, that shouldn't be confused with the weights  $w_i$  of an OWA operator. It is also interesting to note that it is often difficult to specify the values of importance by exact numbers in  $[0, 1]$ ; it would be more natural to specify them either in a linguistic form with the use of qualifiers such as *important*, *very important*, *fairly important*, etc. or by the aid of a graphic representation such as by moving a cursor on a bar or by selecting a grey level on a scale. It has been shown that it is possible to create mapping functions that transform linguistic labels of importance into real values in  $[0, 1]$  and vice-versa.

The adoption of the above described formal framework allows to implement a software environment in which it is possible to select different aggregation operators and obtain therefore different results which can be compared and validated and to attribute relative importance to the contributing factors.

## 3 AN ANOMALY INDICATOR FOR AFRICA

The approach described above has been applied to derive an anomaly indicator for the African continent. Since the work has been developed in the framework of the Geoland-OLF project, the application example presented in the following paragraphs exploits the dataset made available in the context of the project. The anomaly indicator is based on the integration of contributing factors that describe the anomaly of the phenology of the vegetation (start,

peak and length of the vegetative season) and the amount of rainfall occurred during the season. The variables describing the phenology were derived from the analysis of the AVHRR-GAC NDVI temporal profiles as follows:

- Start of apparent growing season ( $f_{start}$ ): the inflexion point of the portion of the NDVI temporal profile that shows an increasing trend from the minimum value. Mathematically the inflexion point is derived as the maximum of the first derivative of the interpolated (piece-wise logistic) NDVI curve [21].
- Date of the peak of the growing season ( $f_{date}$ ): the maximum NDVI value observed during the season.
- Duration of the growing season ( $f_{length}$ ): the time difference between the end and the start of the growing season. The end of the growing season is identified as the time, occurring after the season's peak, when NDVI value reaches a threshold established as a fraction of the difference between the minimum and the maximum values.

Specifically for the example presented here, the phenology variables refer to the last observation preceding the time for which the anomaly indicator is computed.

The cumulated rainfall is computed from the ten-day rainfall data of the Famine Early Warning System Network (FEWS-NET) Meteosat Rainfall Estimation (RFE) dataset. The ten-day rainfall estimates are cumulated over the preceding 12 months.

The anomaly of each contributing factor is derived as the difference between the current and the long-term average values. The phenology and rainfall long term averages were derived from the available historical datasets: 1981-2002 and 1996-2002, respectively.

The GLC2000 land cover map is used to segment the African continent into homogeneous areas: for each land cover class the historical dataset is used to derive the score function. The score anomaly function is derived by a completely data-driven approach, by using the complement of the curve that best interpolates the frequency distribution. Based on the available dataset, the curve found to best interpolate the frequency data was the so-called generalized bell function (Eq. 3) applied to each side of the histogram. The breakout point has been chosen as the data value corresponding to the maximum frequency.

$$f(x) = \frac{1}{1 + \left(\frac{x - \beta}{\delta}\right)^p} \quad \text{if } x > \beta \text{ and } x < -\beta \quad (\beta > 0) \quad ; \quad f(x) = 1 \text{ otherwise} \quad (3)$$

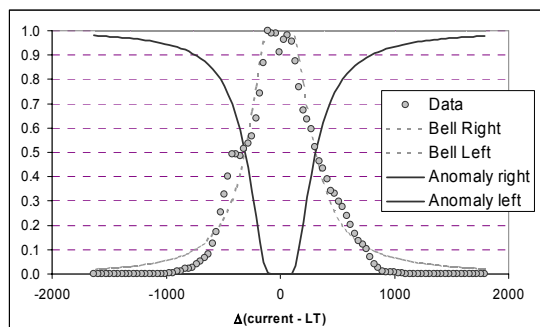
The value of the parameter  $\beta$  is chosen a priori (e.g.  $\beta=100$ ) whereas  $\delta$  and  $p$  are obtained by least square minimization. This function has also been chosen because it is characterised by an asymptotic behaviour that well represents the least anomaly that characterises the values surrounding the frequency peak. An anomaly score equal to 0 is assigned to a range of contributing factor values around the peak value, rather than to the unique most frequent value. Moreover, this formalisation of the score function allows the selection of asymmetric right and left interval around the breakout point to identify the asymptotic range of values (e.g. score=1 if  $\alpha < \text{factor} < \beta$ , where  $\alpha \neq \beta$ ). Finally, the separation into right and left side allows the interpolation of the same type of function although with different parameter values thus taking into account a further level of asymmetry.

Figure 2 shows the histogram (circle markers), the interpolation curve (dotted light grey line) and the anomaly score function (black line) for the rainfall contributing factor. Before interpolation, the frequency values are rescaled between 0 and 1 so that the maximum frequency corresponds to 1 (normality) and the least frequent class to 0 (least frequent cases far from the normal behaviour). The interpolation curve represents the *normal* behaviour based on the underlying assumption that the most frequent cases are the normal ones.

The anomalies of each contributing factor was computed for the last ten-day period of each year from 1996 to 2002 so that the aggregated indicator would represent a synthetic picture of the current year. The anomalies of each contributing factor were aggregated into the Anomaly Indicator ( $AI$ ) by applying the arithmetic mean operator:

$$AI = \frac{1}{n} \sum_{i=1, n} p_i = \frac{(f_{start} + f_{rain} + f_{date} + f_{length})}{n} \quad (4)$$

where  $n = 4$ , since only four contributing factors ( $p_i$ ) are available and factors are assumed to be equally important ( $I_i=1$  for any  $i$ ).

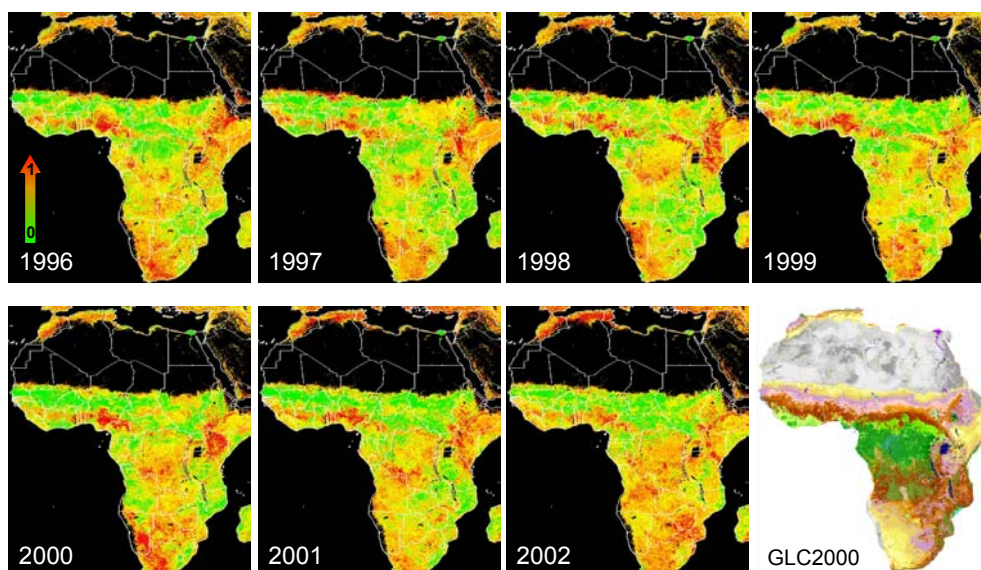


**Figure 2.** The score function derived for the rainfall contributing factor for the Degraded Evergreen Lowland Forest class (source: GLC2000). The x-axes represents the values of the contributing factor ( $\Delta$  = current value of cumulated rainfall - long term average cumulated rainfall).

#### 4 ANALYSIS OF THE RESULTS

Figure 3 shows, as an example, the *AI* derived for the last ten-day period of each year from 1996 to 2002. The red areas highlight the most anomalous regions where changes are likely occurring. The ocean, the inland water basins and deserts have been masked out and therefore appear as the black regions.

The *AI* maps highlight a high inter-annual variability although some constant patterns are clearly visible. The Horn of Africa, Southern Africa and the Sahelian region South of Chad are characterized by a highly anomalous behaviour through the 1996-2002 period.



**Figure 3.** Anomaly Indicator for Africa. The indicator is derived as the average value of the fuzzy scores of the contributing factors. GL2000 map [17] used for the stratification is also shown.

The high and persistent anomaly over East Africa shown by our results is in agreement with the occurrence of several years of below-normal rainfalls that affected this region at the end of the last century. Some region experienced prolonged drought beginning in 1998 and beyond 2001 [22].

The African Sahelian region also is characterised by some persistent patterns of high anomaly that could be due to prolonged dry episodes. Progressive desertification is addressed as the explanation of the drought episodes that have been occurring in this region of Africa where the reduction of rainfall is apparently strongly correlated with human activity [23]. In this specific case the information brought by the *AI* could be integrated with information on the human activity such as grazing (overgrazing) and land cover conversion (from natural to agricultural land).



Our results also show high *AI* values over central Africa, in the forest domain. The inspection of the NDVI temporal signal highlighted a low seasonality (high S/N) of the vegetation that might have affected the accuracy of the phenology parameters' estimates. It is probable that for this specific ecosystem a different set of contributing factors should be chosen to perform environmental status assessment.

The type of indicator proposed in this work could be also correlated with ENSO events that strongly affects the conditions of the environment. For example, during El-Nino years Southern Africa generally receives below-normal rainfall whereas La-Nina years brings above-normal rainfall regimes. Yet during the 1997-98 El-Nino event, which was the strongest on record, not all of South Africa received below-normal rainfall. In fact our results show that 1997 and 1998 were not the most anomalous years despite the occurrence of El-Nino. Therefore attention should be paid when drawing conclusion about the correlation between the climate-related events and the conditions of the vegetation.

Although comparison with independent datasets is necessary, the continental scale of analysis and the synthetic character of the anomaly indicator make this exercise hardly feasible. In fact most of the analysis of anomalous behaviour performed at continental and/or global scales concerns the quantification of the anomaly of a single meteorological parameter such as sea surface temperature and rainfall. It is therefore difficult to compare a synthetic (i.e. integrated) indicator with a single parameter.

However, a first comparison could be attempted with the Vegetation Condition Index (VCI) developed by [8]. Figure 4 shows a zoom over the Horn of Africa for which the VCI was available on the NOAA-NESDIS web site (<http://www.orbit.nesdis.noaa.gov/smcd/emb/vci/index.html>) and it compares it with *AI* derived for 2000 and 2001. Since the *AI* is a synthetic indicator, that depicts a synthetic picture of the events occurred during the whole year, we assumed that it could be in first approximation comparable to the VCI maps derived by [8] for the vegetation growth season of the region under analysis. Both of the panels in figure 4 show that the patterns of stressed vegetation conditions (yellow circle at the centre of the figure) are highlighted by a high anomaly of our indicator. A more exhaustive comparison is difficult to perform mainly due to time lag between the datasets and the lack of ground truth datasets.

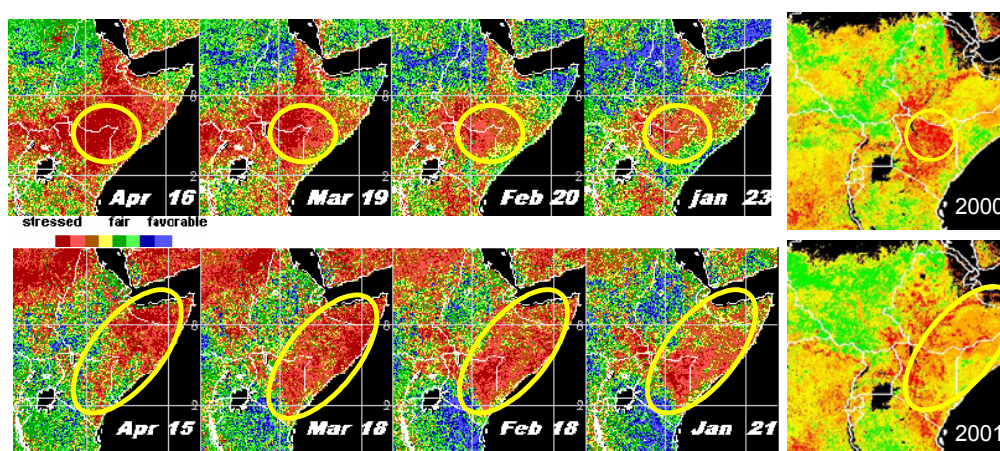


Figure 4. Comparison between VCI maps and Anomaly Indicator maps for the Horn of Africa.

## 5 CONCLUSIONS

We propose an innovative approach to derive an anomaly indicator for environmental status assessment. The methodology is based on the integration of the anomaly of a set of contributing factors; the anomaly is derived from fuzzy score functions extracted from the analysis of the historical dataset. The integration of each factor's anomaly can also be performed by exploiting the advantages offered by fuzzy set theory when dealing with uncertain data.

The proposed approach is suited for global/continental analyses and it has been applied to derive an anomaly indicator over the African continent for the period 1996-2002. For its nature it becomes hardly feasible a validation exercise due to the lack of independent datasets at the appropriate scale.

Since validation and even a comparison to other datasets is difficult to be performed, the strength of the anomaly indicator proposed here mainly derives from the methodological approach. The anomaly indicator is definitely an improvement over previous approaches because it faces the uncertainty involved in environmental

status assessment by exploiting the fuzzy set theory. Moreover, the general scheme of the proposed methodology allows the integration of datasets derived from different sources. A clear example could be the case of desertification where the anomaly indicator could easily accommodate socio-economic data, besides taking into account the vegetation's conditions and the rainfall patterns that highlight the occurrence of drought.

## ACKNOWLEDGMENTS

This work has been carried out within the Observatory for Land cover and Forest change (OLF) of GeoLand, an Integrated Project of European Commission FP-6. Geoland is carried out in the context of GMES (Global Monitoring for Environment and Security).

## REFERENCES

- [1] PYKH, Y.A., KENNEDY, E.T., AND GRANT, W.E., 2000: An overview of systems analysis methods in delineating environmental quality indices. *Ecological Modelling* 130, pp. 25-38.
- [2] TRAN, L.T., KNIGHT, C.G., O'NEILL, R.V., SMITH E.R., RIITTERS, K.H., AND WICKHAM, J., 2002: Environmental Assessment Fuzzy Decision Analysis for Integrated Environmental Vulnerability Assessment of the Mid-Atlantic Region, *Environmental Management* 29, pp. 845-859.
- [3] LAMBIN, E.R., GEIST, H.J., AND LEPERS, E., 2003: Dynamics of Land-Use and Land-Cover Change in Tropical Regions, *Annu. Rev. Environ. Resour.* 28, pp. 205-241.
- [4] SEAQUIST, J.W., OLSSON, L., AND ARDOE, J., 2003: A remote sensing-based primary production model for grassland biomes. *Ecological Modelling* 169, pp. 131-155.
- [5] MAS, J.F., PUIG, H., PALACIO, J.L., AND A. SOSA-LOPEZ, A., 2004: Modelling deforestation using GIS and artificial neural networks. *Environmental Modelling & Software* 19, pp. 461-471.
- [6] MAERTENS, B., AND LAMBIN, E.F., 1997: Spatial modelling of deforestation in southern Cameroon; spatial disaggregation of diverse deforestation processes. *Applied Geography* 17(2), pp. 143-162.
- [7] OTT, W.R., 1978: Environmental indices: theory and practice. Ann Arbor, MI.
- [8] KOGAN, F.N., 2000: Satellite-Observed Sensitivity of World Land Ecosystems to El Nino/La Nina. *Remote Sensing of Environment* 74, pp. 445-462.
- [9] ZADEH, L.A., 1965: Fuzzy sets. *Information and Control* 8, pp. 338-353.
- [10] YAGER, R.R., 1988: On ordered weighted averaging aggregation operators in multi-criteria decision making, *IEEE Trans. Systems, Man and Cybernetics* 18, pp. 183-190.
- [11] ZADEH, L.A., 1975: The concept of a linguistic variable and its application to approximate reasoning, parts I, II. *Information Science* 8, pp. 199-249, pp. 301-357.
- [12] KLIR, G. J., AND YUAN, B., 1995: Fuzzy Sets and Fuzzy Logic: Theory and Applications. Prentice-Hall, Upper Saddle River, NJ.
- [13] TUCKER, C. J., AND CHOUDURY, B. J., 1987: Satellite remote sensing of drought conditions. *Remote Sensing of Environment* 23, pp. 243-251.
- [14] LEVINE, J.S., 1996: Biomass burning and global change. MIT Press, Cambridge, Massachusetts.
- [15] BURROUGH, P.A., 1996: Natural objects with indeterminate boundaries. In: Burrough P.A. and Frank A.U. (eds.): Geographic objects with indeterminate boundaries, pp. 3-28. Taylor and Francis, London.
- [16] OLSON, D. M., AND DINERSTEIN, E., 1998: The Global 200: a representation approach to conserving the Earth's most biologically valuable ecoregions. *Conservation Biology* 16, pp. 502-515.
- [17] BARTHOLOMÉ, E., AND BELWARD, A.S., 2005: GLC2000: a new approach to global land cover mapping from Earth observation data. *Int. J. Remote Sensing* 26 (9), pp. 1959-1977.
- [18] ROBINSON, P.B., 2003: A perspective on the fundamentals of Fuzzy Sets and their use in Geographic Information Systems. *Transactions in GIS* 7(1), pp. 3-30.
- [19] ZADEH, L.A., 1983: A computational approach to fuzzy quantifiers in natural languages. *Computers and Mathematics with Applications* 9, pp. 149-184.
- [20] YAGER, R.R., 1996: Quantifier guided aggregation using OWA operators. *Int. J. Intell. Systems* 11, pp. 49-73.
- [21] ZHANG, X., FRIEDL, M.A., SCHAAF, C.B., STRAHLER, A.H., HODGES, J.C.F., GAO, F., REED B.C., AND HUETE, A., 2003: Monitoring vegetation phenology using MODIS. *Remote Sensing of Environment* 84, pp. 471-475.
- [22] WMO, 2001: Unusual floods and droughts in East Africa. *World Climate News* 19, pp. 3-4.
- [23] CHARNEY, J.G., QUIRK, W.J., CHOW, S.H. AND KORNFIELD, J., 1977: A comparative study of the effects of albedo change on droughts in semi-arid regions. *J. Atmospheric Sciences* 34, pp. 1366-1385.

# How certain is desiccation in the west African Sahel?

A. Chappell<sup>a</sup> and C.T. Agnew<sup>b</sup>

<sup>a</sup> Centre for Environmental Systems Analysis, University of Salford, Manchester, UK,  
email: a.chappell@salford.ac.uk

<sup>b</sup> School of Environment and Development, University of Manchester, Manchester, UK

## ABSTRACT

For well over three decades controversy has surrounded the characteristics of environmental change and environmental degradation. One reason for this prolonged debate is that there has been no assessment of uncertainty in previous Sahelian rainfall work. We used data from the Global Historical Climatology Network to provide an assessment of spatial uncertainty of summer rainfall between 1930 and 1990. Stochastic simulations prioritised the reproduction of global features and statistics over local accuracy to provide a complete assessment of uncertainty. The series of realisations were post-processed and the uncertainty information summarised using the mean per pixel of all realisations and the variance of the conditional distribution of the realisations. The probability of exceeding rainfall was calculated for 200 mm and 500 mm. Denormalised area-weighted rainfall anomalies showed the characteristic decrease in rainfall between the late 1960s and 1990. The annual estimates of the minima and maxima of the simulated rainfall provided a range of possible values for the areal annual rainfall that considerably reduced certainty in that pattern. The maps of spatial uncertainty demonstrated that there was considerable heterogeneity across the region which could not reasonably be estimated by a single areal annual value. Furthermore, the threshold of 200 mm was a very poor approximation of the boundary between the Sahara and the Sahel and that of 500 mm did not adequately represent the boundary of agricultural production. The estimation of spatial uncertainty robustly questioned the methodology used to calculate rainfall anomalies and the assumptions for the use of simple isoline thresholds.

**Keywords:** West African Sahel Rainfall; Geostatistics; Sequential Indicator Simulation; Spatial Uncertainty; Desiccation; Rain-fed agriculture; Sahara desert.

## 1 INTRODUCTION

The summer of 2005 drew world attention to the plight of inhabitants in the West African Sahel (WAS) region of West Africa due to famine, drought and locusts. The FAO and UNICEF reported that in Niger alone some three million people were likely to be affected. Drought related tragedies have been reported several times during the 20<sup>th</sup> Century and the characteristics of environmental change and environmental degradation in the Sahel have been the focus of scientific interest for well over three decades. Controversy has surrounded the scientific work due to natural environmental variability, the paucity of data, misunderstanding of resilience, and institutional facts [1]. Many of the accounts of environmental change have been challenged and new positions adopted. Examples include possible interactions between climate and land cover changes [2],[3]; the relationships between droughts and human activity [4],[5] and increasing desiccation as presented by an expanding Sahara [6],[7],[8],[9]. Such studies have led to recognition that the Sahel is environmentally heterogeneous despite significant sources such as [10] and IPCC [11] portraying the Sahel as a region. The Sahel is a complex mosaic of environments and human activities [12]. Climatologists have also noted the diversity and variability of the Sahelian environment [13] yet the paradigm of widespread persistent drought and desiccation is so well established [14] that few question local variations nor the quality of the data used. This is in stark contrast to the work of ecologists, geomorphologists, and others who have challenged the views of Sahelian environmental change established earlier in the 20<sup>th</sup> Century [15],[16],[17].

There is little support for those whose work questions or offer alternative explanations, as forcibly stated in a paper [18] entitled 'The recent Sahel drought is real'. The paradigm is well established and reinforced by possible explanations of the drying trend. However, drought (a short term, severe reduction in precipitation) is commonly expected in semi-arid regions such as the Sahel whereas desiccation (a long term reduction in precipitation) is an element of climate change which requires an examination of precipitation trends e.g., [19],[13],[20]. Desiccation between the late 1960s and 1990 is explained by comparing empirical evidence or model predictions against 'observations' of Sahelian rainfall e.g., [21],[22]. However, the outcomes of testing these hypotheses are based upon the assumption that aggregated rainfall observations represent the underlying population despite limitations of the observation network and variability in rainfall. Despite consideration of local interpolation errors [23] and



spatial and temporal sampling patterns on the estimation of aggregated climatological variables e.g., [24],[25] there has been no assessment of uncertainty in previous Sahelian precipitation work. Here we provide an assessment of spatial uncertainty between 1930 and 1990. The analyses provide uncertainty about temporal variation of areal rainfall in the region but this is not the main focus. Instead, we consider in detail the spatial variation of the rainfall, its variation and the probability of exceeding thresholds set at 200 mm as an approximation for the edge of the Sahara [8] and at 500 mm as an approximation for the region of rain-fed agriculture [26].

## 2 DATA AND METHODS

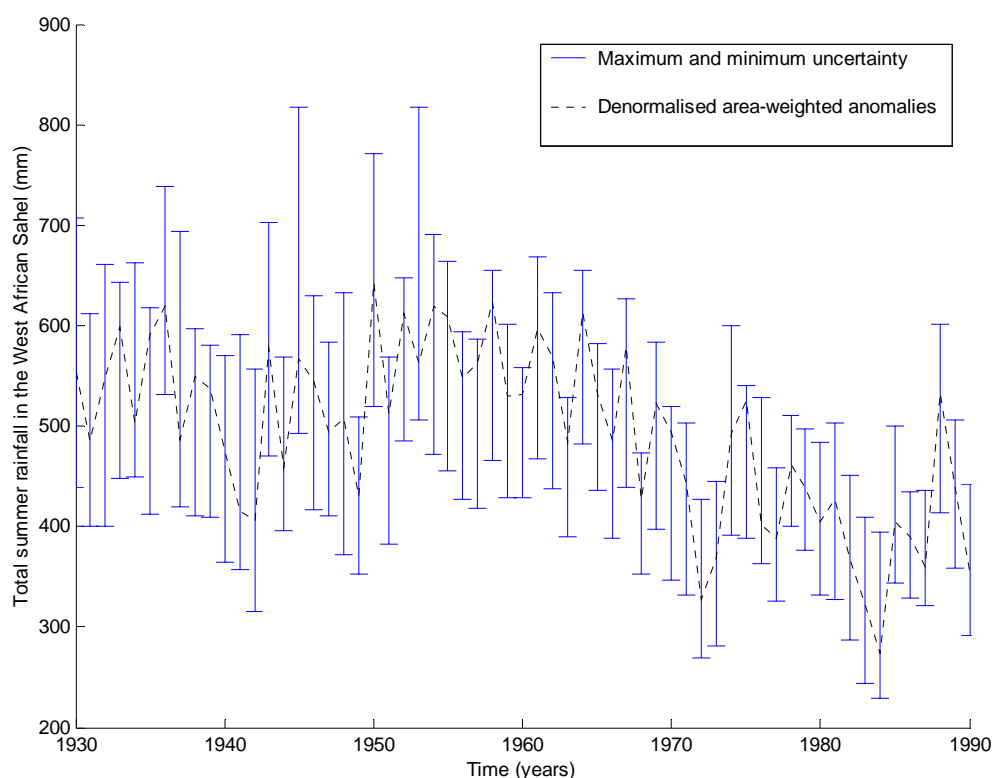
We used the Global Historical Climatology Network (GHCN) v.2 rainfall data [27] and extracted rainfall stations for the years between 1930 to 1990 inclusively, within the west African Sahel (WAS) following the definition of Nicholson [28; 10-20°N, -20°W to 20°E]. Stations locations recorded using latitude and longitude were converted to an equal-area projection using the unit circle. We calculated the total northern hemisphere summer (June, July, August and September) annual rainfall. Therefore, all stations with summer monthly data for a year were extracted from the database. In addition, rainfall anomalies were calculated using the accepted method [29] and the area-weighting scheme [30]. A reference period of 1961 to 1990 was set to achieve the maximum number of stations with the minimum amount of missing data (29%).

Unlike local interpolation algorithms (including kriging) stochastic simulation prioritises the reproduction of global features (texture) and statistics (histogram, covariance etc.) over local accuracy and provides a complete assessment of error or uncertainty [31]. It has been used to good effect in other environmental applications e.g., [32],[33]. Sequential indicator simulation was used here to generate 300 maps or realisations of rainfall and honour the values of the rainfall stations each year, reproduce the declustered sample histogram and reproduce the covariance models for four thresholds (10%, 25%, 75%, 90%) using the mosaic model [34] and the median indicator approximation [31]. The spatial structure of the median indicator rainfall data was calculated using experimental isotropic semi-variograms [35]. The variograms were fitted with several authorised models using non-linear weighted least squares and the model that fitted best, in the least-squares sense, was selected. The west African Sahel was discretised into a grid with 3500 nodes (100 x 35) which was approximately 0.3° and 0.4° in latitude and longitude, respectively. The series of realisations were post-processed and the uncertainty information summarised using the mean per pixel of all realisations and the variance of the conditional distribution of the realisations. In addition, the probability of exceeding rainfall was calculated for two thresholds. The first was set at 200 mm [8] as an approximation for the edge of the Sahara in their experiment to detect expansion and contraction of the desert. The second was set at 500 mm because it was believed [26] to approximately identify the region of rain-fed agriculture. Maps were selected for the years 1935, 1945, 1955, 1965, 1975 and 1985. The minimum and maximum values of the realisation means for every year between 1930 and 1990 were also plotted over time to provide a conservative estimate of uncertainty.

## 3 RESULTS

The rainfall anomalies for each year of data were area-weighted and then denormalised by adding 493 mm, the long-term summer rainfall (Figure 1). The denormalised area-weighted rainfall anomalies (DARA) show the characteristic decrease in rainfall between the late 1960s and 1990. The annual estimates of the minima and maxima of the simulated rainfall are also shown in figure 1. Notably, the uncertainty decreases over time and contributes to the appearance of decreasing rainfall over time. However, this appearance is exaggerated with the inclusion of the drought years of 1972-1973 and 1983-1984 within the context of dessication. With the exception of these years the uncertainty estimates between the late 1960s and 1990 overlap considerably with those of the wet phase in the 1950s and early 1960s and those of the dry phase in the 1940s.

The maps of the per pixel realisations average of summer rainfall for the region are shown every ten years between 1935 and 1985 in figure 2 (a-f). The pattern of rainfall for these years is similar. An area of large rainfall exists in the southwest. Notably, that area extends no further east than the border of Guinea. Two other areas of consistently large rainfall are found in the south-eastern portion of the region (Nigeria, Cameroon and Chad) and over central Niger. Notably, there is a belt of relatively small rainfall that extends from the coast across the region but which terminates at approximately the border with Chad. The low rainfall belt is more or less pronounced in each of the maps and is notably extensive during 1985.

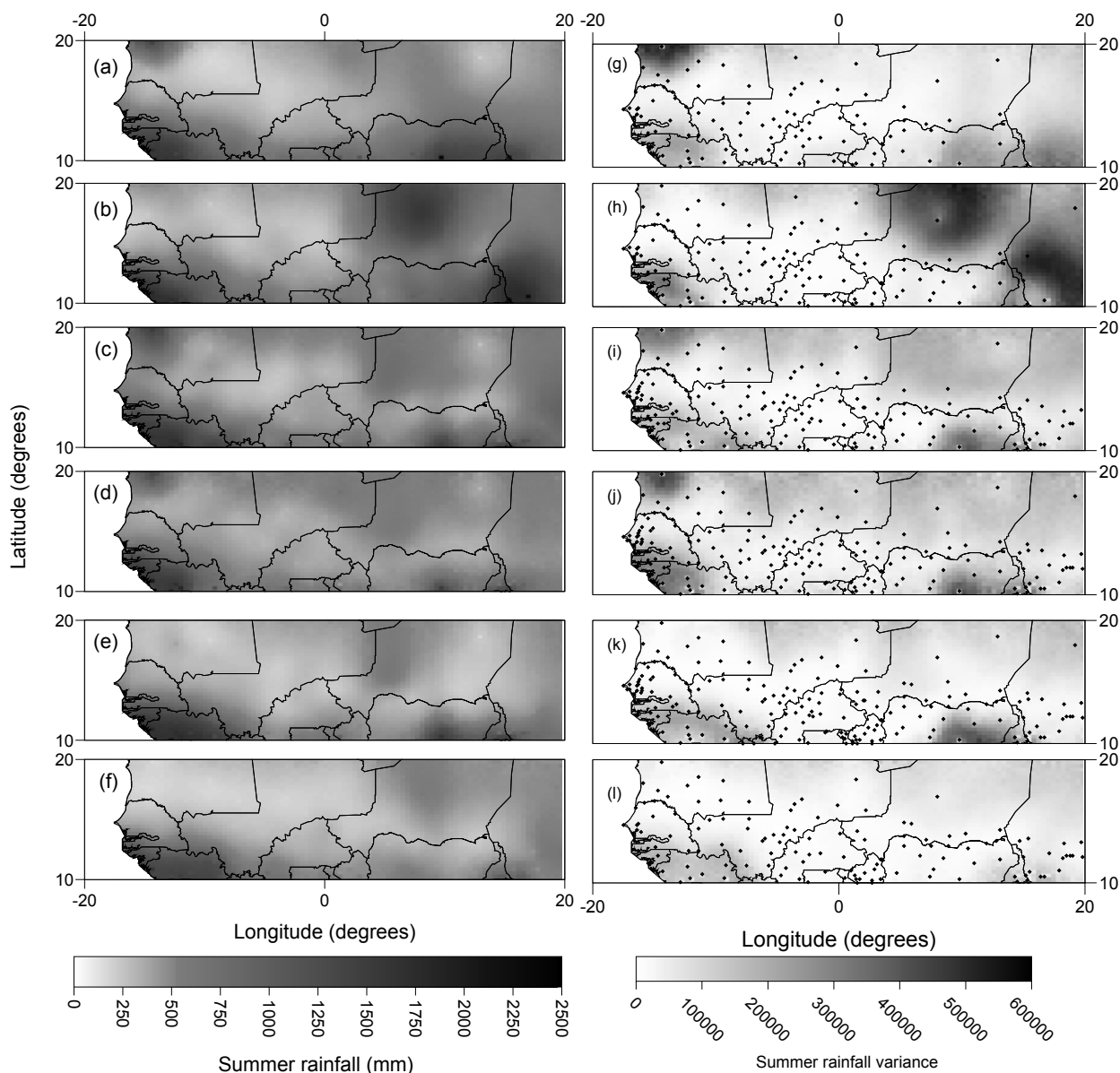


**Figure 1.** Annual variation in summer rainfall for selected stations using the denormalised area-weighted anomalies (--) and the minima and maxima of the 300 averages of the simulation realizations.

The maps of per pixel conditional variance (Figure 2g-l) reveal that those areas of large rainfall previously identified are highly variable in the simulation realisation which suggests that there is considerable uncertainty in the rainfall estimates. Notably, the area adjacent to the Sahara, particularly in northern Mali and Niger, has variances in the estimates that are larger than the majority of the region. The speckled nature of the variance maps is caused by the highly spatially variable nature of the variance.

The maps of the per pixel probability of exceeding the 200 mm and 500 mm threshold of summer rainfall for the region are shown every ten years between 1935 and 1985 in figure 3. Darker shades indicate a tendency to exceed the threshold whilst lighter shades indicate that the threshold is unlikely to be exceeded. As one might expect, the majority of the region has dark shades because of the increased likelihood that each pixel will exceed the 200 mm threshold of summer rainfall (Figure 3a-f). However, the pattern does not produce the typical isoline close to the northern boundary of the region. Instead, clusters of lighter shades are identified where parts of several countries have not exceeded the threshold. Notably, in 1985 a large part of the western portion of the region has light shades but the eastern part of the region is expected to exceed the threshold. The speckled nature of the dark regions is caused by the rainfall values at the rainfall stations that have been retained in the maps.

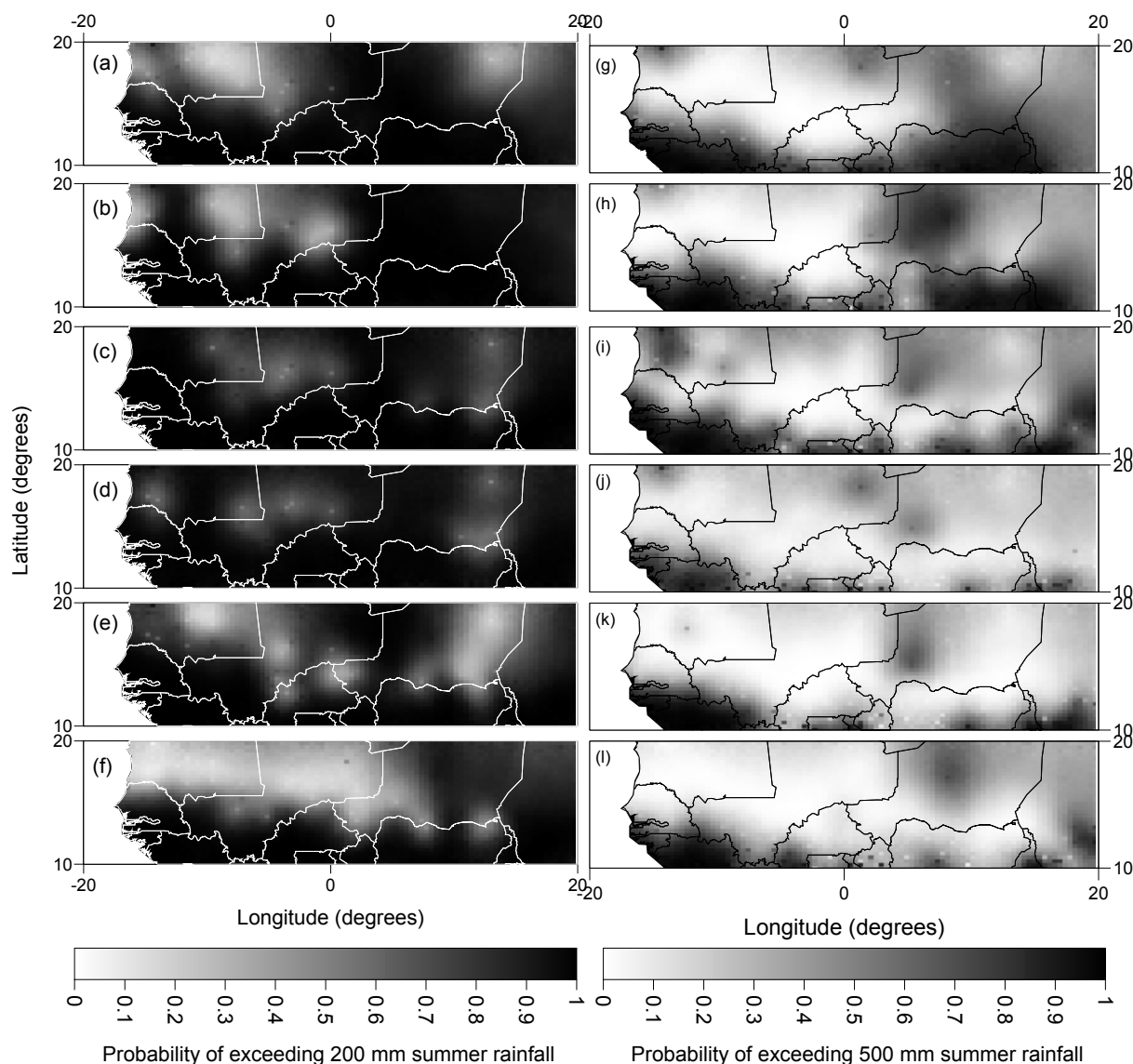
In 1935, 1945 and to a less extent 1955, the areas of the region that exceed the 500 mm threshold of summer rainfall are similar. Large values are found in the lower latitudes of the region including southern Senegal, Mali and Burkina Faso and the border between Nigeria and Niger. In addition, central and northern parts of Mali, Niger and Chad show medium valued clusters that are persistent during these years. In years 1965, 1975 and 1985 the area of the region covered by darker shades has visibly decreased and generally only clusters in the most southern latitudes exceed the 500 mm threshold. However, there also remain a few clusters in central and northern Niger, northern Mali and Chad that exceed the 500 mm threshold.



**Figure 2.** Maps of the per pixel (approximately 0.3° and 0.4° in latitude and longitude, respectively) average of the 300 realisations (a-f) and the variance for the conditional distributions (g-l) of summer rainfall in the West African Sahel for the years of 1935, 1945, 1955, 1965, 1975 and 1985, respectively. The rainfall stations (•) and the political boundaries for countries of the region are also shown.

#### 4 DISCUSSION

The denormalised area-weighted rainfall anomalies (DARA) are commonly used to aggregate observations from across the west African Sahel. A decrease in the anomalies between the late 1960s and 1990 is widely accepted as evidence for a drying trend or desiccation in the region. Unfortunately, the DARA contain no estimate of uncertainty. This is because there is little difference in the temporal pattern between local interpolators or as a result of sampling effects such as the number of stations selected for the aggregation procedure. However, the simulation technique demonstrated that there could be considerable variation in the spatial pattern of rainfall for a given year whilst constrained by global characteristics including, amongst other things, the rainfall measurements. Consequently, the large variation each year between the minimum and maximum values of the simulations considerably reduces the certainty of desiccation in the region. The removal of drought years 1972-1973 and 1983-1984 from the temporal trend makes it easier to appreciate that uncertainty.



**Figure 3.** Maps of the probability that the summer rainfall at each pixel (approximately  $0.3^\circ$  and  $0.4^\circ$  in latitude and longitude, respectively) in the West African Sahel will exceed the threshold at 200 mm (a-f) and at 500 mm (g-l) for the years of 1935, 1945, 1955, 1965, 1975 and 1985, respectively. The political boundaries for countries of the region are also shown.

The source of the variability in the estimate of annual rainfall for the region is contained in the maps of spatial uncertainty. The mean and the conditional variance per pixel for the 300 realisations provide an estimate of that variation. The heterogeneity of the region is evident from the average of the realisations and makes it difficult to appreciate how a single value can reliably estimate that variation. Furthermore, the maps of the per pixel average of the realisations provide only one representation of the spatial pattern of rainfall across the region. The per pixel variance maps show that there is considerable variation in the realisations. The spatial uncertainty is different each year but there are consistently occurring patterns. For example, there is consistently large uncertainty in the lowest and highest latitudes of the region and a belt of small uncertainty that stretches through the central portion of the region. There is considerable uncertainty in the south-west coastal region and in northern Nigeria around the Jos Plateau. The results identify a considerable source of variation that exceeds that of local interpolation errors and sampling effects. That source appears to be highly spatially variable and suggests that the rainfall pattern across the region does have broad bands but also contains considerable clustering.

The per pixel mean maps consistently show larger amounts of annual rainfall along the edge of the Sahara than in a central belt across the region. This is somewhat surprising since rainfall is expected to decrease north across the region. This is the basis for the use of  $200 \text{ mm year}^{-1}$  isoline as an approximation for the boundary between the Sahara zone and the Sahel [8]. However, the annual maps for the probability of exceeding that threshold

substantiate the pattern detected in the maps of the per pixel mean. The probability maps show distinct clusters of areas that are unlikely to exceed this threshold. Only in 1985 is there a tendency for a strong latitudinal gradient to exist and even this does not extend across the entire region. There appears to be little evidence that this threshold can be used to identify the boundary between the Sahara and the Sahel. However, there is some support for the use of 500 mm as a threshold that identifies a distinct boundary, that of rain-fed agriculture [26]. The main exception appears to be the consistent occurrence of an area over central and northern Niger that exceeds the threshold. Results suggest that the boundary is at its most northern extent in years 1935 and 1945. It appears to be confined to the most southerly latitudes during the years 1955, 1965, 1975 and 1985. The speckled nature of the maps is caused by the simulations honouring the values of the rainfall observations. The probability maps suggest that the use of boundaries based on isolines formed from locally optimal maps are simplistic and hide a considerable amount of variation and uncertainty.

## 5 CONCLUSION

The denormalised area-weighted rainfall anomalies for the west African Sahel no longer provide unequivocal evidence of the drying trend or desiccation between the late 1960s and 1990. Stochastic simulations provided a range of possible values for the areal annual rainfall that considerably reduced certainty in that pattern. The estimation of uncertainty renders inconclusive previous comparisons between rainfall anomalies and empirical evidence from related variables (e.g., dust) and model-based predictions.

The maps of spatial uncertainty demonstrate that there is considerable heterogeneity across the region which cannot reasonably be estimated by a single areal mean value that is conventionally used. It is likely that the expectation of being able to estimate rainfall across the region in this manner has reduced the importance of uncertainty. Reconsideration of its importance for the aggregation of climate observations may make an important contribution to temporal and spatial patterns in this region and others around the globe. Spatial uncertainty was also expressed as the probability of exceeding thresholds at 200 mm and 500 mm. The results showed that the former threshold was a very poor approximation of the boundary between the Sahara and the Sahel. Evidently, there is a much more complex relationship than was previously recognised between rainfall and vegetation in the detection of the edge of the Sahara desert. At 500 mm there appeared to be a much stronger boundary. However, its position in years 1955, 1965, 1975 and 1985, well south of the border between Nigeria and Niger, suggests that agricultural production during that period was barely viable. On the contrary, these years are quite wet and instead it is likely that a simple threshold does not adequately represent the complex spatial heterogeneity of the region nor the complexity of rain-fed agriculture.

Challenging the drying trend and the use of simplistic thresholds in the west African Sahel may appear wholly negative with the intention of undermining for example, the ability to better understand the complexity of agriculture or climate systems. However, the absence of critical checks and perspectives allow assumptions and simplifications to go unchallenged and so widely accepted that they become immutable and very difficult to contest. Faced with this situation with respect to west African Sahel rainfall the estimation of spatial uncertainty has robustly questioned the methodology used to calculate rainfall anomalies and the assumptions for the use of simple thresholds.

## ACKNOWLEDGMENTS

We are grateful to NCAR for hosting the provision of the GHCN v.2 data and to Dr. M. Ekström for numerous useful discussions. However, any shortcomings of the manuscript remain the responsibility of the authors.

## REFERENCES

- [1] AGNEW, C.T., 1995: Desertification, drought and development in the Sahel. In: Binns, A.(ed.): People and Environment in Africa, pp.137-49. John Wiley & Sons, Chichester.
- [2] HULME, M. AND KELLY, M., 1993: Desertification and Climate Change. *Environment* 35(6):39-45
- [3] INTERNATIONAL UNION FOR CONSERVATION OF NATURE, 1989: Sahel Studies. IUCN, Nairobi.
- [4] SIVAKUMAR, M.V.K., WALLACE, J.S., RENARD, C. AND GIROUX, C., 1991: Soil Water Balance in the Sudano-Sahelian Zone, IAHS Publication 199, Wallingford
- [5] GLANTZ, M., (ed.) 1994. Drought Follows the Plow. CUP, Cambridge.
- [6] MAINGUET, M., 1999: Aridity, Droughts and Human Development. Springer Verlag, Berlin.
- [7] THOMAS, D.G. AND MIDDLETON, N., 1994: Desertification: Exploding the Myth. J. Wiley, Chichester.
- [8] TUCKER, J.C., DREGNE, H.E. AND NEWCOMB, W.W., 1991: Expansion and contraction of the Sahara Desert from 1980 to 1990. *Science*, Vol. 253, p. 299-301.

- [9] WARREN, A. AND AGNEW, C.T., 1988: An assessment of desertification and land degradation in arid and semi-arid areas. Paper 2, International Institute for Environment and Development, London.
- [10] UNITED NATIONS ENVIRONMENT PROGRAMME, 1992: Atlas of Desertification. UNEP Edward Arnold, London.
- [11] HOUGHTON, J.T., DING, Y., GRIGGS, D.J., NOGUER, M., VAN DER LINDEN, P.J. AND XIAOSU, D., 2001: Climate Change 2001: The Scientific Basis. Cambridge University Press, Cambridge
- [12] RAYNAUT, C., 1997: Societies and Nature in the Sahel. Routledge, London.
- [13] NICHOLSON, S.E. AND PALAO, I.M., 1993: A re-evaluation of rainfall variability in the Sahel. *International Journal of Climatology*, 13: 371-389.
- [14] HULME, M., 2001: Climate perspectives on Sahelian desiccation 1973-1998. *Global Environmental Change* 11:19-29.
- [15] LEHOUEOU, H.N., 1996: Climate change, drought and desertification. *Arid Environments*, 34:133-85
- [16] GARCIA, R.V., 1981: Drought and Man. Pergamon press, Oxford.
- [17] FRANKE, F. AND CHASIN, B., 1980: Seeds of Famine. Allanheld Osman & Co. New Jersey.
- [18] DAI, A., LAMB, P.J., TRENBERTH, K.E., HULME, M., JONES, P.D. AND XIE, P., 2004: The recent Sahel drought is real. *International Journal of Climatology*, 24, 1323-13331.
- [19] FOLLAND, C.K., PALMER, T.N. AND PARKER, D.E., 1986: Sahel rainfall and worldwide sea temperatures, 1901-85. *Nature*, 320:, 602-606.
- [20] ZENG, N., NEELIN, J.D., LAU, K.-M., TUCKER, C. J., 1999: Enhancement of interdecadal climate variability in the Sahel by vegetation interaction. *Science*, 286: 1537-1540.
- [21] GIANNINI, A., SARAVANAN, R. AND CHANG, P., 2003: Oceanic forcing of Sahel rainfall on interannual to interdecadal time scales. *Science*, 302: 1027-1030.
- [22] TAYLOR, C.M., LAMBIN, E.F., STEPHENNE, N., HARDING, R.J. AND ESSERY, R.L.H., 2002: The influence of land use change on climate in the Sahel. *Journal of Climate*, 15: 3615-3629.
- [23] HULME, M. AND NEW, M., 1997: Dependence of large-scale precipitation climatologies on temporal and spatial sampling. *Journal of Climate*, 10, 1099-1113.
- [24] MADDEN, R.A., SHEA, D.J., BRANSTATOR, G.W., TRIBBIA, J.J. AND WEBER, R.O., 1993: The effects of imperfect spatial and temporal sampling on estimates of the global mean temperature: experiments with model data. *Journal of Climate*, 6: 1057-1066.
- [25] WILLMOTT C.J., ROBESON, S.M., AND JANIS, M.J., 1996: Comparison of approaches for estimating time-averaged precipitation using data from the USA. *International Journal of Climatology*, 16: 1103-1115.
- [26] AGNEW, C.T., 1990: Spatial aspects of drought in the Sahel, *Journal of Arid Environments*, 18, 279-293.
- [27] PETERSON, T.C. AND VOSE, R.S., 1997: An overview of the Global Historical Climatology Network temperature data base, *Bulletin of the American Meteorological Society*, 78, 2837-2849.
- [28] NICHOLSON, S.E., 1993: An overview of African rainfall fluctuations of the last decade. *Journal of Climate*, 6: 1463-1466.
- [29] JONES, P.D. AND HULME, M., 1996: Calculating regional climatic time series for temperature and precipitation: methods and illustrations. *International Journal of Climatology*, 16, 361-377.
- [30] Dai, A., Fung, I.Y. and Del Genio, A.D., 1997: Surface observed global land precipitation variations during 1900-88. *Journal of Climate*, 10, 2943-2962.
- [31] CHAPPELL, A., MCTAINSH, G., STRONG, C. AND LEYS, J., 2003: Simulations to optimise sampling of aeolian sediment transport for mapping in space and time. *Earth Surface Processes and Landforms*, 28: 1223-1241.
- [32] CHAPPELL, A. AND EKSTRÖM, M., 2005: The importance of de-clustering and uncertainty in climate data: a case study of west African Sahel rainfall. International Geostatistics Congress, Banff (in press)
- [33] JOURNEL, A.G., 1984: The place of non-parametric geostatistics. In Verly, G., David, M., Journel, A.G. and Marechal, A., (eds.): Geostatistics for Natural Resources Characterization, V1 pages 307-355. Reidel, Dordrecht.
- [34] DEUTSCH C.V. AND JOURNEL, A.G., 1998: GSLIB Geostatistical Software Library and User's Guide. OUP, Oxford.
- [35] GOOVAERTS P., 1997: Geostatistics for Natural Resources Evaluation. OUP, Oxford.

# Combined Land Surface Water and Vegetation Indices for Land Degradation Studies in Dryland Ecosystems

A.R. Huete<sup>a</sup>

<sup>a</sup>Department of Soil, Water and Environmental Science, P.O.B. 210038, University of Arizona, Tucson, Arizona USA, email: [ahuete@ag.arizona.edu](mailto:ahuete@ag.arizona.edu)

## ABSTRACT

Arid and semiarid ecosystems are experiencing rapid land cover changes (e.g. woody plant encroachment, invasive species) with significant shifts in the physiognomic makeup of the vegetation with consequences to surface hydrologic processes, productivity, and land surface moisture conditions. Water is the most limiting resource to biological activity in these dryland zones, however, the relationship moisture and biological activity as it relates to drought and land degradation is not simple with differential sensitivities existing across land cover types. In this study we combined remotely-sensed vegetation indices and canopy moisture indices to improve the prediction of land degradation and drought and to provide a mechanism in which spatiotemporal variability in water availability and productivity may be analyzed in order in response to climate change and human land cover modifications. We used field optical measurements, AVIRIS, Hyperion, and 5 years of MODIS time series data to analyze seasonal patterns of LSWI and VI and provide a contextual array of measurements for assessing 'greenness' and vegetation water content and ascertain variations specific to each. Combined vegetation index and land surface water indices (VI- LSWI), describing moisture status achieved per unit 'greenness' were found to vary uniquely with phenology phase, vegetation type, water availability, drought, and land degradation. The slope of VI- LSWI relationships shifted with drought status and stage of degradation. Our results show that combined greenness and water indices offer improved sensitivity to ecosystem health assessment and drought detection and analysis.

**Keywords:** Vegetation indices, canopy moisture indices, land degradation, drought.

## 1 INTRODUCTION

Canopy moisture plays a critical role in the evaluation of terrestrial environmental conditions with important influences on hydrologic, pedologic, biogeochemical, ecologic and atmospheric processes [1]. Knowledge of the water status of a vegetation canopy can provide valuable information on soil moisture condition, vegetation stress, and drought status. The process of degradation, however, results in simultaneous and complex variations of many interrelated soil and vegetation biophysical parameters rendering it difficult to develop simple and robust remote sensing mapping and monitoring approaches. Nevertheless, remote sensing offers a feasible method to collect spatial information on vegetation canopy optical features. In this paper, we investigate the relationship between chlorophyll-based and water-based vegetation indices for drought and land degradation applications.

### 1.1 Vegetation Moisture Indices

Vegetation water indices employing the 1240 nm, 1640 nm, or 2100 nm wavelengths in lieu of the red band used in vegetation indices, have recently been used as independent vegetation measures related to canopy moisture condition instead of chlorophyll amount. Laboratory studies and canopy radiant transfer model simulations have shown that changes in leaf water content have a large effect on reflectances in portions of the near-infrared (NIR) and shortwave infrared (SWIR) spectral regions. Important liquid water absorptions are found at 1640 nm and 2100 nm, with a weaker absorption feature at 1240 nm, which result in negative relationships between reflectances at these wavelengths and leaf water content [2, 3]. Several studies have shown increases in leaf reflectance associated with plant stress across the SWIR region [4, 5] providing useful information to infer soil moisture status in the plant root zone. The SWIR reflectance values alone, however, are not suitable for retrieving vegetation water content as variations in leaf internal structure and leaf dry matter content as well as canopy geometry, shadowing, and soil surface moisture also influence SWIR reflectance [6, 7].

The assessment of vegetation water content or equivalent water thickness (EWT, g-H<sub>2</sub>O/cm<sup>2</sup>-leaf area) is significantly improved by the combination of NIR and SWIR bands [8]. Land surface water indices (LSWI) employing the 1640 nm or 2100 nm wavelengths in lieu of the red band used in VIs, have been used as independent vegetation measures related to canopy moisture condition instead of chlorophyll amount [9, 10].

$$LSWI = [\rho_{860nm} - \rho_{swir}] / [\rho_{860nm} + \rho_{swir}] \quad (1)$$

with  $\rho_{swir}$  representing one of the shortwave infrared bands. Many Earth Observing sensors have SWIR bands of potential use in surface moisture studies, including Landsat Thematic Mapper bands 5 and 7 (1550- 1750 nm, 2080- 2350 nm), MODIS bands 6 and 7 (1628- 1652nm, 2105- 2155nm), and SPOT-VEGETATION (1580- 1750nm), and offer potential canopy moisture indicators [8, 11, 12]. The Normalized Difference Water Index (NDWI) uses two reflectance bands in the high NIR reflectance plateau of vegetation canopy spectra, at 860 nm and 1240 nm wavelengths [3],

$$NDWI = [\rho_{860nm} - \rho_{1240nm}] / [\rho_{860nm} + \rho_{1240nm}] \quad (2)$$

with the weaker, liquid water absorption feature enhanced by the high NIR scattering in the leaf. This formulation was applied to MODIS bands 5 (1230 -1250nm) and 2 (841 - 876nm) and was found to be a strong indicator of canopy water content during the growing season in the Sahel [12]. Whereas, the SWIR region responds to both vegetation water content and soil surface moisture, the weaker 1240 nm, water absorbing region has been shown to respond to canopy moisture status only and be insensitive to surface soil moisture. However, it was found that in dry years the vegetation cover was too dry and sparse to provide information on canopy water content suggesting that a minimum, threshold vegetation amount must be present for the water indices to work [12].

## 1.2 Combined Moisture and Vegetation Indices

Although vegetation indices (VIs) have also been correlated with vegetation water content, they are physiologically related to canopy chlorophyll content and absorbed photosynthetically active radiation [13]. Thus, VIs generally would depict decreases in plant growth (or senescence) caused by water stress rather than lower water contents. At the Soil Moisture Experiments 2002 (SMEX02) field and satellite campaign, Jackson et al. [14] found the water indices to be superior to VIs in mapping vegetation water content (VWC), as the NDVI was found to saturate while the water indices continued to show changes in VWC with increasing amounts of green vegetation. Ceccato et al. [8] concluded that VIs were unsuitable for retrieving VWC since relationships between chlorophyll and VWC are specific to each species. Furthermore, decreases in chlorophyll content do not imply a decrease in VWC, and vice-versa, a decrease in VWC does not imply a decrease in chlorophyll content. The two VIs adopted as standard MODIS products are the normalized difference vegetation index (NDVI) and enhanced vegetation index (EVI) [15],

$$NDVI = [\rho_{NIR} - \rho_{Red}] / [\rho_{NIR} + \rho_{Red}] \quad (3)$$

$$EVI = 2.5 [\rho_{NIR} - \rho_{Red}] / [1 + \rho_{NIR} + 6 \rho_{Red} - 7.5 \rho_{Blue}] \quad (4)$$

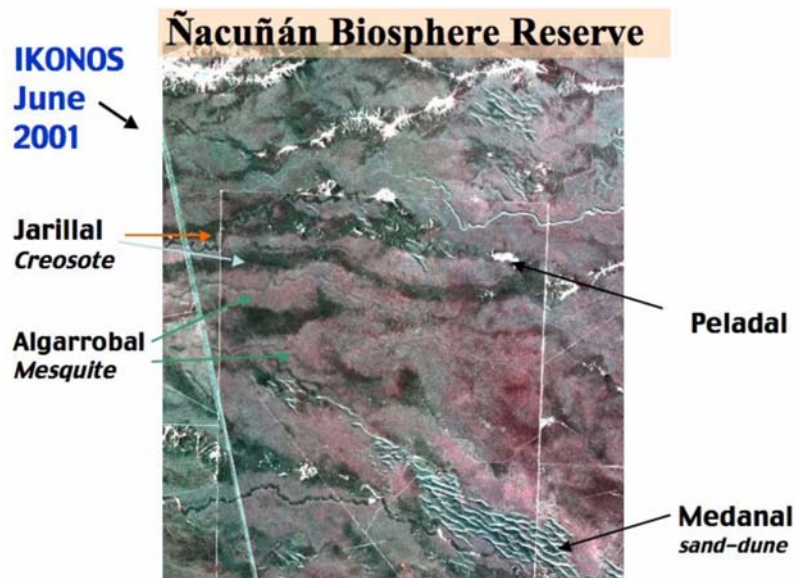
Maki et al. [16] and others have combined use of NDVI and NDWI to generate vegetation dryness measures involving both indices. A combined VI- LSWI approach would provide a contextual array of remotely sensed measurements, increasing the measurement domain and reducing the under-determination problem for assessing soil moisture and vegetation water content [1, 17]. Our objectives in this study were to combine land surface water indices with 'greenness'-based vegetation indices to utilize their unique biophysical properties in the assessments of drought and land degradation in semiarid environments. We expect that the decoupling of moisture and chlorophyll parameters may provide early warning indicators for land health and degradation analysis.

## 2 METHODS

Vegetation index and canopy water index relationships were investigated in both spatial and temporal domains with field data sets, fine resolution AVIRIS (4m) and Hyperion imagery (30m) and MODIS time series data (1km). A field measured seasonal data set of irrigated wheat (Seri) crop under normal and stressed water treatments was used to analyze VI- water index relationships under relative wet and dry conditions. We also utilized fine resolution AVIRIS and Hyperion imagery acquired over the protected Ñacuñán Biosphere Reserve and surrounding degraded areas within the Mendoza region of Argentina. The EO-1 Hyperion sensor imaged the Ñacuñán Reserve on January 24, 2001. All hyperspectral imagery were corrected for atmospheric effects and converted to surface reflectances with the aid of an atmosphere correction program, ATREM, constrained with co-registered, surface ASD radiometric measurements, used as calibration ground control points. Hyperion is a pushbroom sensor providing 220, 10 nm bands covering the spectrum from 400 to 2500 nm. Hyperion and AVIRIS imagery have demonstrated their utility in characterizing the ecological variance and complexities of landscapes, including species composition, ecosystem functioning, biogeochemical cycles, and land use, land cover change, and largescale ecological changes. The Ñacuñán Biosphere Reserve is located in a warm semi desert shrubland steppe ecosystem in the province of



Mendoza (34°02'S; 67°54'W). This designated UNESCO Biosphere Reserve comprises an area of 12,271 ha and is administered by the Instituto Argentino de Investigaciones de las Zonas Aridas (IADIZA). It is at a mean altitude of 540 m with an average annual temperature of 15.8 C and 200 mm annual precipitation. The site consists of floristically diverse vegetation communities, characterized by open forests of mesquite (*Prosopis spp.*) and creosotebush (*Larrea divaricata* and *L. cuneifolia*), locally known as algarrobal and jarillal communities, respectively [18]. These open forest communities were totally cut down between the years 1907 and 1937 and are now protected under a restoration and protection plan. The algarrobal community of mixed mesquite-creosotebush is the main cover type inside the reserve followed by the jarillal (creosotebush) community. The dark green leaves of the creosotebush render this community very dark in appearance in satellite imagery relative to the algarrobal vegetated areas (Fig. 1). There are two additional vegetation formations resulting from previous and current phases of land degradation, including a 'medanal' community consisting of both mesquite and creosotebush species and characterized by sand dune formations and a 'peladal' community which is severely degraded, has stunted creosotebush, and appears very bright (Fig. 1). These degraded vegetation communities are present inside the reserve but are much more prominent outside the reserve, particularly to the north.



**Figure 1.** Ikonos image (June 2001) depicting the vegetation communities at the Ñacuñán Biosphere Reserve, Argentina.

### 3 RESULT

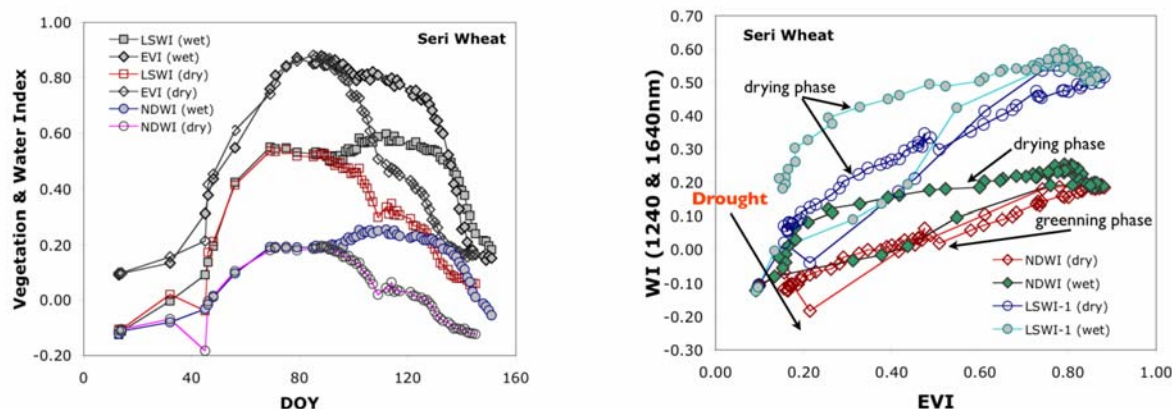
#### 3.1 Wheat Phenology

We first examined the phenology profiles of a wheat canopy (Seri) with the EVI, NDWI, and LSWI under normal irrigation (wet) and water stressed (dry) treatments (Fig. 2a). There is little variation during the green-up phase between treatments and for all indices. As water was not withheld from the dry treatment until mid-way into the growing season, no signs of water stress were evident in the greening and peak phases. The dry-down phase was noticeably different between wet and dry treatments with a large lag in drying occurring in the wet treatment. Thus, both chlorophyll activity and water contents declined rapidly in the dry treatments while in the wet treatment, rapid declines in the EVI, NDWI, and LSWI lagged by more than one month (~40 days). The two water indices show extended peak values through to DOY 130 before initiating a drying phase while the EVI declined gradually during this lag period and was the first index to commence dry-down. Thus, the chlorophyll and water indices depicted a net loss in chlorophyll signal followed by a delayed decline in moisture content.

The combined VI - WI crossplot using NDWI and LSWI as the water indices is shown in Fig. 2b for both wet and dry treatments. There was a single, positive and linear relationship between the water index and EVI during the green-up period when using NDWI or LSWI. For the dry wheat treatment, green-up and dry-down follow the same relationship, but in the wet treatment, the dry-down relationship is different from the green-up relationship. A hysteresis effect was observed such that during the dry down phase, the NDWI was consistently higher for any specific EVI value (greenness condition) compared with the green-up phase. In the case of VI - LSWI

relationships, the hysteresis effect was observed for both dry and wet wheat treatments. In this case the dry down phase exhibits a separate relationship for the dry treatment, as well as the wet treatment. In all cases, the dry down phase does not follow the green-up relationship. However, the dry down phase of the wet treatment shows the highest LSWI values per unit of VI (greenness).

This effect is most likely due to the cessation of chlorophyll production at peak greenness with no concurrent effect on leaf moisture status. During green-up the chlorophyll concentration or amount of chlorophyll per unit amount of leaf tissue is high, but there is less leaf biomass (less LAI) for the moisture signal. At dry-down, LAI is maximum, biomass is maximum, and although it is becoming less green, it is still transpiring and with moisture. The ratio of chlorophyll to leaf biomass is lower, but the ratio of leaf moisture to biomass remains high.



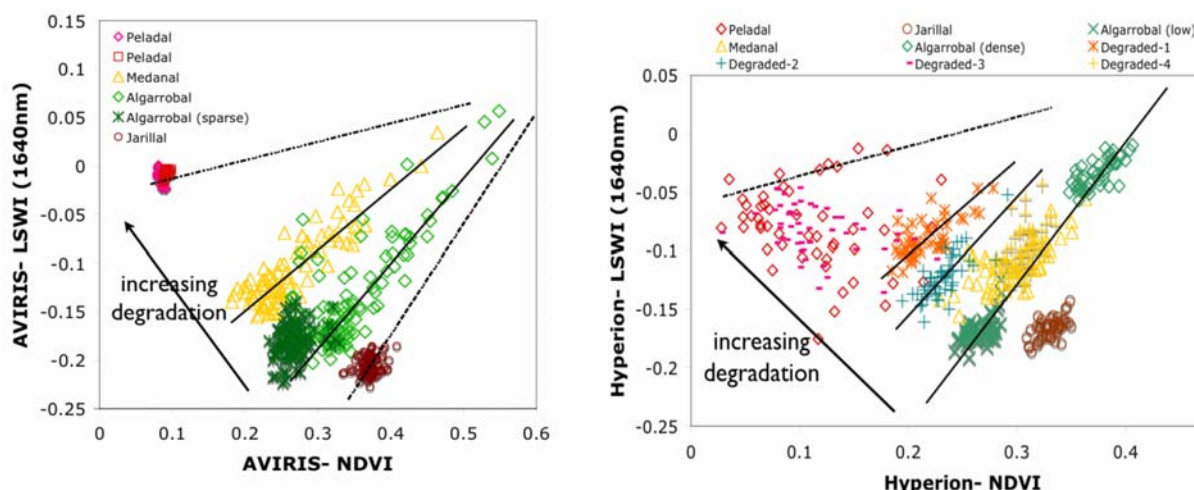
**Figure 2.** Seasonal profiles of EVI, NDWI, and LSWI for Seri Wheat crop under irrigated (wet) and water stressed (dry) treatments (left). LSWI at 1240 nm and 2130 nm relationships with EVI obtained from the seasonal profile data (right).

The drying phase from the water-stressed treatment may also show higher LSWI values, relative to the greening phase, due to canopy architecture differences. In the green-up period, there is little biomass nor canopy structure, while in the dry-down phase, the canopy is fully developed, and structurally complex, casting shadows which may cause increased absorption over the SWIR wavelengths, raising the LSWI. This did not occur in the NDWI measurements of the stressed wheat canopy in the dry-down phase, indicating that the NDWI measurements were not influenced by canopy architecture. However, the NDWI involves only NIR bands, which may not decrease in values with canopy architecture, as is the case in the SWIR.

### 3.2 Land Degradation

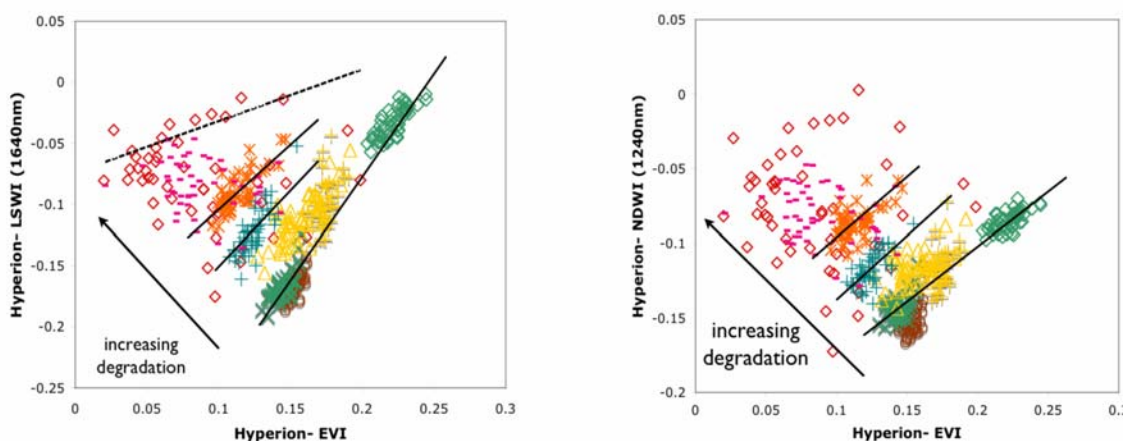
The AVIRIS data showed more complex LSWI- VI relationships among the various land cover classes at different stages of degradation (Fig. 3). Overall, there is an inverse relationship between these two canopy measures with the most degraded site (peladal) exhibiting the lowest NDVI values with highest LSWI values. For a particular land cover class, however, there is a positive relationship between these two indices encompassing the range of variability and vegetation densities. The slopes of these specific LSWI- NDVI relationships appear to decrease with severity of land degradation, indicating that for given amounts of canopy moisture, there is less chlorophyll or greenness signal with increasing stages of degradation. The change in moisture content per unit increase in VI is greater in the healthier landscapes. The peladal sites had unusually high LSWI values, equivalent to that or greater than all other land cover conditions. These sites were dry during the AVIRIS overflights and these high values over bare and dry surfaces have been reported in other studies where strong negative, 'soil-line' relationships among bare soils, as well as surface litter, were seen in the NDWI - NDVI plot [19].

Although there is a strong and positive relationship between NDVI and NDWI for vegetated points, it is worth noting that both indices are needed for maximum discrimination of the land degradation classes as well as detection of variations in land degradation (Fig. 3). The LSWI by itself, would not be able to unambiguously distinguish among the land degradation conditions, particularly given the high peladal (bare playa) values.



**Figure 3.** AVIRIS LSWI – NDVI relationships (left) and Hyperion derived LSWI – NDVI relationships (right) for various land degradation land cover classes at Ñacuñán Biosphere Reserve, Argentina (Monte desert).

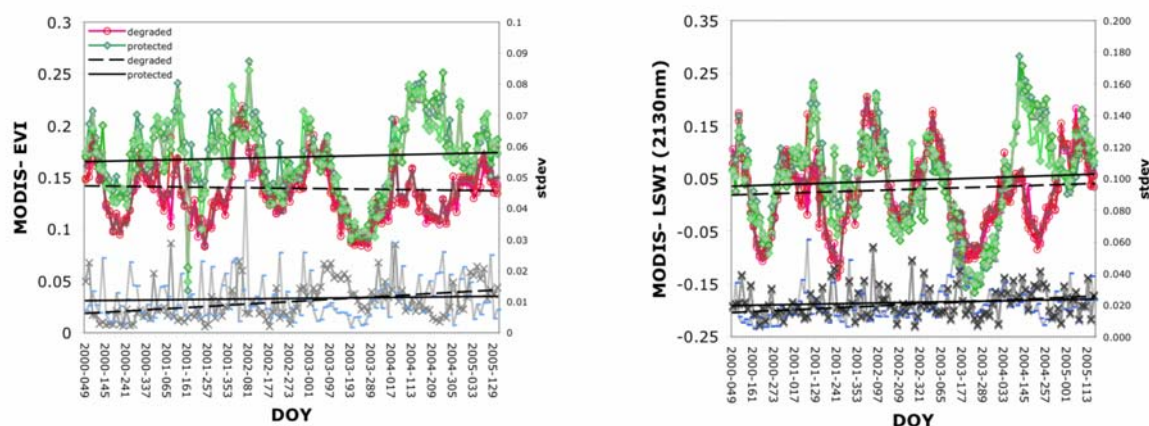
The relationships among Hyperion-derived LSWI and NDVI with EVI were mostly similar to those encountered with the NDVI. The Jarillal community, however, was integrated with the Algarrobal vegetation communities in the case of the EVI (Fig. 4). Also, in the case of the NDVI, there were parallel lines of NDVI- EVI relationships (constant slopes) shifting negatively toward higher NDVI and lower EVI with increasing degradation (Fig. 4b).



**Figure 4.** Hyperion-based EVI-LSWI (left) and EVI-NDWI (right) relationships at the Ñacuñán Biosphere Reserve and surrounding degraded areas.

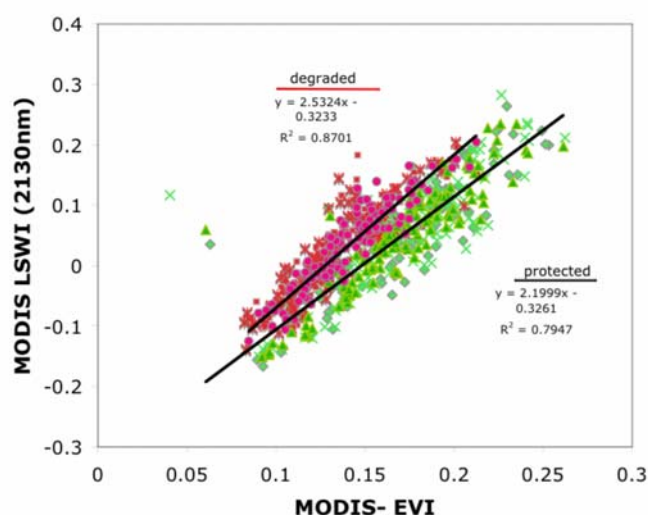
### 3.3 MODIS TIME SERIES DATA

The MODIS time series profiles of the protected and degraded sites at Ñacuñán Biosphere Reserve show an upward 5-year trend with EVI and LSWI values (Fig. 5). The degraded areas surrounding the Reserve exhibit an increasing LSWI but decreasing EVI trend over the 5 years. The EVI standard deviation values of the degraded areas increased more sharply than in the protected areas (Fig. 5a). In the case of the LSWI, both degraded and protected areas show a similar upward trend with standard deviations that also increase, but with a slightly higher increase in the degraded areas. The protected area has a slight upward trend and the standard deviation values increased slightly.



**Figure 5.** MODIS time series profiles of protected and degraded sites at Ñacuñán Biosphere Reserve for EVI (left) and LSWI (right). Trend lines depict spatially-based average and standard deviation values.

The combined LSWI-EVI MODIS plot (Fig. 6) show a steeper slope in the degraded areas outside the Ñacuñán Biosphere Reserve and a negative shift toward higher LSWI and lower EVI values.



**Figure 6.** Combined LSWI and EVI plot of MODIS time series data in the protected Ñacuñán Biosphere Reserve and the surrounding areas.

#### 4 CONCLUSIONS & DISCUSSION

Remotely-sensed land surface water indices combined with greenness-based vegetation indices resulted in useful information for the prediction of vegetation health response to climate change and human land cover modifications. Spectral retrievals of both chlorophyll and water estimates in vegetation canopies better depicted plant physiological status and provide opportunities for improved drought, soil water deficit, and vegetation stress analysis. Furthermore, the combined indices resulted in better characterization of land degradation and land cover conversions. In all VI- water index cases, there were strong differences between wet and dry treatments of potential value in assessing land degradation and drought. The slope of the moisture index- vegetation index relationship varied with moisture availability and became steeper with a much lower intercept term with increasing drought. The canopy water index- vegetation index slopes varied with phenology phase, species, land degradation, and moisture availability. The combined vegetation and water indices were particularly useful in discriminating among stages of land degradation. These involved differences in biological moisture availability, chlorophyll activity, plant species



and physiognomy, and altered phenology patterns. The patterns and shifts in LSWI- VI relationships were opposite in the case of drought-induced vegetation stress and degradation- induced vegetation health. With increasing drought, we found a shift in LSWI- VI toward higher VI values and lower LSWI values while in the case of land degradation, we found decreasing VI values and increasing LSWI values with land degradation severity. The slope variations with land degradation were difficult to analyze given that land degradation may be result in excess water availability per unit of green biomass (lower green cover but constant rainfall conditions) or if significant erosion has occurred, there may be less biological available water (drought effects) as runoff from rainfall may be more pronounced. Thus, with land degradation, there may be excess water or a deficiency in water availability. Much remains to be done in the application of combined indices to land degradation studies and the extraction of moisture availability and biological production information. However, the combined approach may provide new insights into complex hydrologic processes, fluxes, and feedbacks among soil moisture, atmosphere moisture, and ecosystem metabolism and development. A combined VI and vegetation water index with thermal or microwave remote sensing approaches would also greatly enhance our understanding of land surface moisture dynamics.

## ACKNOWLEDGMENTS

We acknowledge NASA MODIS contract #NNG04HZ20C and NASA EO-1 grant for supporting this study. We would like to thank Hojin Kim, Youngwook Kim, and Andree Jacobson for help in data extraction and processing.

## REFERENCES

- [1] GOWARD, S.N., Y. XUE, AND K.P. CZAJKOWSKI, 2002: Evaluating land surface moisture conditions from remotely sensed temperature/ vegetation index measurements: An exploration with the simplified simple biosphere model. *Remote Sens. Environ.*, 79: p. 225-242.
- [2] HUNT, E. R. AND B.N. ROCK, 1989: Detection of changes in leaf water content using Near- and Middle-Infrared reflectances. *Remote Sens. of Environ.*, 30(1): p. 43-54.
- [3] GAO, B.C., 1996: NDWI- A normalized difference water index fro remote sensing of vegetation liquid water from space. *Remote Sens. Environ.*, 58: p. 257-266.
- [4] TUCKER, C.J., 1980: Remote sensing of leaf water content in the near infrared. *Remote Sens. Environ.*, 10(1): pp. 23-32.
- [5] GAUSMAN, H.W. AND W.A. ALLEN, 1973: Optical parameters of leaves of 30 plant species, *Plant Physiology*, 57-62.
- [6] COHEN, W.B., 1991: Response of vegetation indices to changes in three measures of leaf water stress. *Photogram. Eng. & Remote Sensing*. 57(2): p. 195-202.
- [7] CECCATO, P., ET AL., 2001: Detecting vegetation leaf water content using reflectance in the optical domain. *Remote Sens. Environ.*, 77(1): p. 22-33.
- [8] CECCATO, P., ET AL., 2002: Designing a spectral index to estimate vegetation water content from remote sensing data: Part 1: Theoretical approach. *Remote Sens. Environ.*, 82(2-3): p. 188-197.
- [9] HUNT, E.R., B.N. ROCK, AND P.S. NOBEL, 1987: Measurement of leaf relative water content by infrared reflectance. *Remote Sens. Environ.*, 22: p. 429-435.
- [10] HARDISKY, M.A., KLEMAS, V. AND SMART, R.M., 1983: The influences of soil salinity, growth form, and leaf moisture on the spectral reflectance of *Spartina alterniflora* canopies. *Photogramm. Eng. & Remote Sensing*, 49: p. 77-83.
- [11] XIAO, X., ZHANG, Q., BRASWELL, B., URBANSKI, S., BOLES, S., WOFSY, S., MOORE, B., OJIMA, D., 2004: Modeling gross primary production of temperate deciduous broadleaf forest using satellite images and climate data. *Remote Sens. Environ.*, 2004.
- [12] FENSHOLT, R. AND I. SANDHOLT, 2003: Derivation of a shortwave infrared water stress index from MODIS near- and shortwave infrared data in a semiarid environment. *Remote Sens. Environ.*, 87(1): p. 111-121.
- [13] TUCKER, C.J. AND P.J. SELLERS, 1986: Satellite remote sensing of primary production. *Int. J. of Remote Sensing*, 7(11): p. 1395-1416.
- [14] JACKSON, T.J., DAOYI CHEN, MICHAEL COSH, FUQIN LI, MARTHA ANDERSON, CHARLES WALTHALL, PAUL DORIASWAMY AND E. RAY HUNT, 2004: Vegetation water content mapping using Landsat data derived normalized difference water index for corn and soybeans. *Remote Sens. Environ.*, 92(4): p. 475-482.
- [15] HUETE, A., ET AL., 2002: Overview of the radiometric and biophysical performance of the MODIS vegetation indices. *Remote Sens. Environ.*, 83(1-2): p. 195-213.

- [16] MAKI, M., ISHIAHRA, M., AND TAMURA, M., 2004: Estimation of leaf water status to monitor the risk of forest fires by using remotely sensed data. *Remote Sens. Environ.*, 90: p. 441-450.
- [17] ZARCO-TEJEDA, P.J., RUEDA, C.A., & USTIN, S., 2003: Water content estimation in vegetation with MODIS reflectance data and model inversion methods. *Remote Sens. Environ.*, 85: p. 109-124.
- [18] OJEDA, R.A., C.M. CAMPOS, J.M. GONNET, C.E. BORGHI, AND V.G. ROIG, 1998: The MaB reserve of ñacuñán, Argentina: its role in understanding the Monte Desert biome, *J. Arid Environ.*, 39: p. 299-313.
- [19] HUETE, A., 2005: Hydrological Applications of Remote Sensing: Surface States – Soil Properties (hyperspectral VIS/IR), in Wood, B. (ed.): Editor. *Encyclopedia of Hydrology*.

# Contribution of Meteosat Second Generation (MSG) to drought early warning

B. Lacaze<sup>a</sup> and J.-C. Bergès<sup>a</sup>

<sup>a</sup> PRODIG, CNRS UMR 8586, Paris, France

## ABSTRACT

Several low resolution satellite sensors are now available and can provide near real-time monitoring of vegetation cover seasonal changes on a large scale basis. This paper presents a comparison of NDVI derived from SPOT-VEGETATION and MSG-SEVIRI for the whole continent of Africa.

Dekadal NDVI from VEGETATION data are available, obtained from maximum NDVI compositing technique. VEGETATION data from July 1-10, 2004, have been re-sampled at 0.025° spatial resolution (= resolution of MSG-SEVIRI data) for whole Africa. In the case of SEVIRI data, a 2-steps procedure is used: first daily compositing is implemented through analysis of thermal data (maximum surface temperature compositing), followed by dekadal NDVI synthesis.

Results include the observed correlations and discrepancies of NDVI products of the 2 sensors. Results suggest that, due to higher temporal frequency (1 image each 15 mn), MSG-SEVIRI data can be used to obtain improved NDVI products through better removal of cloud-contaminated pixel.

**Keywords:** Remote sensing, drought, vegetation, NDVI, temporal compositing, Africa.

## 1 INTRODUCTION

Several low resolution satellite sensors are now available and can provide near real-time monitoring of vegetation cover seasonal changes on a large scale basis. In addition to NOAA-AVHRR sensor operated and archived since more than 20 years, new sensors became recently available for continental or global vegetation monitoring, like SPOT-VEGETATION (since 1998), EOS-MODIS (since 2000) or MSG-SEVIRI (since 2004). In this paper, the emphasis will be put on MSG-SEVIRI instrument. The high temporal frequency allows a new approach to temporal compositing inducing an improved removal of cloud-contaminated pixels. The derived NDVI product will be compared to similar product obtained from SPOT-VEGETATION data during the same compositing period (July 1-10, 2004).

## 2 SATELLITE DATA ACQUISITION AND PROCESSING METHODS

### 2.1 MSG Data acquisition

MSG-1, the first of the Meteosat Second Generation geostationary satellites, has been launched on August 28, 2002. Due to technical problems, it was fully operational only on January 29, 2004 and took the name Meteosat 8.

MSG transmits raw data to the Eumetsat control and processing centre in Darmstadt (Germany), via the primary ground station, for processing. The raw data consists mainly of images generated by the SEVIRI (Spinning Enhanced Visible and Infrared Imager) instrument and the Geostationary Earth Radiation Budget Experiment on board the satellite. Once processed, the data is sent back to the satellite for broadcasting to users.

SEVIRI radiometer is the main instrument on board MSG. It provides images of the Earth disc with 3km resolution at nadir in 11 bands (visible, near infrared, shortwave infrared and thermal infrared). Main features of optical bands are indicated in table 1.

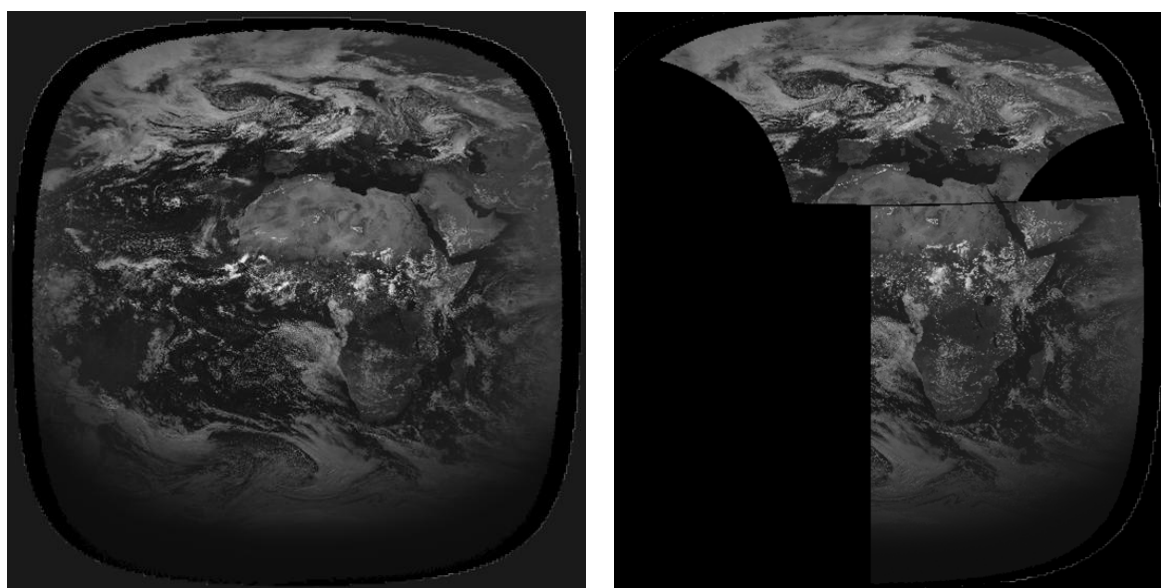
**Table 1.** Spectral characteristics of 3 optical bands of SEVIRI instrument.

Channel	Spectral domain	$\lambda_{cen}$	$\lambda_{min} - \lambda_{max}$
VIS 0.6	Green - Red	0.635	0.56 – 0.71
VIS 0.8	Near Infrared	0.810	0.74 – 0.88
NIR 1.6	Shortwave IR	1.640	1.50 – 1.78

MSG takes one full resolution image every 15 minutes, thus illustrating the weather in motion. In addition, a panchromatic image is taken with 1km resolution, covering partly the Earth disc, as indicated at Figure 1. Image dimensions are 3712 x 3712 pixels in channels 1 to 11, and 5568 x 11136 pixels in channel 12.

### 1.2 Deriving NDVI from MSG data

Temporal compositing of NDVI data is generally based upon the computation of maximum NDVI from a set of multi-temporal data. This technique can not be applied to MSG data taken during a diurnal cycle: due to changes in solar zenithal and azimuthal angles, NDVI exhibit variations which are not related with ground cover. An alternative technique is to follow the diurnal cycle of brightness temperature: the identification of the maximum value during the day is an efficient mean to eliminate pixels contaminated with clouds or cloud-shadows, characterized by low temperatures. Then NDVI is computed for each pixel, using red and near infrared radiances recorded at the time of day of maximum temperature. This procedure has been implemented by the MSG-ATR team (MSG-ATR, 2005). NDVI is multiplied by 1000, and coded as integer value, ranging from -1000 to + 1000. It must be noted that the procedure is applied to raw radiance data (no atmospheric corrections).



**Figure 1.** Example of MSG images at 3km resolution, full disc (left) and 1km resolution (right).

A sub-image covering the whole continent of Africa has been extracted (38°N to 35°S, 26°W to 60°E); data have been re-sampled at 0.025 degree resolution in Plate-Carrée projection (geographic): the size of resulting image is 3440 x 2920 pixels.

### 1.3 SPOT VEGETATION NDVI data

Dekadal NDVI data are available freely from SPOT VEGETATION distributor (VITO, 2005). NDVI data can be obtained for the whole continent of Africa (38°N to 35°S, 26°W to 60°E) in a geographic projection, with spatial



resolution of 0.00892857 degree (~1 km) : the size of image is 9633 x 8177 pixels. Data are available in *hdf* format; one channel “quality of data” is also available, which indicates pixels affected by clouds or cloud-shadows.

NDVI data are given in byte format (Digital counts DC between 0 and 255). NDVI values range between -0.1 (DC = 0) and 0.92 (DC = 255), and the relationship between NDVI and digital counts is given by :

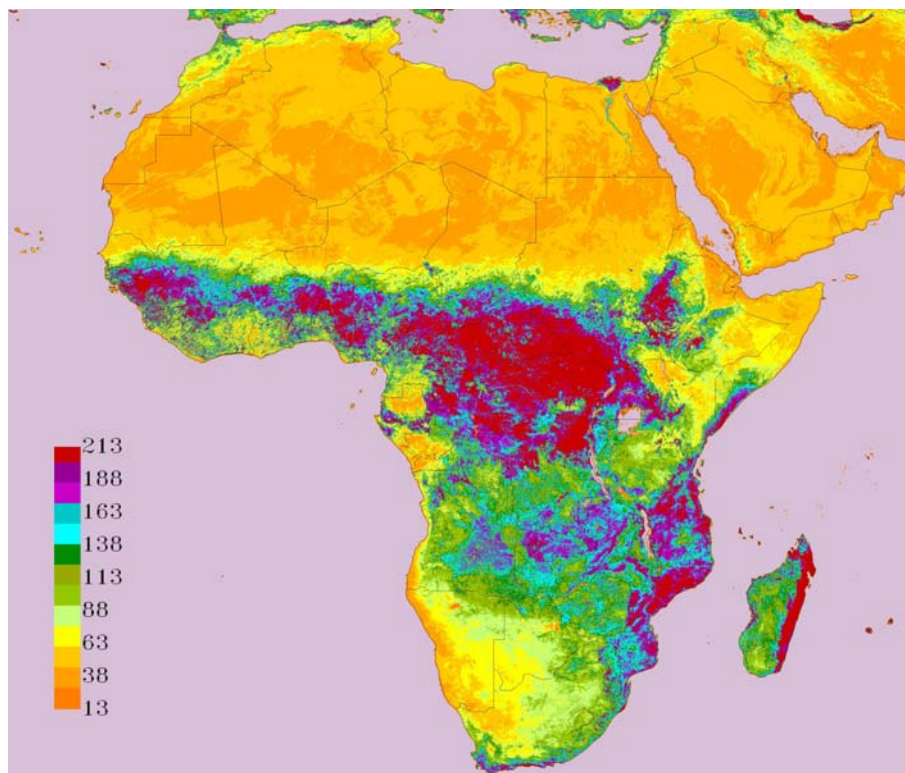
$$\text{NDVI} = 0.004 * \text{DC} - 0.1 \quad (1)$$

To compare with MSG data, SPOT VEGETATION NDVI image has been re-sampled at 0.025° resolution, using the nearest neighbour algorithm.

## 2 RESULTS

### 2.1 SPOT-VEGETATION NDVI data

Re-sampled NDVI image from July 1-10, 2004 is displayed at Figure 2. Although resulting from a 10 days synthesis, the image is still affected by cloud contaminated pixels. This is the case in the West Africa tropical region, as indicated at Figure 3.



**Figure 2.** Dekadal NDVI image derived from SPOT-VEGETATION data (July 1-10, 2004).



**Figure 3.** Cloud-contaminated pixels (white pixels) in SPOT-VEGETATION dekadal image.

### **1.2 MSG SEVIRI data**

MSG SEVIRI data (temporal synthesis, July 1-10, 2004) are depicted at Figure 4. The following procedure has been followed, before displaying the results: first, transformation into byte format, using the same scaling procedure as SPOT VEGETATION data:  $DC = (NDVI + 0.1)/0.004$ ; second, a linear contrast stretch has been applied to the data, as the range of MSG SEVIRI NDVI values is narrower than the range of SPOT- VEGETATION data (see below). The resulting value is defined by:

$$NDVI_{stretched} = 1.73 * NDVI_{byte} - 2.16 \quad (2)$$

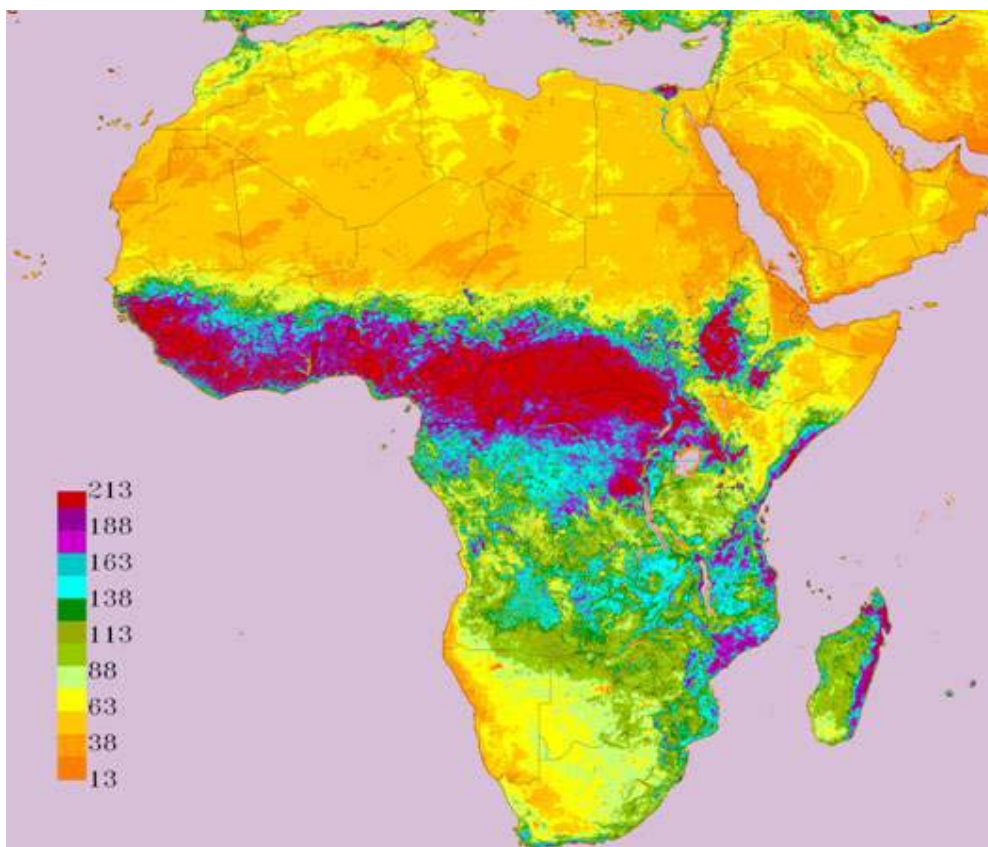


Figure 4. Dekadal NDVI image derived from MSG-SEVIRI data (July 1-10, 2004).

### 2.3 Correlations between MSG SEVIRI and SPOT data

Histograms of SPOT-VEGETATION NDVI and MSG SEVIRI NDVI are presented at Figure 5. Only the cloud-free part of the African continent has been considered. One can notice the wider range of values of SPOT VEGETATION data, which can be explained by the fact that atmospheric corrections have been applied, prior to compute NDVI.

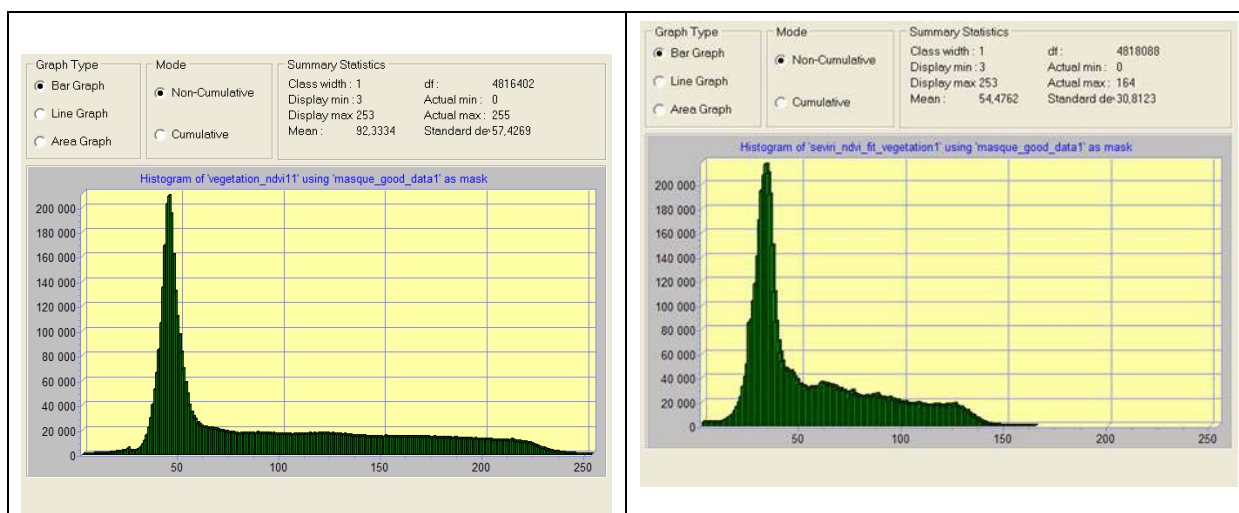


Figure 5. Histograms of NDVI data : SPOT-VEGETATION (left) and MSG SEVIRI (right).

Excluding cloud-contaminated pixels, the correlation between SPOT VEGETATION NDVI and MSG SEVIRI NDVI appears rather high (cf. Figure 6), with a correlation coefficient  $r^2 = 0.87$ .





### 3 CONCLUSIONS AND PERSPECTIVES

Most monitoring studies and early warning procedures rely on present vegetation condition assessment with reference to some statistical values derived from historical data (KOGAN, 1998 and 2000; DePAUW, 2000). Dekadal NDVI derived from NOAA-AVHRR has been routinely used for drought early warning, in spite of coarse spatial resolution of archived data. SPOT VEGETATION provides since 1998 dekadal NDVI data at 1km resolution (VITO, 2005), and operational systems like Drought Global Watch (HEWS,2005) make use of both data sources, with 10 days or one month compositing periods.

The availability of MSG data can contribute to improve drought early warning systems, because of the following advantages:

- data are easily accessible to users, in real time through low cost receiving systems (free data for research purposes, requiring EUMETSAT agreement);
- many receiving systems have been installed in meteorological offices of developing countries through the E. U.-funded Meteorological Transition in Africa Project (PUMA, 2005), non-meteorological applications are now planned with the launch of the AMESD project : African Monitoring of the Environment for Sustainable Development (AMESD, 2005);
- procedures are now developed, based on open software (Linux) to process data and extract daily parameters like NDVI and surface temperature (MSG-ATR,2005);
- as shown in this study, dekadal syntheses of MSG SEVIRI NDVI are of better quality than those of SPOT-VEGETATION, because of improved removal of cloud-contaminated pixels;
- in most areas, it is suggested that MSG SEVIRI can provide NDVI syntheses of good quality for periods of 5 days or less;
- coarse spatial resolution (3 km) remains a limiting factor, but higher resolution is achievable through data fusion of multispectral bands with panchromatic band at 1 km resolution.

### REFERENCES

- [1] AMESD, 2005: African Monitoring of the Environment for Sustainable Development; cf Internet site <http://www.msgafrica.net/>
- [2] DEPAUW E., 2000: Drought Early Warning Systems in West Asia and North Africa. In "Early Warning Systems for Drought Preparedness and Drought Management" (D. A. Wilhite, M. V. K. Sivakumar & D. A. Wood Eds), Proceedings of an Expert Group Meeting held September 5-7, 2000, Lisbon, Portugal. WMO/Technical Document N° 1037, pp. 65-85. World Meteorological Organization, Geneva, Switzerland. available at Internet site [http://www.drought.unl.edu/monitor/EWS/EWS\\_WMO.html](http://www.drought.unl.edu/monitor/EWS/EWS_WMO.html)
- [3] HEWS, 2005: Humanitarian Early Warning Service/Drought Global Watch: Internet Site <http://www.hewsweb.org/drought/>
- [4] KOGAN F., 1997: Global Drought Watch From Space. Bulletin of the American Meteorological Society, 78, 4; 621-636.
- [5] KOGAN F., 2000: Contribution of Remote Sensing to Drought Early Warning of Remote Sensing. In "Early Warning Systems for Drought Preparedness and Drought Management" (D. A. WILHITE, M. V. K. SIVAKUMAR & D. A. WOOD EDS), Proceedings of an Expert Group Meeting held September 5-7, 2000, Lisbon, Portugal. WMO/Technical Document N° 1037, pp. 86-100. World Meteorological Organization, Geneva, Switzerland. available at Internet site [http://www.drought.unl.edu/monitor/EWS/EWS\\_WMO.html](http://www.drought.unl.edu/monitor/EWS/EWS_WMO.html)
- [6] MSG-ATR, 2005: Groupe de Recherches Météosat Seconde Génération-Analyse en Temps Réel. cf. Internet address <http://prodig.univ-paris1.fr/msg/>
- [7] PUMA, 2005: Meteorological Transition in Africa (PUMA Task Team Project). See Internet Page: <http://www.oosa.unvienna.org/SAP/act2003/austria/doc5a.pdf>
- [8] VITO, 2005: Free VEGETATION products. cf. Internet address <http://free.vgt.bitto.be/>

# Sandification Monitoring Using Remote Sensing

X. Wang<sup>a</sup>, Z. Li<sup>a</sup>, Z. Gao<sup>a</sup>, L. Bai<sup>a</sup>, X. Che<sup>a</sup> and F. Wang<sup>a</sup>

<sup>a</sup> Institute of Forest Resource Information Techniques, Chinese Academy of Forestry, Beijing 100091, China, email: wangxh@forestry.ac.cn, zengyuan.li@forestry.ac.cn

**Key words:** multi-temporal images, multi-layer extraction, sandification degree, NDVI, change detection

## 1 INTRODUCTION

China is one of the countries in the world most seriously affected by sand disaster. In 2004, the total sandy land area was 17,397 ha, accounting for 18.12% of the total national land territory. Although sandification condition is much better than that in the late 1990's preliminarily controlling sandy land expansion in whole, sandy land is expanding in part and the whole situation of sandification is serious. Therefore, detection of the status and dynamic of sandy land in time plays an important role in making sandification control strategy.

Remote sensing provides the possibility for monitoring and assessment of sandy land over large areas because of its capability of collecting data frequently, synoptically, and objectively. In recent years, scientists of many countries in the world have studied monitoring and assessment of sandification. It is still an important topic to establish a simple, applicable and operational remote monitoring system of sandification. The paper selected Dengkou county as study area, extracted sandy land based on field survey and image spectral analyses, determined the degree and development of sandy land, and implemented change detection of land cover during the last 10 years with PCA to derive land cover change map.

## 2 STUDY AREA

Dengkou County lies in the southwest of Bayannaoermeng, Inner Menggolia, at 106°9'-107°10'E and 40°9'-40°57'N. This area consists of hilly area, desert, plateau and river. It has a semi-temperate continental monsoon climate dominated by strong winds, rich sand and little rain. The average annual precipitation is 142.7 mm. The average and maximum annual wind velocity is 3 m/s and 24 m/s respectively. The average annual strong wind and sand storm days are 20.2 and 20 respectively. The Soil consists of aeolian sandy soil, ortho brown soil, grey desert soil, saline soil, irrigated warped soil and meadow soil. It is distinctly distributed according to region, with ortho brown soil in hilly area, aeolian sandy soil, grey desert soil and saline soil in desert area, and irrigated warped soil and saline soil in river bend area. The vegetation is desert steppe, including Compositae, Leguminosae, Gramineae, Chenopodiaceae, Zygophyllaceae, and so on. From east to west, xerophyte and extreme xerophyte plants are increasingly dominated.

## 3 METHODOLOGY

### 3.1 Field Survey

In August 2003 and July 2004, two field surveys were performed in Dengkou County. 38 sample plots were investigated in detail. The investigated contents included topography, land use, soil type, soil texture, vegetation coverage, vegetation height, vegetation distribution, vegetation growth, degree of sandification and degree of salinization. Precise position was determined using GPS in each sample plots. To establish the relationship between vegetation coverage and NDVI, line-transect was main method, point sampling and visual observation as ancillary methods [1].

### 3.2 Image Selection and Analyses

Landsat 7 ETM+ images of 4 May 2001 and 20 August 2002 covering Dengkou County were selected for information extraction of sandy land.

Spectral characteristics of shifting sandy land, lake, river, saline and alkaline land, barren mountain and residential land were similar in spring image to those in summer image, but spectral characteristics of farmland, shrub land, semi-fixed and fixed sandy land on which vegetation grew were different in spring and summer image.

In May 2001, semi-fixed and fixed sandy land overlaid with germinating shrub and grass mainly presented the spectral characteristics of sandy land in the image. Some crop came out and didn't come into blossom. Some soil accumulated salt in the surface. According to diversities of crop growth period, farmland presented three types in the image, namely vegetation-covered land, salt-accumulated land and barren land, out of which spectral characteristics of barren farmland and sandy land were difficult to distinguish. Extracted sandy land was often overestimated.

In August 2002, vegetation on sandy land grew vigorously. In the image sandification degrees were divided based on vegetation coverage. On some fixed sandy land vegetation grew too vigorously to cover the land surface. Therefore extracted sandy land was often underestimated. But in the whole spectral value of fixed sandy land was lower than that of farmland.

The paper used multi-temporal images to extract sandy land exactly. Spring image was used to extract sandy land, and then summer image was used to eliminate farmland.

Landsat ETM+ images covering Dengkou County in 20 August 2002 and Landsat TM image in 24 August 1989 were used in change detection of land cover during the last ten years.

### 3.3 Image Preprocessing

Standard atmosphere correction method described in the Landsat 7 Science Data User's Handbook was used in radiometric correction procedure.

Geometric correction of image 2002 was processed based on 1:50000 topographic maps covering the area. More than thirty ground control points (GCP) were used and evenly distributed in the whole image. The nearest neighbor algorithm was used to resample and the second-order polynomial model was used to rectify image. The final root-mean-square error (RMSE) was less than 1 pixel.

Geometric correction of image 1989 was carried out with image 2002 as reference image. The final RMSE was less than 0.5 pixel.

Regression method was processed in relative correction of image 1989 with image 2002 as reference image. Sample sites were selected according to the following criteria, the same elevation, relatively flat areas, and the same amount of vegetation [2], [3].

### 3.4 Information Extraction and Degree Classification

Multi-layer remote sensing information extraction method of sandy land using multi-temporal images was developed based on spectral characteristic analyses.

Sandification degrees were determined according to the land classification standard of China national desertification survey. It was shifting sandy land with vegetation coverage of less than 10%, semi-fixed sandy land with that between 10% and 30%, and fixed sandy land with that of more than 30% [4]. NDVI reflected the relationship between spectral response and vegetation coverage. By regression model, the relationship between NDVI and vegetation coverage was established [5]. Sandification degrees were divided with the threshold of NDVI and the degree map of sandy land was derived.

### 3.5 Change Detection

Image 2002 and image 1989 were stacked to create a twelve-band composite. The composite was used in a PCA to produce six components. Analyzing the components, suitable component was selected. By identifying the threshold of change/non-change, change information was derived [6].

## 4 RESULTS AND ANALYSES

### 4.1 Spectral Analyses

According to the spectral profile of training sites in spring image (Figure 1), the reflectance of clay barren land, sandy land and the gobi was obviously higher than that of other objects in TM band 5 and band 7. TM band 5 and band 7 were middle infrared bands, sensitive to variations in moisture content of soil and vegetation, and reflected the variations of land surface in arid area. TM band 7 was used to separate clay barren land, sandy land and the gobi from other land covers. The reflectance of the gobi and sandy land was similar, but the texture was obviously different. The gobi was smooth in texture and distributed in diluvial fan. Sandy land exhibited dune chain mixed with vegetation. Based on the topography, the gobi was separated. The reflectance of clay barren land was much

higher than that of sandy land in TM band 4. With suitable threshold in TM band 4, clay barren land was separated. The remainder of sandy land and some bare farmland was not distinct from each other. In summer image the reflectance of agriculture plants was relatively low in TM band 3 and high in TM band 4 (Figure 2). According to this, farmland was separated, thus the extraction of sandy land was realized.

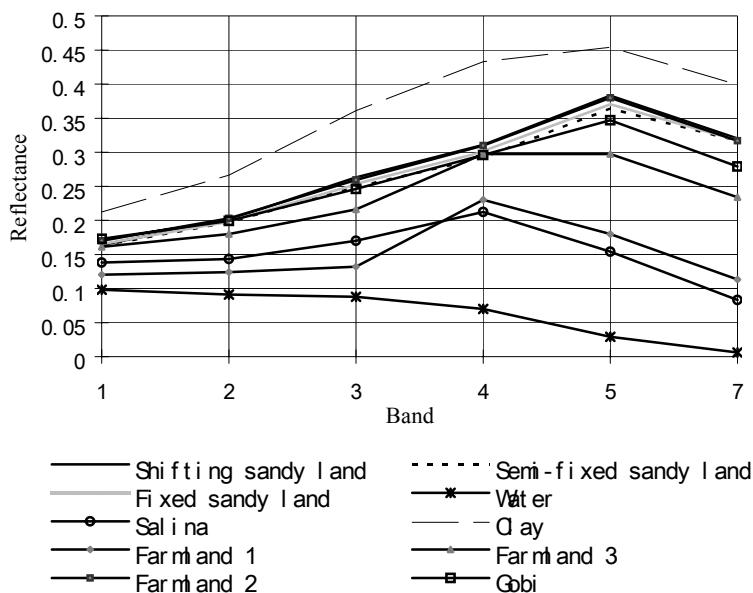


Figure 1. Spectral profile of spring image.

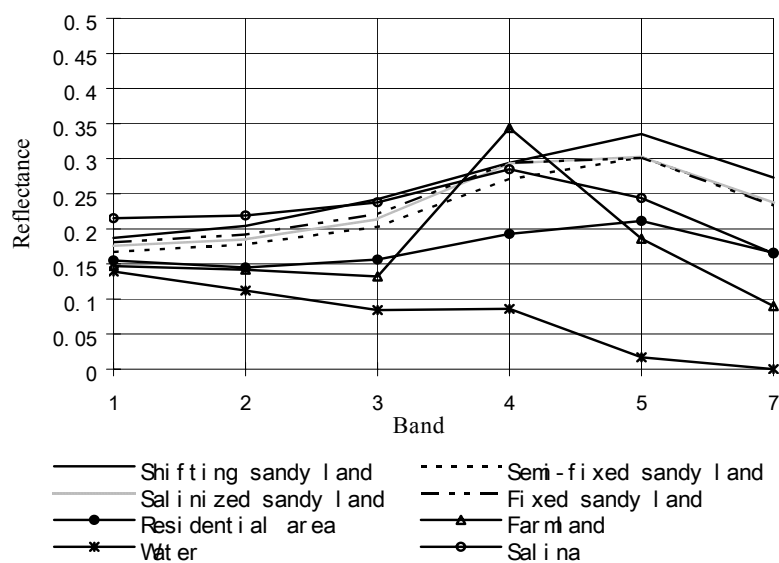


Figure 2. Spectral profile of summer image.



### 4.2 Sandy Land Extraction

According to spectral analyses, multi-layer information extraction of sandy land with spring and summer images in Dengkou was implemented. Figure 3 was flow figure of sandy land extraction.  $\rho_3, \rho_4$  and  $\rho_7$  was reflectance in band 3, band 4 and band 7 respectively, a, b, and c was empirical value determined by interactive method.

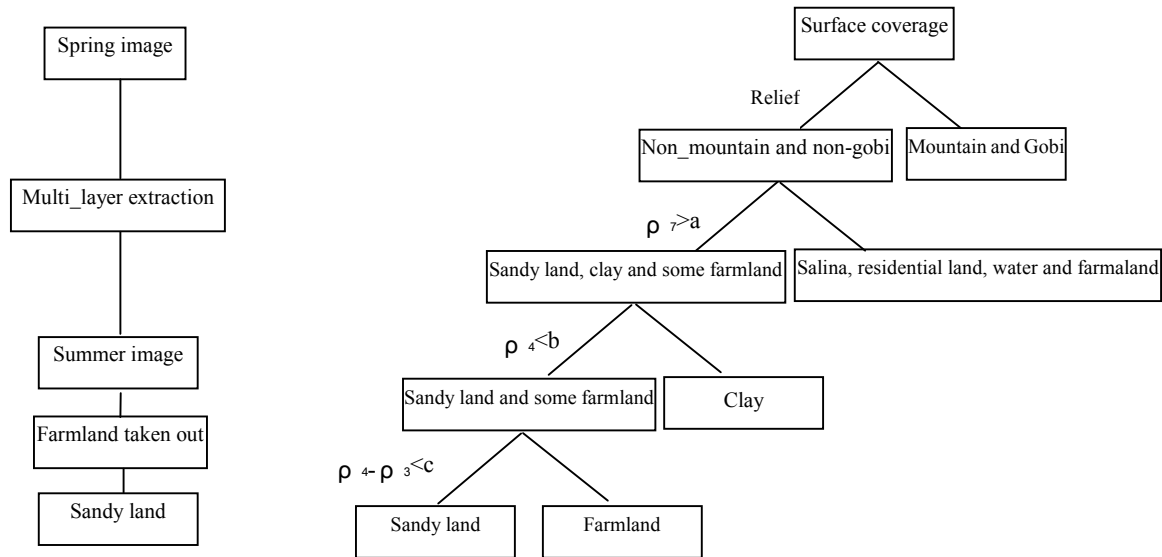


Figure3. Multi-layer extraction of sandy land.

### 4.3 Determination of Sandification Degrees

In the field of remote sensing application, vegetation index was used to quantitatively and qualitatively assess vegetation coverage and energy as an important information source to reflect vegetation information in the land surface. The paper used empirical model to derive vegetation coverage. Empirical model of ground-truth data and NDVI was established. The model was extended to larger region. According to the relationship between vegetation coverage and NDVI, sandification degrees were divided with the threshold of NDVI. The degree map of sandy land was derived.

NDVI was mapped using August 2002 image. 11 sample plots of fixed, semi-fixed and shifting sandy land were chosen to establish the relationship between NDVI and ground-truth vegetation coverage (Figure 4). Linear, polynomial and power regression analyses were implemented, with correlation coefficient of 0.7677, 0.8096 and

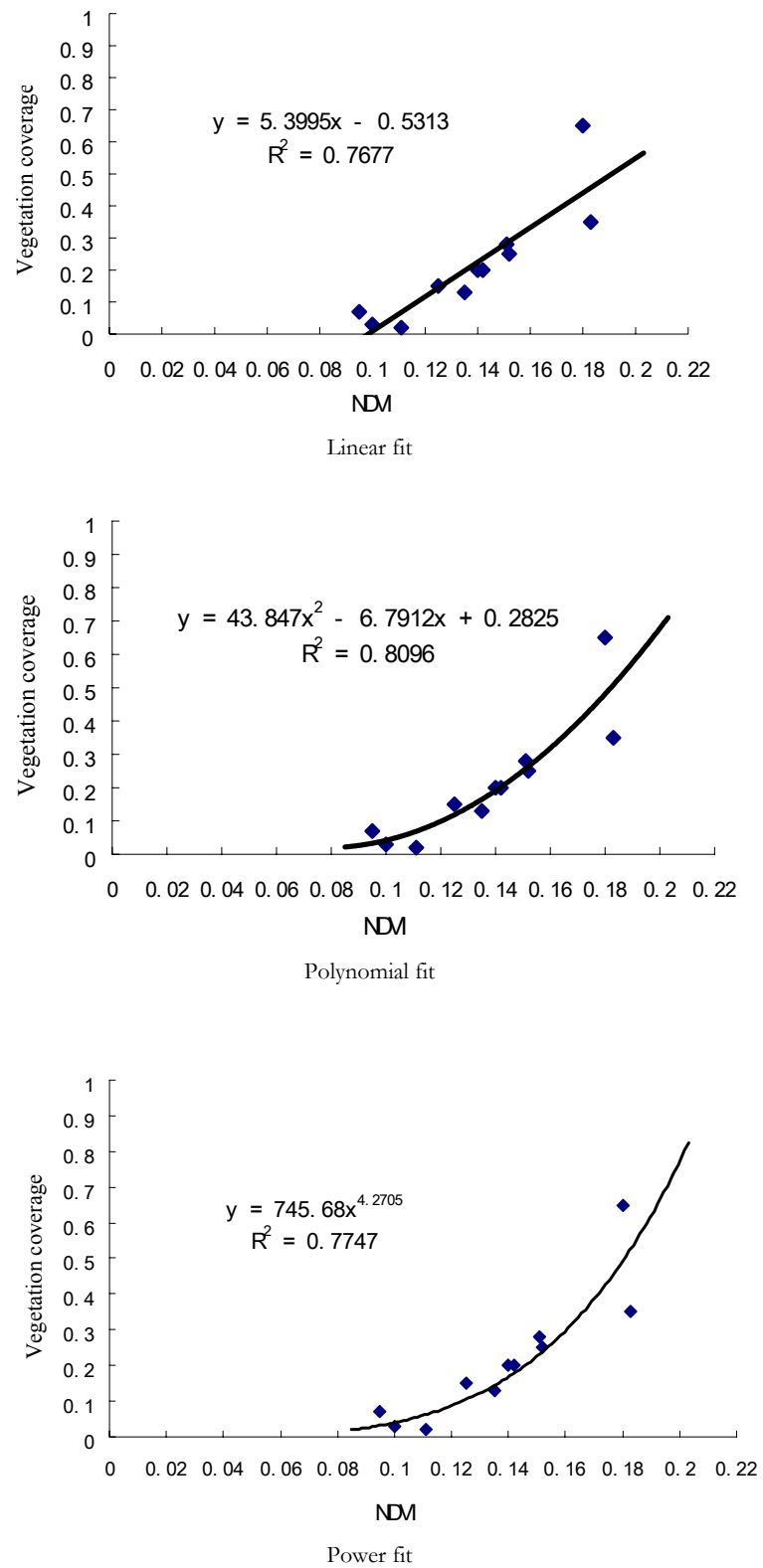
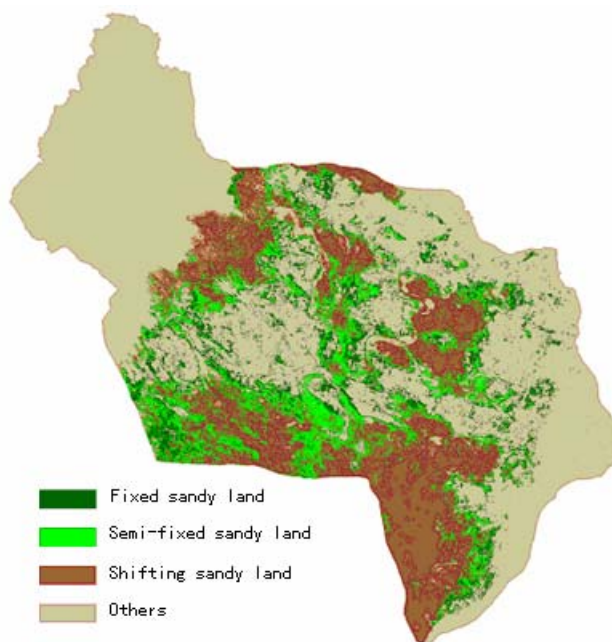


Figure 4. Fit formula of vegetation coverage and NDVI.

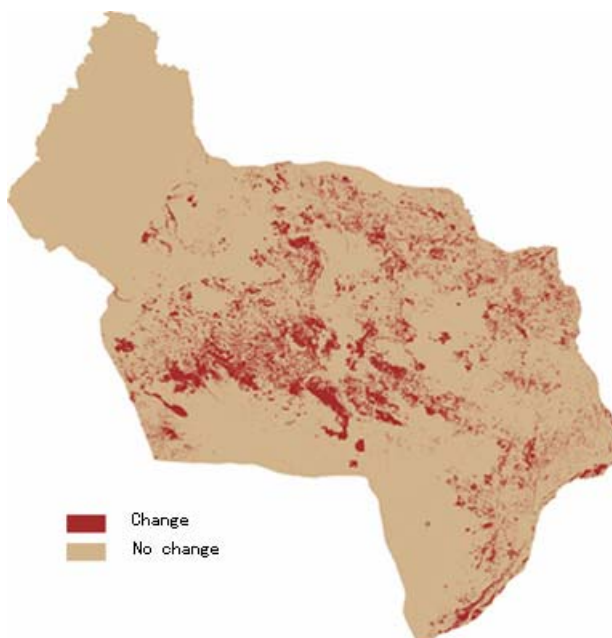


**Figure 5.** Sandy land distribution map in Dengkou.

0.7747 respectively. The second-order polynomial regression has the best fit effect. When vegetation coverage was 10% and 30%, corresponding NDVI was 0.120 and 0.156 respectively, which was used to divide sandification degrees. Distribution map of sandy land was derived (Figure 5).

#### 4.4 Change Detection

Comparing components, the second component had a good effect on change detection. The threshold was selected with statistical measure and interactive procedure [7]. The change image was derived (Figure 6).



**Figure 6.** Land cover change map in Dengkou.

#### 4.5 Accuracy Assessment

Accuracy assessment included three aspects, namely sandy land extraction, degree classification and change detection.

Area-based accuracy assessment was carried out with differential GPS. Accuracy (%) = Total pixels classified correctly / Total pixels. The result was in Table 1. The accuracy of sandy land extraction was 90.8%. The accuracy of non-sandy land extraction was 91.9%. The total accuracy was 90.9%.

**Table 1.** Accuracy assessment of sandy land extraction.

<b>GPS polygon</b>	<b>Total pixels classified correctly</b>	<b>Total pixels</b>	<b>Accuracy (%)</b>
Sandy land	1050	1156	90.8
Among which, Fixed sandy	250	338	74.0
Semi-fixed sandy land	606	624	97.1
Shifting sandy land	194	194	100.0
Non-sandy land	124	135	91.9
Sum	1174	1291	90.9

According to accuracy assessment, the errors were mostly due to omission of some fixed sandy land. Overlaying the image with GPS polygons and contrasting to field survey data, some fixed sandy land missed by extraction was found to lie near the oasis and farmland with good water condition and high vegetation coverage, and during the period of sandy desertification reverse. Other missed class was salinized sandy land mistakenly judged as saline and alkaline land. Other information sources, such as soil and site information should be used to promote the accuracy of sandy land extraction.

Degree classification of sandification was implemented in the inner sandy land. To be independent of sandy land extraction, accuracy assessment of degree classification of sandy land was carried out with GPS points (Table 2).

**Table 2.** Accuracy assessment of sandification degrees.

<b>Type</b>	<b>Producer accuracy</b>	<b>User accuracy</b>	<b>Average accuracy</b>
Fixed sandy land	75.0	100.0	87.5
Semi-fixed sandy land	77.8	70.0	73.9
Shifting sandy land	87.5	77.8	82.7
Total accuracy	80.0		
Kappa	0.7		

Overall accuracy was 80%. Classes of fixed sandy land have the highest user's accuracy of 100%. Classes of semi-fixed sandy land have the lowest user's accuracy of 70%. In sample sites, no semi-fixed and shifting sandy land was misclassified as fixed sandy land. Lots of fixed and shifting sandy land was misclassified as semi-fixed sandy land. More fixed and semi-fixed sandy land was misclassified than shifting sandy land. Semi-fixed and shifting sandy land was misclassified as each other.

For sandy land related changes, including sandy land – farmland, sandy land – water area, shifting sandy land – semi-fixed and fixed sandy land, the overall accuracy was 82.2% (Table 3). The detection effect of change from sandy land to farmland, from sandy land to water area was relatively good, with the accuracy of 80% and 100% respectively. The detection effect of change between shifting sandy land, semi-fixed sandy land and fixed sandy land was relatively worse, with the accuracy of 50%. The method performed well in change detection of sandy land and the other land cover.

**Table 3.** Accuracy assessment of change detection.

Type	Accuracy
Sandy land – Farmland	80.0
Sandy land – Lake	100.0
Shifting sandy land – Semi-fixed and fixed	50.0
Overall accuracy(%)	82.2

## 5 CONCLUSIONS AND DISCUSSION

(1) Remote sensing image with suitable time could have the maximum spectral distinction between sandy land and the other land cover, benefit to sandy land extraction. The paper used integrated multi-season method, overcoming the limitation of single season method that overestimated or underestimated sandy land, thus realized the correct extraction of sandy land.

(2) Based on the image analyses, multi-layer method was used to extract sandy land.

(3) Establishing the relationship between NDVI and vegetation coverage, it was an effective way that sandification degrees were divided with the threshold of NDVI.

(4) To determine sandification degrees, some aspects should be improved in the respect of radiometric correction and field survey. a) The radiometric correction model was improved; b) Visual observation should not be used when investigating vegetation coverage on the sample plot because of its subjectivity; c) The same method was used to measure vegetation coverage in order to avoid from various systematic error. d) Sample plot was located in large and vegetation evenly-distributed area with less variation of land surface type; e) Differential GPS was positioned in the center of sample plot.

(5) PCA has a good result on change detection for sandy land and other land cover. But the method could only provide change/non-change information, which integrates other classification method could provide specific change class information.

## ACKNOWLEDGMENTS

This research is supported by the scientific project of China national “Tenth Five-year Plan”, the study on the integrated technical system of sand control.

## REFERENCES

- [1] YUNXIA, Z., XIAOBING, L. AND YUNHAO, C., 2003: Overview of field and multi-scale remote sensing measurement approaches to grassland vegetation coverage. *Advance in Earth Sciences*, 18, pp. 85-93
- [2] SONG, C., WOODCOCK, C.E., SETO, K.C., PAX LENNEY, M. AND MACOMBER, S.A., 2001: Classification and Change Detection Using Landsat TM Data: When and How to Correct Atmospheric Effects. *Remote Sensing of Environment*, 75, pp. 230-244
- [3] JIANWEN, M., QIQING, L., SIBAGEN, H. AND ZHILI, L., 2003: The endangered rare plant coverage change detection in twelve years by using TM/ETM data. *IEEE*, pp. 3266-3268
- [4] JUNFENG, Z., ZHENDA, Z., ET AL, 1999: *Combating Desertification in China*. China Forestry Press, Beijing
- [5] WENYI, F., CHENGYANG, X., RONGHUA, Y., 2000: Application of hyperspectral remote sensing to desertification monitoring. *Journal of Northeast Forestry University*, 28, pp. 139-141
- [6] MUNYATI, C., 2004: Use of Principle Component Analysis (PCA) of Remote Sensing Images in Wetland Change Detection on the Kafue Flats, Zambia. *Geocarto International*, 19, pp. 11-22
- [7] LU, D., MAUSEL, P., BRONDI'ZIO, E. AND MORAN, E., 2004: Change detection techniques. *Journal of Remote Sensing*, 25, pp. 2365-2407

# Using Earth Observation Data for Assessing Development Impact and Environmental Change in Arid Regions – The Case of the Tarim Basin in Western China

D. Werle<sup>a</sup>, T. Boivin<sup>b</sup>, G. Bruce<sup>b</sup> and W. Yu<sup>c</sup>

<sup>a</sup> Ærde Environmental Research, P.O. Box 1002, Halifax, Nova Scotia, Canada, B3J 2X1  
email: dwerle@ca.inter.net

<sup>b</sup> Hatfield Consultants Ltd., West Vancouver, BC, Canada  
email: tboivin@hatfieldgroup.com and gbruce@hatfieldgroup.com

<sup>c</sup> PetroChina / RIPED, Beijing, China  
email: yuwy@petrochina.com.cn

## ABSTRACT

Western China has been a focus of intensive development for several decades, starting in the late 1950s with the expansion of agricultural oases and, more recently, with oil and gas exploration activities. In 1999, the Central Government of the People's Republic of China has initiated an ambitious "Western Development Strategy". Over a ten-year span, this major government program initially concentrated on development planning and policy formulation and is now proceeding with investments in transportation, energy, communications, urban infrastructure, forestry, mining, minerals and agriculture. The paper examines the potential usefulness of Earth observation satellite data in support of natural resource development and oil and gas exploration activities in the Tarim basin of western China. Project background, scope and the objectives are illuminated first. Then the role of satellite imagery, including Canadian Radarsat-1 data, and its application in oil & gas exploration and environmental assessments is examined. This is followed by a demonstration of the technical remote sensing and geographic information system (GIS) capabilities, using the Kuche area in the Tarim Basin of Xinjiang, western China, as an example. The overview concludes with a discussion of results, an outline of potential benefits and recommendations regarding further Earth observation satellite contributions to ongoing exploration and environmental analysis work.

**Keywords:** Environmental assessment, Tarim Basin, Earth observation satellite data collection and analysis.

## 1 INTRODUCTION

Western China has been a focus of active oil and gas exploration for several decades. The recent discovery of considerable gas reserves in the Tarim Basin has accelerated the development of this natural resource. In 1999, the Central Government of the People's Republic of China has initiated an ambitious "Western Development Strategy". Over a ten-year span, this major government program will concentrate initially on development planning and policy formulation and proceed with investments in transportation, energy, communications, urban infrastructure, forestry, mining, minerals and agriculture.

Natural resources in western China continue to be mapped and inventoried. The exploitation of oil and gas reserves, which account for more than 80 per cent of the national total, awaits the provision of infrastructure and other incentives to ensure profitability. A key component identified and approved by the Chinese government is a major pipeline network to transport natural gas from the production areas in western China to the consumer markets in the East. Environmental assessment, monitoring and management are important components of the development strategy.

The project examines the potential usefulness of Earth observation satellite data in support of specific oil and gas exploration activities and for human safety and environmental assessments in general. It is the result of an international cooperation that has brought together experts from the Remote Sensing Geology Department of PetroChina's Research Institute of Petroleum Exploration and Development (RIPED) and a consortium of Canadian companies under the aegis of Hatfield Consultants Ltd. and Ærde Environmental Research. The Canadian Space Agency and its Earth Observation Applications Development Program (EOADP) provided funding support for the team members to bring this 'Western China Oil & Gas Project' to a successful completion [1].

## 2 PROJECT BACKGROUND, SCOPE, AND OBJECTIVES

The central Government of China and enterprises such as PetroChina are interested in attracting investment and expertise in order to accelerate the development of resource-rich western regions of the country. This includes Chinese businesses as well as international entrepreneurs. In the past, PetroChina's RIPED has had fruitful cooperation with Canada to foster their oil & gas exploration activities. Canada is also being recognized as a leader in Earth observation technology and environmental resource management. These sectors are expected to play a prominent role as the western regions of China develop at a fast pace over the present decade and beyond.

Earth observation satellites as well as GIS are innovative and useful tools for addressing these concerns. Experience in China and in North America has shown that both optical and radar-based imaging instruments can be a reliable source of information. The successful process of image selection, acquisition and analysis not only guides geological and geophysical exploration efforts, but it also assists in the surveillance, assessment and monitoring of environmental conditions in which the exploration and the development effort is taking place.

The RIPED Remote Sensing Geology Department has used routinely American LANDSAT image analysis as an integral part of their mapping program in various parts of the country. The work under the EOADP project offered an opportunity to evaluate the advantages and limitations of imaging radar technology in arid regions. The project team selected as a test area in the Tarim Basin, Xinjiang, and conducted the work with a view toward practical application of two components: (i) oil and gas exploration activities and (ii) environmental monitoring and assessment.

The rationale for the first component is obvious given RIPED's mandate. The rationale for the second component is a result of changing realities within China and the world at large. Multi-national oil and gas companies involved in exploration and development of reserves must, at a minimum, meet environmental standards of their host countries, and ensure that operations interfere as little as possible with local communities and their environments. PetroChina has accepted a stewardship role in this regard, as manifested by strong support for the collaborative Sino-Canadian EOADP project in Xinjiang.

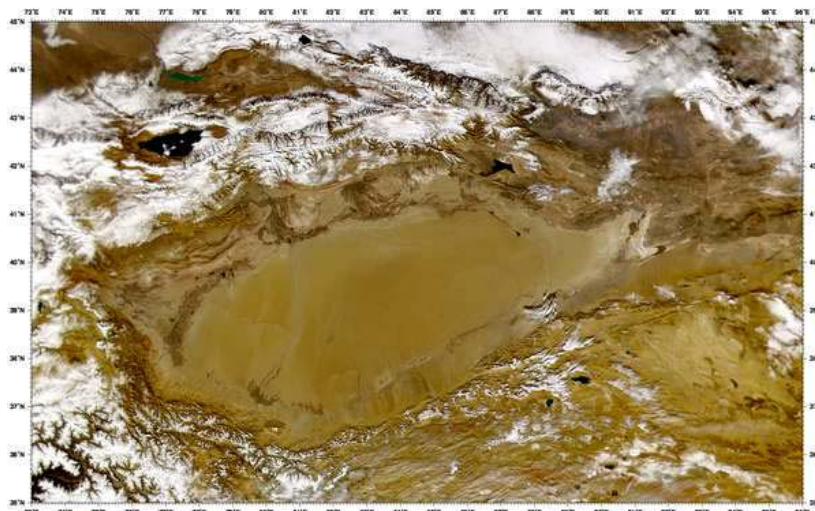
## 3 ENVIRONMENTAL SETTING

The Tarim Basin in western China is one of the world's driest and most land-locked areas with unique environmental systems (Figure 1, Table 1). The area is of historic significance as it was an important part of the transcontinental trade route network, the ancient 'Silk Road'. Today, the Tarim Basin is considered by many to be a frontier region. This perception pertains to the rugged natural setting of the enormous oil and gas exploration and production activities that China is vigorously pursuing within the framework of its national 'Western Development' plans.

The challenges of the physical environment are formidable. The western region as a whole receives little precipitation, and the Tarim Basin, being shielded by the high mountain ranges of the Tian Shan, Pamir, and Kunlun Shan, is particularly arid. The sand desert of the Taklimakan covers a vast territory of more than a quarter million square kilometers, and diluvial gravel gobis, located in the piedmont region around the edges of the basin, are equally expansive.

Kuche, the EOADP project area, is one of the major oases along the edge of the Tarim Basin. Over the course of many centuries, the cultivated area of the oases has expanded and contracted, partly because of natural fluctuations in environmental conditions, and partly because of historical, political and cultural factors. During the 1950's, shortly after the formation of the People's Republic of China, agricultural production in the Tarim Basin, as elsewhere in Xinjiang, received a boost as army construction corps reclaimed large tracts of marginal lands and constructed new irrigation and drainage canals and water reservoirs.

Geological exploration efforts over the past decades have led to rich discoveries. PetroChina has found 12 gas fields in Tarim Basin, with proven gas reserves of 450 billion cubic meters and possible gas reserves of 400 billion cubic meters. The Kuche Depression, as it has been named by geologists, may become one of the most important gas regions in China, with potential gas resources of more than 2.2 trillion cubic meters. The exploration activities have culminated in the current development boom that started during the 1990's with major infrastructure projects, including highways, railroad, pipelines and other petro-chemical installations, and a vigorous urban expansion program.



**Figure 1.** Satellite image map of the Tarim Basin showing the Taklamakan Desert (1) in the centre of the basin, surrounded by numerous oases, such as Kuche (2), that are fed by meltwater streams from the snow-covered mountain ranges. The image was acquired by the SeaWiFS sensor on December 7, 1999. (Source: SeaWiFS Project, NASA/Goddard Space Flight Center, and Orbimage.).

**Table 1.** List of main geographical features and environmental issues in the Kuche project area.

Features / Issues	Tien Shan (southern slopes)	Tarim Basin (northern periphery)
Topography	Erosional high mountains (fold block system with intermontane rift basins (2,000-6,000m)	Denudational mountains & hills (piedmont foothills, 1,000-2,000m). Stony, gravel terrain (gobi), sandy terrain (sandy desert)
Climate	Nival alpine terrain (>3,500m) Air current barrier, air subsidence (foehn) effects Strong local wind regimes	Clay silt terrain (alluvial plains, marshes) Warm-temperate climate with scarce rainfall (<100mm/yr) and high evapo-transpiration, 180-240 frost-free days, 3,000-5,000 hours of sunshine
Vegetation	Arid & semi-arid montane desert, Grasses & meadows Periglacial cushion vegetation	Low density, xerophilous shrubs (Tamarisk steppe, goosefoot)
Land use	Meso-xerophilous shrubs, small tracts of birch & spruce woodland Animal husbandry (grasslands) Grazing on mountain slopes	Salt marshes, desert reeds Poplars Oasis agriculture (intensive, with irrigation), animal husbandry (extensive)
Settlements & transportation	Small hamlets Some historic fortifications at important passes	Regional center (Kuche), towns, villages Highway & sand road, roads & trails, rail road, airport
Resource extraction	Small mining operations Road construction	Oil & gas exploration & production Small mining operations Highway & road construction
Desertification	Potential overgrazing	Water reservoir, drainage/dyke construction Reduction in stream flow, Reservoir siltation Soil salinization of arable land Lowering of ground water levels
Natural hazards	Erosion, landslides, flashfloods Snow & ice storms	Floods & flashfloods Sand storms, drought
Regional development	Construction & maintenance of roads, mountain passes	Human safety & environmental protection; O&G exploration and production sites, roads, settlements, water supply



#### 4 EARTH OBSERVATION DATA

There are extensive on-line archives available at various space agencies and affiliate organizations around the world. The EOADP project relied on high resolution LANDSAT and RADARSAT image archives and MODIS data banks in North America, although SPOT and ERS archives in Europe also contained valuable high-quality Earth observation data (Table 2, 3). An often overlooked source of information is the growing archive of astronaut photography reaching back to the early days of manned space flight in the 1960s. The recent addition of high quality photography from the International Space Station has added even greater value to the archive.

The record of available LANDSAT imagery for the Kuche area goes back more than four decades (Table 3). The recent release of American spy satellite data collected during the Cold War period under the CORONA Program represents an additional and surprisingly detailed source of imagery that predates the LANDSAT program by a full decade. The experimental Shuttle Imaging Radar A and Shuttle Imaging Radar SIR-C/X-SAR missions were carried out for short periods of time in the 1980s and 1990s. They also offer a unique, if only selective, perspective on the varied terrain features of the Tarim Basin. The ASTER instrument is able to record detailed imagery at a 10 m resolution.

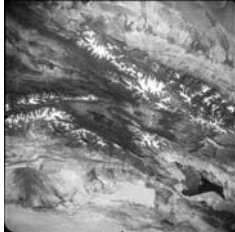
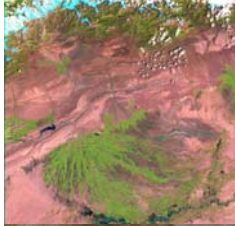

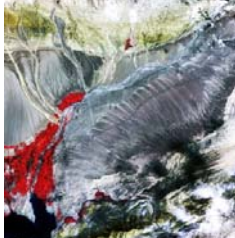

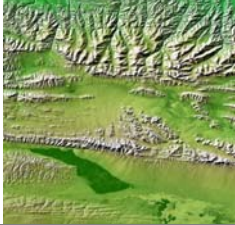
On a daily basis, the NASA and affiliate organizations in the United States provide a near-real time MODIS data stream over the World Wide Web at resolutions as good as 250m and as coarse as 2 km. At a higher spatial resolution, albeit at coarser temporal resolution of about once a week, the Canadian RADARSAT program is also capable of providing imagery on a near-real time basis, where data delivery can be arranged within an hour or two of the actual radar data acquisition. The main advantage for using radar is the fact that imagery can be recorded independent of cloud cover or day time / night time, especially during environmental emergency situations.

The satellite data selection strategy for the EOADP project was threefold: (i) to obtain good area coverage for landform and terrain analysis; (ii) to obtain good spectral coverage, in terms of both visible and infra-red bands for land cover, hydrology and geology analyses and radar for cloud-penetration and special terrain identification; and (iii) to obtain good temporal coverage, in terms of both long-term (*e.g.* decadal) and short term (*e.g.* seasonal) change detection in the landscape, for land cover and for land use.

**Table 2.** Summary of the main data and information sources for the EOADP project.

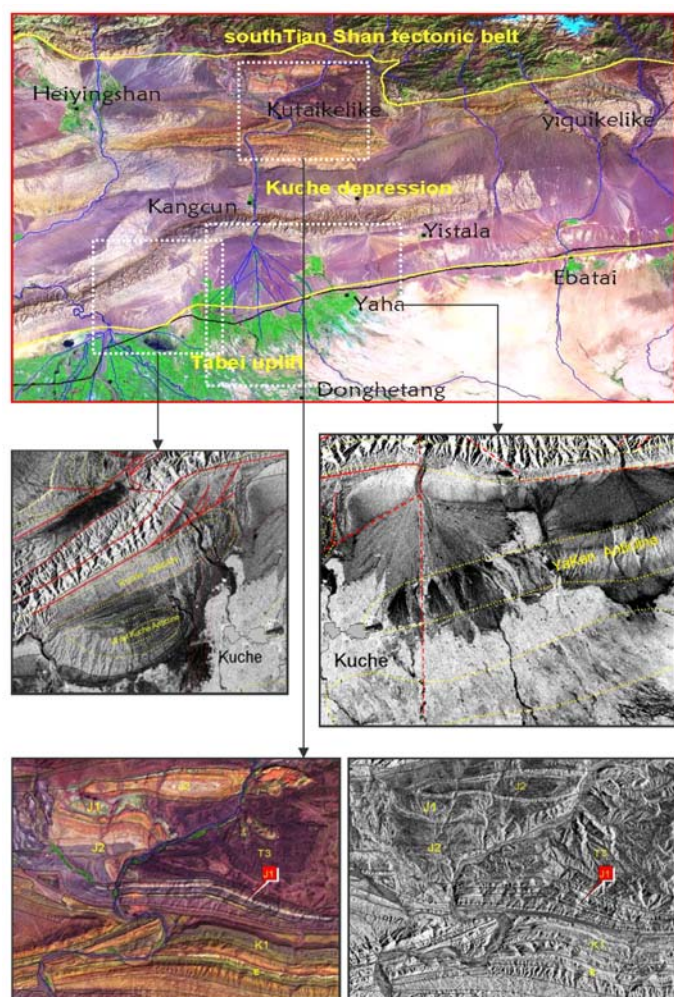
Remote Sensing	Thematic Maps	Literature	WWW
Astronaut photography: Space Shuttle International Space Station	Topographic maps: various scales from 1:50,000 to 1:2M	Scientific journals: RS / GIS, Environmental management, earth sciences & geography	Queries: Satellite image archives, thematic maps, literature
Satellite imagery (archive data): Landsat MSS & TM, Radarsat-1, X-SAR, Corona, Aster, MODIS, SeaWiFS	Digital elevation models (DEM): Various scales from 1:100,000 to 1:1M	Monographs: Oil exploration in China, regional geography, remote sensing	Data access and ordering: Landsat, Radarsat, Corona, Modis, X-SAR
Satellite imagery (near-real time): MODIS, Radarsat-1, weather satellites	Thematic maps: Land use & land cover maps at various scales from 1:100,000 to 1:1M	Reports: Government publications, contractor reports	News items: Oil & gas sector, regional news

**Table 3.** Selected remote sensing data sets for the Tarim Basin, their sources, and their characteristics in terms of spatial, spectral and temporal resolution and coverage.

Satellite Sensor & Application	Resolution	Bands	Coverage	Tarim Sample Imagery
CORONA (1960s US spy satellite) <a href="http://usgs.gov">http://usgs.gov</a> (Earth explorer) Historic land cover data, topographic mapping and terrain analysis (1960s)	1-8 meter	Panchromatic black & white photography	Intermittent; 10 to 300 km wide swath	
LANDSAT MSS and TM (1972 - present) <a href="http://glovis.usgs.gov/">http://glovis.usgs.gov/</a> Regional geological mapping, land use mapping and seasonal environmental monitoring	15-30 meter	5-8 bands in the visible & IR, pan	>2-3 weeks; large archive (3 decades); 185km wide swath	
MODIS (1999 - present) <a href="http://rapidfire.sci.gsfc.nasa.gov/">http://rapidfire.sci.gsfc.nasa.gov/</a> Basin-wide environmental surveillance and monitoring (e.g. snow, vegetation, flood)	250 meter - 4km	36 bands in the visible & IR	< 1 day, 2200 km wide swath	
ASTER (2000 - present) <a href="http://glovis.usgs.gov/">http://glovis.usgs.gov/</a> Detailed regional land use mapping and terrain analysis	15-90 meter	14 bands in the visible & IR	Infrequent (experimental), 60 km wide swath	
RADARSAT-1 Synthetic aperture radar (SAR) (1995 - present) <a href="http://www.ccrs.nrcan.gc.ca">www.ccrs.nrcan.gc.ca</a> Basin-wide and regional terrain analysis, structural-geological mapping, land use monitoring	10-100 m	C-band SAR with different angles of illumination	Every 5 to 24 days 50-500 km wide swath	
SIR-C/X-SAR and SRTM (1994/95, 2000) <a href="http://southport.jpl.nasa.gov/">http://southport.jpl.nasa.gov/</a> <a href="http://isis.dlr.de/XSAR">http://isis.dlr.de/XSAR</a> Experimental mapping	20-30 meter	SIR-C: C & L band X-SAR: X-band only	Experimental missions in 1994/95 and in 2000; 20-50 km wide swath; large area DTM mosaics	

## 5 FIELD PROGRAM AND TECHNICAL CONSULTATIONS

The Sino-Canadian study team planned and executed a field program in Xinjiang, western China, during the month of September 2002, and conducted several technical consultation meetings in Vancouver, Ottawa and Montreal, Canada, during the months of June, 2002, and February, 2003.



**Figure 2.** Example of satellite image analyses pertaining to geological structure in the Kuche region. The regional overview image (top) consists of a Landsat TM image; it also indicates the location of the three detailed study areas depicted below. The black & white subsets consist of Radarsat-1 SAR imagery. These tend to enhance structural detail (centre, bottom right), whereas Landsat TM colour imagery provides better indication of lithological differences (bottom left). (Source: Radarsat imagery courtesy of the Canadian Space Agency and RSI; Landsat TM imagery courtesy of the US Government.)

requirements and expectations for the environmental assessment component of the study.

### 5.1 Example: Geology and Oil & Gas Exploration

The Tarim Basin formed as the result of relatively recent plate tectonic movements of the Indian subcontinent and the Asian landmass. The dominant factor influencing the northern margin of Tarim Basin lies at the ENE right slip fault. This tectonic movement has not ceased, as was demonstrated by the major earthquake in the Aksu region in February, 2003. RIPED has conducted extensive research on the surface stratigraphy and internal structure of the Kuche Depression and Tabei Uplift using optical LANDSAT and SPOT imagery as well as airborne remote sensing data. With the exception of one IRSA research project using SIR-C imagery, little experience is available with regard to the potential of radar. Hence, this project concentrated on a comparative analysis of both LANDSAT and RADARSAT imagery after integrating, or fusing, the data sets in a digital fashion. Standard techniques such as Intensity – Hue – Saturation (IHS) were used to enhance the detection of lithological and structural features within various terrains.

The primary objective of the program in Xinjiang was the collection of field observations and the verification of the remote sensing image analysis results. Canadian team gained a first hand perspective of the social and natural environment in the study area and had an opportunity to meet with local and regional officials. The visit allowed the project team to assess terrain conditions, geological features, as well as environmental concerns and management practices in order to better validate the use of satellite data. Despite the remoteness of the study area in general and specific test sites in particular, the excellent coordination, planning, and field logistics provided by RIPED made the trip successful. The project team was also well prepared from a technical perspective for the fieldwork. The team had all the necessary data, maps, and images to conduct their fieldwork and contributed valuable information to the project. During the field program there was considerable discussion about the environmental requirements for the project. The need for a multi-disciplinary approach towards managing and assessing environmental issues was emphasized. The exchange demonstrated the value of increased cooperation between remote sensing and GIS experts and environmental experts across the boundaries of professional disciplines and administrations. The technical consultation meetings in Canada proved beneficial from several perspectives. Visiting delegations from RIPED's Remote Sensing Geology Department gained a first-hand appreciation for environmental assessment procedures and practitioners in Canada and formed linkages with the Earth observation sector in various parts of the country through visits at industrial facilities and institutions such as the Canada Centre for Remote Sensing and the Canadian Space Agency. The consultation program provided an opportunity to exchange ideas and gain an appreciation for the data

Radar has some unique imaging capabilities that set it apart from optical sensors. It can detect dielectric features and surface roughness and has the ability to undertake Earth observation under all weather conditions. The Canadian RADARSAT is very flexible imaging system. A variety of imaging modes can acquire data at various angles of radar illumination (incidence angles), at various levels of spatial detail (10-100 m resolution) and areal coverage (50 to 500 km swath widths). These qualities are advantageous for detailed terrain observation in arid regions such as the Kuche area in Xinjiang. At a very detailed scale, RADARSAT can detect changes in micro-topography by detecting changes in surface roughness. Take the Yaken anticline as an example: this subtle structural feature near Kuche is covered by Quaternary alluvium. There is a clear difference in the radar signatures between the northern and the southern section of the alluvial fan. This is related to the difference in particle sizes in the alluvial fan, revealing the position of the anticline as its westward dip. By comparison, the LANDSAT TM image primarily reveals little difference in the spectral reflectance behaviour of the surface materials and the existence of the anticline in this area remains obscure (Figure 2).

At a regional scale, RADARSAT Standard mode imagery also highlighted a group of nearly north-south trending linear features. These are closely related to tension and compression structures in the margins of the upper Basin. The shear-tension fault system in the Shaya marginal uplift zone is of the middle Mesozoic, Cretaceous – Tertiary age and often associated with oil and gas deposits. Studies have shown that structural network of these faults act as vertical passages for oil and gas migration and allows for the formation of traps over deep-seated oil and gas deposits. On the radar images five left slipping faults along the northern Kuche anticline are clearly identified in the images. These features are not easily identified in the LANDSAT TM imagery.

However, in terms of its ability to detect the lithology of rock outcrops, RADARSAT is considered inferior compared with LANDSAT. This was found to be the case especially in areas of high relief. The interpretation of formations in this study has relied heavily on Landsat TM images while Radarsat images were used primarily as reference. The analysis of faults in high relief areas was also primarily based on Landsat TM images (Figure 2). At a basin-wide scale, the collection of MODIS imagery provided synoptic views of the diverse topography and the drainage network, and their relationship to important structural setting of the entire Tarim Basin. Year-round monitoring of environmental conditions can be of considerable benefit to geological analyses.

## 5.2 Example: Environmental Monitoring and Assessment

Environmental Assessment is a process that identifies and documents potential environmental, social and economic implications associated with proposed development activities. Specific development options are evaluated according to their potential to cause significant impacts on environment, society, and economy. The process ultimately results in the selection of the most appropriate development strategy.

The EOADP project explored how components such as baseline data collection, environmental monitoring, and the management of spatial data sets associated with environmental assessments can be implemented through the use of a satellite remote sensing and GIS. The team of experts reviewed general background and descriptions of Environmental Impact Assessments and provided an overview of how the EIA regulatory and procedural framework evolved in China. The “Management Procedures for Environmental Protection of Capital Construction Projects” issued by China’s State Council in 1998 show the trend toward specific provisions regarding cleaner production, the inclusion of ecological effects, and the introduction the “regional environmental impact assessment” concepts.

Currently, resource extraction and exploration activities in Xinjiang are primarily assessed according to project specific impacts on the receiving environment, and to a lesser degree by the regional environmental impacts associated with multiple developments. Field observation by the EOADP team revealed that PetroChina’s site operations were very well managed, with limited environmental impacts. Environmental protection, engineering and management appeared to be of a high standard at the facilities visited.

However, the implementation of oil and gas extraction facilities in Xinjiang will incur environmental impacts not only from exploration, site development, extraction, product storage and transportation, and site closure and rehabilitation, but also from all the activities that are necessary to support these facilities; these include increases in: population, primary resource demand, urban sprawl, waste-streams, public health requirements and infrastructure. In fact, the environmental implications of secondary activities are considerably greater than the direct impacts resulting from the development of oil and gas extraction facilities.

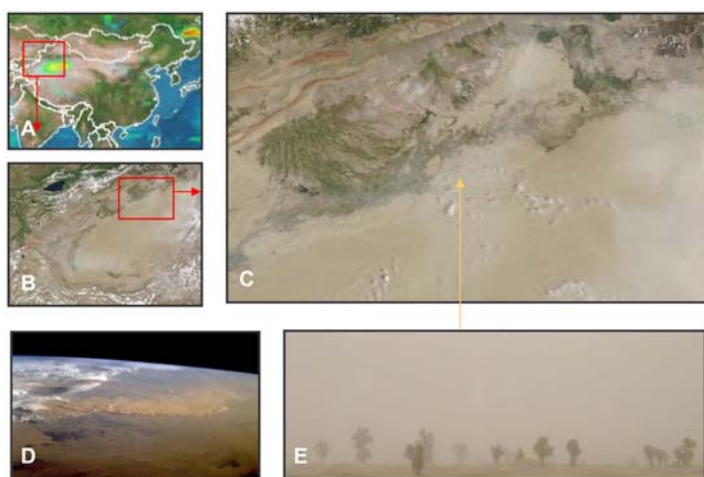
Earth observation satellite data and GIS are the ideal tools for managing strategic environmental assessments given the regional scope of development activities in Xinjiang. The EOADP project provided several examples of how satellite imagery can be used to advantage for environmental assessment at the basin-wide level, as well as on the regional and, to albeit limited extent, at the local level (Figure 3, 4 and 5). At the regional level, limited time series of RADARSAT and LANDSAT imagery provided an excellent account of land use features as well as changes in



the natural and made-made environment (Figure 6). A combination of multi-temporal RADARSAT imagery and Landsat imagery not only revealed the present status of the oasis agriculture and the hydrological network, but it also showed the dynamic nature during different seasons. Moreover, a comparison of recent satellite data with older LANDSAT MSS imagery collected during the 1970s and CORONA satellite photos collected during the 1960s provided an excellent 'historic' perspective on land use development and environmental changes in the Kuche region of the Tarim Basin.



**Figure 3.** MODIS image of the Tarim river flood during the month of August, 2002. The main course of the river and flooded areas are depicted in black; the oases appear in green, and the snow- and glacier-capped mountains in red. The image covers an area of 850 km by 350 km; the spatial resolution is 500 m. (Source: MODIS Science Team, NASA).



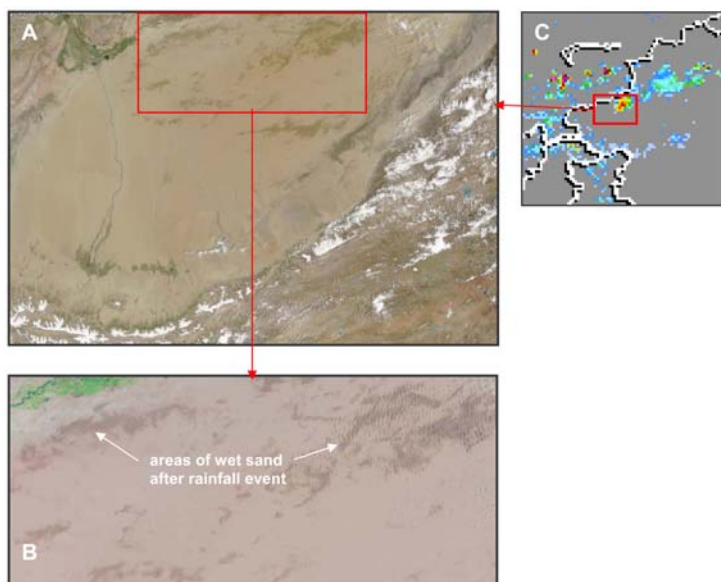
**Figure 4.** Satellite imagery (A,B, C), astronaut photography (D) and ground photograph (E) of a dust storm event in the Tarim basin on May 10, 2003. The concentration of airborne dust particles, or aerosols, is recorded daily (A, top left), at low resolution in near-real time by TOMS, a Total Ozone Mapping Spectrometer. The MODIS imagery (B, C) records dust storms at a far more detailed resolution of 500 m. (Source: Spaceborne images courtesy of NASA, Ground photo courtesy of RIPED).

## 6 CONCLUSIONS

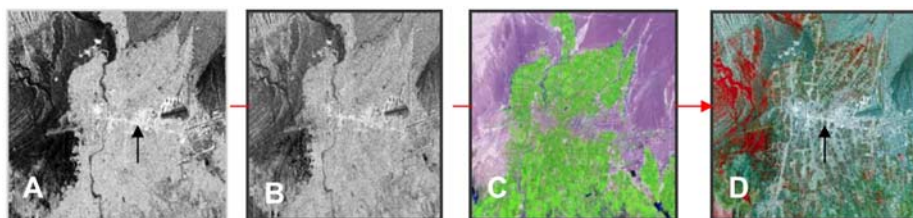
The Sino-Canadian EOADP team met two broad sets of objectives during the execution of this project. These relate to overall project goals and to technical achievements.

In a programmatic sense, the project helped all parties involved to better achieve their mandate and commitments. It provided RIPED technical staff with opportunities to handle and process RADARSAT and other Earth observation satellite data and to gain an appreciation of its strengths and weaknesses. It provided Canadian team members with insights of opportunities within China, whereas Chinese team members were able to assess first-hand a variety of Canadian technologies and get to know Canadian institutions dealing with space technology and environmental issues in arid regions. The second broad set of objectives relate to the specific technical goals of the project, aimed at investigating the use of satellite remote sensing and GIS for the dual purpose of oil and gas exploration and environmental assessment in the Kuche region of Xinjiang. The following conclusions were developed related to these two technical components. The project demonstrated to remote sensing and geological experts at RIPED that MODIS and RADARSAT provide useful information to complement LANDSAT satellite data for the purposes of oil and gas exploration in dry regions. In fact, information on geological structures was derived from a variety of satellite data sources, and it was used to support and guide other types of geological studies, for example seismic surveys. RADARSAT data support observations of subtle anticlines and other structural features that are less prominent on optical imagery. Analysis of multiple sources of radar and optical remote sensing data were used to develop and test structural-tectonic models based on a combination of underlying geological and tectonic principles and observable terrain features. Furthermore, multi-date comparisons of satellite data provided a unique regional perspective of seasonal fluctuations of environmental processes and land use patterns. Long-term trends on the order of decades can often also be discerned using archival LANDSAT MSS and CORONA imagery in conjunction with recent data acquisitions. MODIS satellite data offered regional and basin-wide perspectives and

context for local and regional trend analyses concerning urbanization, agriculture, as well as water distribution and use. A combination of multi-source satellite data and GIS provides an ideal platform for developing water resource monitoring and management strategies. The environmental impacts of individual oil and gas exploration and extraction facilities appeared to be minor. Facilities were engineered to a high standard with small environmental “footprints”. Most of the environmental impacts were related to the overall rapid pace of regional development. Yet, the two issues are closely linked. Systematic collection and careful analysis of Earth observation satellite data can potentially play an important role to improve environmental management at various scales ranging from the site and project specific scale to synoptic and strategic considerations.



**Figure 5.** MODIS satellite imagery collected on July 15, 2003 after a significant rainfall event in the Tarim basin. The overview (A) and detailed (B) images show in dark image tone the location of wet sand surfaces in the Taklamakan desert; area B covers an area of ~ 400 km x 200 km. The rainfall event (C) was recorded days prior by the Tropical Rainfall measurement Mission, TRMM; area C depicts the westernmost portion of China; areas of high intensity precipitation are shown in yellow and red. (Source: MODIS and TRMM imagery courtesy of NASA).



**Figure 6.** Example of merging Radarsat-1 SAR imagery (~15x15 km) of different dates (A, B) with Landsat TM imagery (C) to form a colour composite SAR-TM image (D). This type of imagery is useful for land use analyses and change detection. Note the very bright signatures of built-up areas (in this case the city of Kuche, see black arrow) provided by the radar data. (Source: Radarsat imagery courtesy of the Canadian Space Agency and RSI; Landsat TM imagery courtesy of the US Government).

## ACKNOWLEDGMENTS

The work described in this paper is the result of an international cooperation that has brought together experts from the Remote Sensing Geology Department of PetroChina’s Research Institute of Petroleum Exploration and Development (RIPED) and a consortium of Canadian companies under the aegis of Hatfield Consultants Ltd. and Ærde Environmental Research. The Canadian Space Agency (CSA) and its Earth Observation Applications Development Program (EOADP) provided funding support for the team members to bring this ‘Western China Oil & Gas Project’ to a successful conclusion.

## REFERENCES

[1] HATFIELD CONSULTANTS LTD., 2003: Applying remote sensing to oil and gas exploration and environmental assessment in western China. HCL Summary Report, 31 p., West Vancouver, Canada.

# Monitoring floodplain dynamics in the Sahel region to detect land degradation processes

T. Westra<sup>a</sup> and R.R. De Wulf<sup>a</sup>

<sup>a</sup>University of Ghent, Department Forest and Water Management, Coupure Links 653, 9000 Ghent, Belgium, email: Toon.Westra@UGent.be

## ABSTRACT

Most of the major rivers in the Sahel region of West-Africa contain extensive floodplains. These floodplains have a high ecological and economical value. Local communities make use of the floodplain for agriculture, fishing and dry season grazing. The productivity and carrying capacity of the Sahelian floodplains are highly correlated with the extent of the flooding.

Fourier analysis of Moderate Resolution Image Spectrometer (MODIS) time-series data was applied to monitor flooding extent of the Waza-Logone floodplain, located in the north of Cameroon. Fourier transform (FT) enabled the quantification of the temporal distribution of the MIR band and three different indices: the Normalized Difference Vegetation Index (NDVI), the Normalized Difference Water Index (NDWI) and the Enhanced Vegetation Index (EVI). The resulting amplitude, phase and amplitude variance images were used as inputs for an Artificial Neural Network (ANN) to calculate flooding extent for the different years in the time-series. Different combinations of input variables were evaluated by calculating Kappa Index of Agreement (KIA) of the resulting classification maps. The combinations MIR/NDVI and MIR/EVI resulted in the highest KIA values. When the ANN was trained on pixels from different years, a more robust classifier was obtained, which could consistently separate flooded land from dry land for each year.

A rainfall-runoff model will be used to simulate streamflow of the Logone river based on 10-day African Rainfall Estimates (RFE). Once such a model is calibrated for the catchment area, the relationship between streamflow distribution and flooding extent will be analyzed.

**Keywords:** Floodplains, Sahel, time-series analysis, MODIS, rainfall – runoff model

## 1 INTRODUCTION

Most of the major rivers in the Sahel region of West-Africa contain extensive floodplains. These floodplains are temporally inundated most years, caused by over bank flooding of the rivers. Flooding starts at the end of the wet season and lasts three to five months, providing the floodplain with nutrients and sediments. The maximum extent of the flooding varies one year to another in response to the amount rainfall in the catchments area. In an average year the total inundated area of the major floodplains in the Sahel is about 67,000 km<sup>2</sup> [1].

The Sahelian floodplains are of high ecological value. They play an important role in the conservation of biological diversity both on a global and a local scale. The floodplains have an important economical value as well. Local communities, both resident and nomadic, make use of the floodplain for agriculture, fishing and dry season grazing. The vegetation on the floodplains consists mainly of perennial grasses. These grasses have a higher annual biomass production and a longer growing cycle than annual grasses and therefore provide high quality fodder for wildlife and livestock during the dry season. In areas where floodwater is absent for several years, soil condition deteriorates, since soil moisture and nutrients are not replenished anymore, and perennial grasses are replaced by less productive annuals. The availability of perennial grasses, the size of the fish stock and the soil moisture availability for the growing of crops are all correlated with the extent of the flooding. As a consequence the income of the local communities highly depends on the flooding extent as well [1].

Due to their extent and inaccessibility, monitoring the Sahelian floodplains is only feasible by means of remote sensing. In this study, a Moderate Resolution Image Spectrometer (MODIS) 16-day 250m time-series data is used to monitor the yearly flooding extent for the Waza-Logone floodplain, located in the North of Cameroon. Both the MIR band and the Normalized Difference Water Index (NDWI) [2] are sensitive to the presence of water, whether it is free water or water contained in plants, providing information on the inundation pattern. Analysis of the temporal profiles of the Normalized Difference Vegetation Index (NDVI) and the Enhanced Vegetation Index

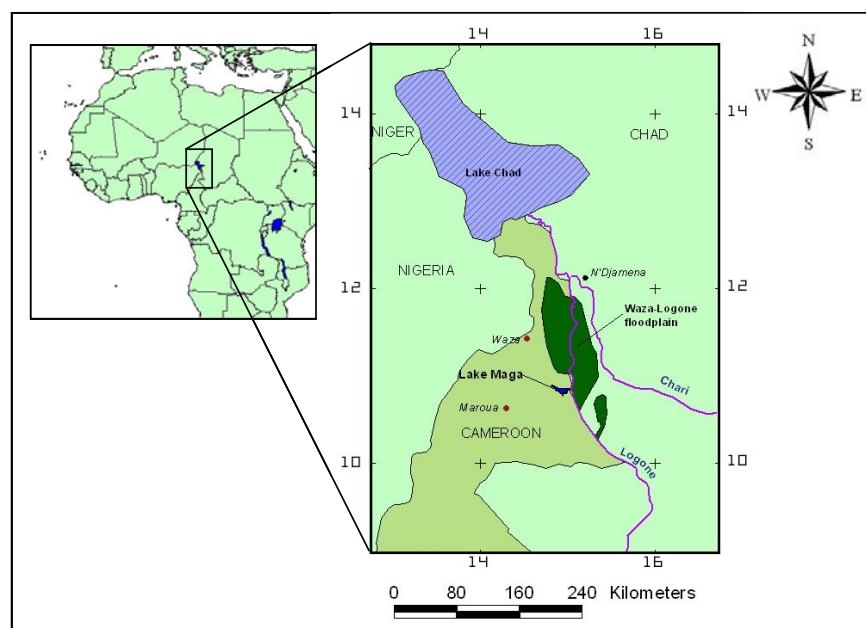
(EVI) [3] enables differentiation between perennial grasses covering the floodplain and annual grasses covering the surrounding dry land, the latter having a shorter growing cycle.

The Fourier Transform (FT) will be used to quantify the intra-annual changes of the different indices and the MIR band. FT decomposes a time-series into a number of periodic signals with different frequencies, characterized by a phase and amplitude value. Similar approaches have been used to classify vegetation types, based on Advanced Very High Resolution Radiometer (AVHRR) NDVI time-series [4] [5] [6]. In this study, phase and amplitude values for those periodic signals explaining most of the time-series variance will be used to differentiate between flooded land, dry land and irrigated rice utilizing an artificial neural network (ANN).

To model the relationship between the amount and distribution of precipitation in the catchments area of the Logone River and the predicted flooding extent, 10-day rainfall estimates (RFE) for Africa [7] will be used. First, a rainfall-runoff model will be established to simulate streamflow in the Logone catchment area. subsequently, the relationship between streamflow and flooding extent will be analyzed.

## 2 STUDY AREA

The Waza-Logone area is located in the Far North province of Cameroon, i.e. in the semi-arid zone of Africa (figure 1). It stretches from Nigeria across northern Cameroon to Chad, approximately between 10°50'N and 12°30'N, and between 14°0'E and 15°20'E. The average rainfall in the area is 650 mm/ year and the rainy season is from May to September [8]. Rainfall is highly unpredictable, both in space and time, yet all the rain is concentrated in the wet season. Locally, the amount of rainfall may vary greatly, depending on whether or not a storm cell generates precipitation. Flooding starts at the end of the rainy season and lasts for a period of three to five months. Two mechanisms are involved in the seasonal flooding of the floodplain. The first is rain-induced local runoff and the second and most important one is over bank flooding of the Logone River. The volume of floodwater depends mainly on the magnitude of the flood peak, and the duration of the floodwater exceeding the bank full capacity of the Logone River [9].



**Figure 1.** The study area.

The floodplain vegetation consists of species-poor perennial grasslands [10]. *Oryza longistaminata* and *Echinochloa pyramidalis* constitute single or two-species stands on the floodplain, but *Vetiveria nigritana* is abundant on the levees of the drainage ditches and on the higher parts of the intact plain. Hardly any perennial grasses can be found in the non-inundated areas, where annual grasses and herbs, and locally thickets of *Acacia seyal* and *Piliostigma reticulatum* occur [11].

More than 100,000 people, both resident and nomadic, use the floodplain area for fishing, dry season grazing and agriculture. Exploitation may vary by site and by season, corresponding to the dynamic

character of the floods and the cultural background of the floodplain users. During the dry season particularly, the area plays an essential role in sustaining the rural economy of the region. Fish and wetland sorghum are exported and herds from the wider surroundings in Cameroon, Chad and Nigeria can find fresh pastures and water for their survival in the dry season [1].

Natural floodplains are among the most biologically productive and diverse ecosystems on earth [12]. However, they are also among the most threatened ecosystems. The main causes of floodplain degradation are habitat



alteration, flow and flood control, species invasion and pollution [12]. In 1979, a dam was built across the Waza-Logone floodplain, creating Lake Maga, and embankments were constructed along the Logone River, as part of an irrigated rice cultivation program. In combination with a succession of years of below average rainfall, this resulted in a decrease of depth and extent of the flooding. Perennial grasslands were replaced by less productive annual-grass dominated stands, reducing the carrying capacity for wildlife and cattle [13]. From 1988-2003, the World Conservation Union (IUCN), has been working to rehabilitate the degraded Waza Logone floodplain. The general objective of this project was to achieve long-term enhancement of the biodiversity of the Waza Logone area and to provide a sustainable improvement to the quality of life of its population. One of the actions taken to achieve this goal was partial reflooding of the floodplain. This resulted in an increased biodiversity and a partial recovery of the natural resources [1]

### 3 CALCULATION OF FLOODING EXTENT

#### 3.1. Data

The 16-days composite MODIS Vegetation Indices Product (MOD13Q1) with a spatial resolution of 250 meter was used to calculate flooding extent. It includes two vegetation indices, NDVI and EVI, in addition to composited surface reflectance bands 1-3 and 7 (red, NIR, blue, and MIR). EVI has been developed to optimize the vegetation signal with improved sensitivity in high biomass regions and improved vegetation monitoring through a decoupling of the canopy background signal and a reduction of atmosphere influences [3]. The two indices are calculated as follows:

$$NDVI = \frac{\rho_{NIR} - \rho_{red}}{\rho_{NIR} + \rho_{red}} \quad (1)$$

$$EVI = 2.5 \cdot \frac{\rho_{NIR} - \rho_{red}}{\rho_{NIR} + 6 \cdot \rho_{red} - 7.5 \cdot \rho_{blue} + 1} \quad (2)$$

Additionally, the Normalized Difference Water Index (NDWI) [2] was calculated, based on the NIR and the MIR band:

$$NDWI = \frac{\rho_{MIR} - \rho_{NIR}}{\rho_{MIR} + \rho_{NIR}} \quad (3)$$

16-day composite MODIS data, covering the Waza-Logone floodplain, was collected for five years, April 2000 – March 2001 to April 2004 – March 2005, with each year containing 23 MODIS images.

#### 3.2. Methodology

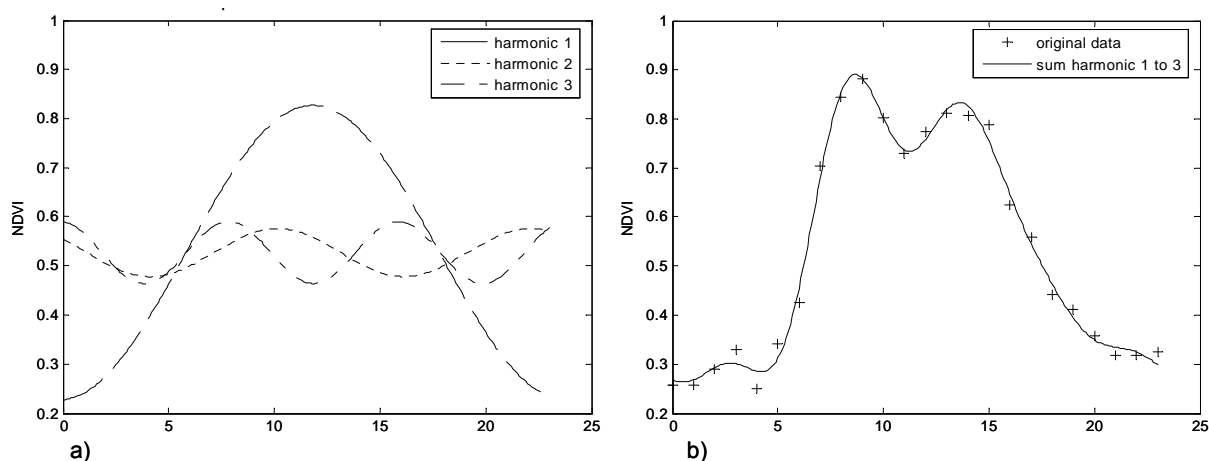
The Fourier Transform (FT) was applied to quantify the intra-annual changes for the different time-series (NDVI, EVI, NDWI and the MIR band). FT decomposes a signal into a series of cosine waves (harmonics) and an additive term (the mean). Each harmonic is defined by unique amplitude and phase angle values, where the amplitude is half the height of the harmonic and the phase angle defines the offset between the origin and the peak of the harmonic. The FT is illustrated in figure 2. In figure 2a, the first three harmonics are depicted, resulting from the decomposition of the 2000 – 2001 NDVI time-series for a wetland pixel. In figure 2b, the sum of harmonic 1 to harmonic 3 and the mean is compared with the original signal.

For each year, Fourier analysis was performed on a per-pixel basis, using the Fast Fourier Transform (FFT) algorithm [14]. For ease of computation and interpretation the Fourier analysis was applied on 24 samples instead of 23, by adding an extra image to each time-series. This resulted, for each year and for each variable, in a mean image and a set of amplitude and phase images for the 1st to the 12th harmonic term, corresponding with the

frequencies  $\frac{1}{24}, \frac{1}{12}, \frac{1}{8}, \dots, \frac{1}{2}$ .

Subsequently, the percent variance each harmonic accounts for was calculated, by dividing the variance of each harmonic term with the total variance of all terms using the amplitude values:

$$\text{variance } j^{\text{th}} \text{ harmonic} = \frac{(\text{amplitude}_j)^2}{\sum_{r=1}^{r=N/2} (\text{amplitude}_r)^2} \quad (4)$$



**Figure 2.** a) Fourier transform of 2001 – 2002 NDVI time-series for wetland pixel; b) Comparison between sum of harmonic 1 to 3 and original NDVI signal.

Based on the amplitude, amplitude variance and phase images resulting from the Fourier transform, a supervised land cover/ land use classification of the Waza-Logone area was performed for each year. Four relevant classes were considered: dry land, flooded land, irrigated rice cultivation and open water. An Artificial Neural Network (ANN) was applied to perform the supervised classification. The main advantage of an ANN classifier over a Maximum Likelihood classifier is that it is distribution-free, that is, no underlying model is assumed for the multivariate distribution of the class-specific data in feature space [15]. For a comprehensive discussion of ANNs, the reader is referred to [16]. For this study LNNS, an in-house developed neural network simulator, was used, which can be downloaded from <http://dfwm.ugent.be/forman/projecten/bof2002/html/index.htm>. Background information about this ANN is described in [17].

For the year 2003, training and test pixels were selected of the different classes (except for the open water class, that was separated by thresholding it in the MIR band) based on field data information, and visual interpretation of the original MODIS time-series. Only data from the 0<sup>th</sup> (the mean) to the 3<sup>rd</sup> harmonic were used for training the ANN, since the other harmonics contained mainly noise. First the ANN was trained for the vegetation indices and the MIR band separately. Then, different combinations of variables (MIR/NDVI, MIR/EVI, NDWI/NDVI and NDWI/EVI) were used as input to the ANN, each time combining a 'wetness' indicator with a 'greenness' indicator. Performance of each trained ANN was evaluated calculating the Kappa Index of Agreement (KIA) [18] based on the test pixels. Finally, the ANN with best performance was retained and used to carry out a classification for the other years.

To calculate the flooding extent, pixels classified as flooded land, belonging to a region smaller than a predefined size and located further away than a predefined distance from the Logone River, were eliminated. Inundation of these regions was most probably not caused by over bank flooding of the Logone River. These pixels could represent rain-fed depressions or simply be misclassified. The minimum area threshold was set to 25 pixels (15.6 km<sup>2</sup>) and the minimum distance threshold was set to 5 km.

### 3.3 Results and discussion

**Table 1.** The Kappa Index of Agreement (KIA) for the classifications obtained by ANNs with different combinations of inputs.

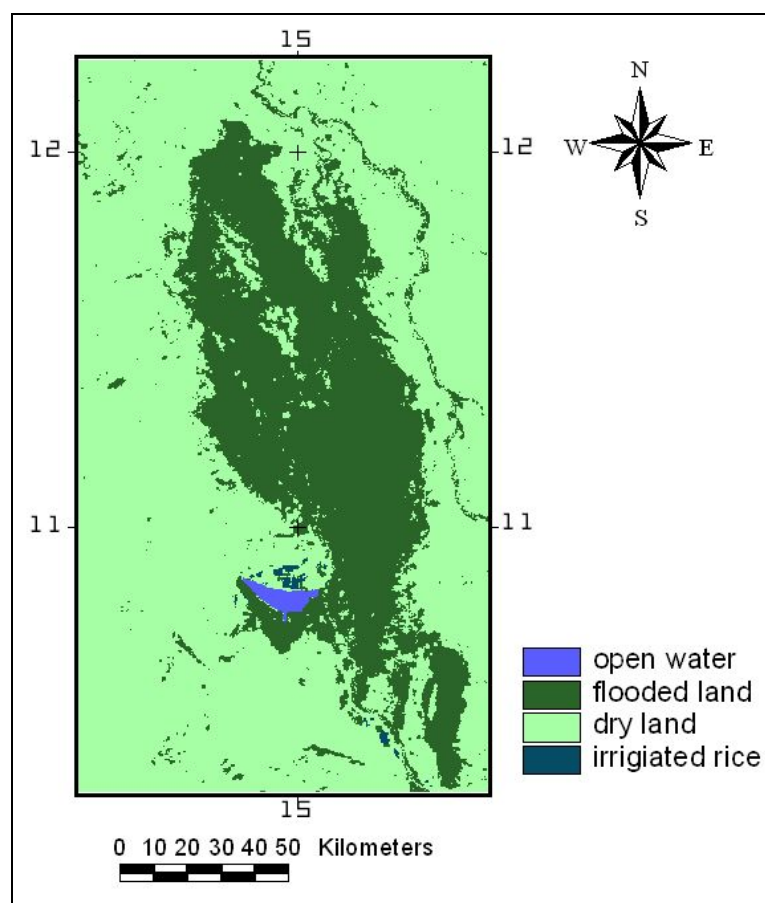
Input	KIA
MIR	0.935
NDVI	0.950
NDWI	0.924
EVI	0.932
MIR/NDVI	0.985
MIR/EVI	0.984
NDWI/NDVI	0.961
NDWI/EVI	0.969

The KIA for the 2003 classification maps resulting from the ANNs, trained with different combinations of input variables are shown in table 1. When only one variable is used as input to the ANN, the highest KIA value is obtained with amplitude, amplitude variance and phase images of the NDVI time-series (0.950). When a combination of variables is used (MIR/NDVI, MIR/EVI, NDWI/NDVI and NDWI/EVI) as input data, the highest KIA is obtained with the combinations MIR/NDVI and MIR/EVI (0.9853 and 0.9841, respectively). The MIR band outperforms NDWI for all combinations used.

The classification resulting from the ANN trained with the combination MIR/NDVI is shown in figure 3. When this ANN is used to perform a classification for the other years, visual inspection reveals numerous obvious classification errors. Mainly in wet years such as 2001, dry land pixels are misclassified as flooded land. For this reason, extra training and testing pixels were collected for the 2000 – 2001 and 2001 – 2002 time-series based on visual image interpretation.

Subsequently, the ANN was trained using the training pixels of the 2000 – 2001, 2001 – 2002 and 2003 – 2004 time-series. In table 2, the KIA of the classifications resulting from ANN trained on the 2003 – 2004 time-series and the ANN trained on the different time-series are compared. When training pixels from different years are combined, the KIA increase considerably for the 2000 and 2001 classification maps and only a slight decrease can be observed for the KIA of the 2003 classification map.

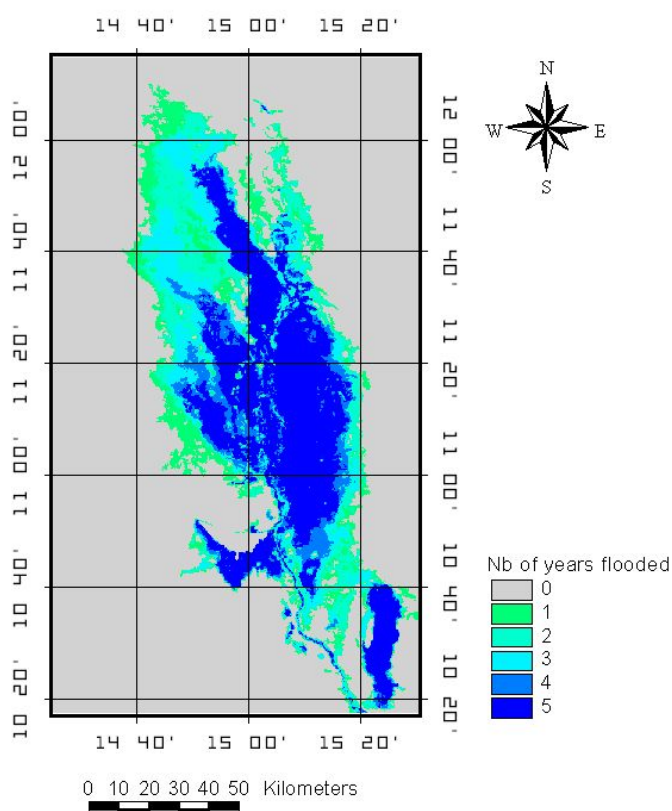
When classifications were performed for each time-series, pixels were eliminated according to the minimum distance and minimum area criteria mentioned above. Next, the maximum flooding extent for each year was calculated. As can be concluded from table 3, large inter-annual differences exist. For example, in 2001 an area more than double the size of 2002 was flooded. Figure 4 shows the number of years flooding occurred during the period 2000 – 2004. It can be noticed that the largest inter-annual differences in flooding extent occur on the Cameroonian side of the Logone (to the west of the river).



**Figure 3.** Classification map for 2003 – 2004 based on 0<sup>th</sup> to 3<sup>rd</sup> harmonic images of MIR and NDVI time-series.

**Table 2.** Comparison of ANN performance, when trained on data from a single year, and when trained on data from several years.

Year	KIA	
	ANN trained on 2003 data set	ANN trained on 2000, 2001 and 2003 data set
2000 – 2001	0.860	0.950
2001 – 2002	0.760	0.920
2003 – 2004	0.985	0.968

**Figure 4.** Number of years in which flooding occurred in the Waza-Logone area for the period 2000 – 2004**Table 3.** Extent of the flooding in Waza-Logone region for different years

Year	Area (km <sup>2</sup> )
2000 – 2001	5982
2001 – 2002	9204
2002 – 2003	4081
2003 – 2004	7918
2004 – 2005	4810

#### 4 HYDROLOGICAL MODELLING

A hydrological model will be established to simulate streamflow in the Logone catchment area based on 10-day rainfall estimates RFE [7]. Streamflow data from two gauging station, Bongor and Moundou will be used for calibration. When such a model is developed, stream flow can be related to flooding extent. The main problem is the large number of missing streamflow data. For this reason the Pitman model [19] will be used. The advantage of this model is the availability of guidelines for parameter estimation provided by the WR90 study [20] These parameters can then be refined by local calibration. The model is an explicit soil moisture accounting model representing interception, soil moisture and ground water storages, with model functions to represent the inflows and outflows from these. It has been especially developed for semi-arid catchments in the South-African subcontinent, but has also been applied outside the region [21].

##### 4.1. Input data

Based on the GTOPO30 1 km DEM data set [22], eight sub-basins were delineated within the Logone catchment area. 10-day rainfall estimates RFE for Africa [7] were used to calculate monthly rainfall for each sub-basin. The RFE data is processed by NOAA's Climate Prediction Centre for the United States Agency for International Development (USAID) Famine Early Warning System (FEWS) to assist in the drought and flood monitoring efforts for the African continent. Computation of RFE is based on METEOSAT 7 satellite data, Global Telecommunication System (GTS) rain gauge reports, model

analyses of wind and relative humidity, and orography. This data is available for the period 1996 – 2004.

Streamflow records for the period 1996 – 2004 were available for two gauging stations in the catchment area. For Bongor station, situated approximately 100 kilometers upstream from the Waza-Logone floodplain, only three years of streamflow data was available within the period 1996 – 2004. For Moundou station, located 300 kilometers upstream from Bongor, seven years of streamflow data was available within this period.

Information on Potential Evapotranspiration (PET), land cover, soil type and geology was collected for each sub-basin using following data sets:

- Global map of monthly reference evapotranspiration - 10 arc minutes [23]
- 1-km land cover map of Africa [24]
- The digitized soil map of the world [25]
- Map showing geology, oil and gas fields, and geologic provinces of Africa [26]

#### 4.2. Pitman monthly time-step model

The monthly time-step model has two main functions that generate runoff. The first is a symmetrical triangular distribution, defined by two parameters ( $ZMIN$  and  $ZMAX$ ), representing the catchment absorption rate. If the rainfall in any iteration step  $\Delta t$  is greater than  $ZMIN*\Delta t$ , then some runoff occurs. The greater the difference between the two parameters, the wider the range of the cumulative distribution and the lower the runoff rate for any rainfall greater than  $ZMIN$ . The other function is mainly controlled by a maximum moisture storage parameter ( $ST$ ). If the storage level exceeds this value all further rainfall becomes runoff. The moisture storage is depleted by evapotranspiration and drainage using a non-linear soil moisture runoff formulation. This equation is based on a non-linear relationship between current soil moisture storage and runoff from soil moisture. Once the runoff is generated by either of these functions it much reach the catchment outlet as there are no loss functions except those related to artificial abstractions. [27]

#### 4.3. Expected results

The rainfall-runoff model is currently being calibrated. Once the first results are available, the relationship between simulated streamflow at Bongor station (closest to the floodplain) and rainfall in the floodplain area, on one hand, and flooding extent, on the other hand, will be analyzed. Rainfall in the floodplain area influences the soil moisture prior to inundation, while streamflow data of the Logone River determines the duration and the intensity of the over bank flooding.

### 5 CONCLUSIONS

The flooding extent of the Waza-Logone floodplain, located in the north of Cameroon, was studied using time-series of MODIS 16-day 250m data. Fourier analysis was applied to quantify the temporal distributions of the MIR band and three indices (NDVI, NDWI, and EVI). The resulting amplitude, phase and amplitude variance images for harmonics 0 to 3 were used as inputs for an ANN to differentiate between the different land cover/ land use classes. When the combinations MIR/NDVI and MIR/EVI were used as input to the ANN, the classification map with the highest Kappa Index of Agreement (KIA) was obtained. When the ANN was trained on pixels from different years, a more robust classifier was obtained, which could consistently separate flooded land from dry land for each year. During the period 2000 – 2004 flooded area varied highly from one year to another, reaching a maximum in 2001 – 2002 and a minimum in 2002 – 2003. The extent of the flooding strongly influences the availability of natural resources in the dry season. The considerable interannual differences in flooding extent should therefore be taken into account in view of a sustainable management of these natural resources.

Flooding extent differs from one year to another in response to rainfall in the floodplain area prior to flooding and the streamflow distribution of the Logone river. Streamflow can be simulated using the Pitman model based on African Rainfall Estimates (RFE) data. Subsequently, a model could be constructed that can estimate flooding extent based on the simulated streamflow data. Such a model would enable prediction of possible impacts of a changing climate due to Global Warming, and detection of human-induced anomalies such as hydropower and irrigation projects.

## ACKNOWLEDGEMENTS

This project was funded by BOF, the Special Research Fund of Ghent University, Belgium, under contract number B/05884/01.

## REFERENCES

- [1] LOTH, P. (EDITOR), 2004: The return of the water: restoring the Waza Logone Floodplain in Cameroon. IUCN, Gland, Switzerland and Cambridge, UK.
- [2] GAO, B.G., 1996: NDWI – a normalized difference water index for remote sensing of vegetation liquid water from space. *Remote Sensing of Environment* 58, pp. 257-266.
- [3] HUETE, A., DIDAN, K., MIURA, T., RODRIGUEZ, E.P., GAO, X., AND FERREIRA L.G., 2002: Overview of the radiometric and biophysical performance of the MODIS vegetation indices. *Remote Sensing of Environment* 83, pp. 195-213.
- [4] OLSSON, L. AND EKLUNDH, H., 1994: Fourier Series for analysis of temporal sequences of satellite sensor imagery. *International Journal of Remote Sensing* 15, pp. 3735-3741.
- [5] MOODY, A. AND JOHNSON, D. M., 2001: Land-surface phonologies from AVHRR using the discrete fourier transform. *Remote Sensing of Environment* 75, pp. 305-323.
- [6] JAKUSBAUSKAS, M.E., LEGATES, D. R. AND KASTENS, J.H., 2001: Harmonic analysis of time-series AVHRR NDVI data. *Photogrammetric Engineering & Remote Sensing* 67, pp. 461-470.
- [7] XIE, P. AND ARKIN, P. A., 1997: A 17-year monthly analysis based on gauge observations, satellite estimates, and numerical model outputs. *Bulletin of the American Meteorological Society*, 78, pp. 2539-2558.
- [8] BEAUVILAIN, A., 1995: Tableau de la pluviométrie dans les bassins du Tchad et du Benoué. Tableaux et documents scientifiques du Tchad. Documents pour la recherche III, CNAR, N'djamena.
- [9] MACDONALD, M., 1999: Logone Floodplain Model Study Report. Mott MacDonald, Cambridge.
- [10] DENNY, P., 1985: The ecology and management of African wetland vegetation. Geobotany 6. Dr W. Junk Publishers. Dordrecht/Boston/Lancaster.
- [11] BURGIS, M. J. AND SYMOENS J. J., 1987: African wetlands and shallow water bodies. Editions de l'ORSTOM. Institut Français de recherche scientifique pour le développement en coopération. Collection TRAVEAUX et DOCUMENTS no. 211. Paris.
- [12] TOCKNER, K. AND STANFORD, J. A., 2002: Riverine flood plains: present state and future trends. *Environmental Conservation* 29, pp. 308-330.
- [13] SCHOLTE, P., KIRDA, P., SALEH, A. AND BOBO, K., 2000: Floodplain rehabilitation in North Cameroon: Impact on vegetation dynamics. *Applied Vegetation Science* 3, pp. 33-42.
- [14] SINGLETON, R. C., 1969: An Algorithm for Computing the Mixed Radix Fast Fourier Transform. *IEEE Transactions on audio and electroacoustics* 17, pp. 93-103.
- [15] ATKINSON, P. AND TATNALL, A., 1997: Neural networks in remote sensing. *International Journal of Remote Sensing* 18, pp. 699-709.
- [16] HAYKIN, S., 1999: Neural networks: A comprehensive foundation. Prentice-Hall, New Jersey.
- [17] VERBEKE, L.P.C., VAN COILLIE, F.M.B. AND DE WULF, R.R., 2004: Reusing back-propagation artificial neural networks for land cover classification in tropical savannahs. *International Journal of Remote Sensing* 25, pp. 2747-2771.
- [18] COHEN, J., 1960: A coefficient of agreement for nominal scale. *Educational and Psychological Measurement* 20, pp. 37- 46.
- [19] PITMAN, W.V., 1973: A mathematical model for generating monthly flows from meteorological data in South Africa. Report No. 2/73, Hydrological research Unit, University of the Witwatersrand, South Africa.
- [20] 1994: Surface Water Resources of South Africa 1990. Water Research Commission Reports MIDGLEY, D.C., PITMAN, W.V. AND MIDDLETON, B.J., No. 298/1.1/94 to 298/6.194, Pretoria, South Africa.
- [21] WILK, J. AND HUGHES, D.A., 2002: Calibrating a rainfall-runoff model for a catchment with limited data. *Hydrological Sciences Journal* 47, pp. 3-17.
- [22] GESCH, D.B., VERDIN, K.L., AND GREENLEE, S.K., 1999: New land surface digital elevation model covers the Earth. *EOS, Transactions of the American Geophysical Union* 80, pp. 69-70.
- [23] FAO, 2004: Global map of monthly reference evapotranspiration - 10 arc minutes. FAO, Rome, Italy.
- [24] MAYAUX, P., BARTHOLOME, E., FRITZ, S. AND BELWARD, A., 2004: A new land-cover map of Africa for the year 2000. *Journal of biogeography* 31, pp. 861-877.
- [25] FAO, 1997: Digitized Soil Map of the World (1:5,000,000). FAO, Rome, Italy.
- [26] USGS, 2002: Map showing geology, oil and gas fields, and geologic provinces of Africa. USGS, Reston, USA.
- [27] HUGHES, D.A., 1995: Monthly rainfall-runoff models applied to arid and semiarid catchments for water resource estimation purposes. *Hydrological Sciences Journal* 47, pp. 751-769.